Review—Ionizing Radiation Damage Effects on GaN Devices

S. J. Pearton,[a,*,z] F. Ren,[b,*] Erin Patrick,[c,] M. E. Law,[c,**] and Alexander Y. Polyakov[d]**

[a]*Department of Materials Science and Engineering, University of Florida, Gainesville, Florida 32606, USA*
[b]*Department of Chemical Engineering, University of Florida, Gainesville, Florida 32606, USA*
[c]*Department of Electrical and Computer Engineering, University of Florida, Gainesville, Florida 32606, USA*
[d]*National University of Science and Technology MISiS, Moscow 119049, Russia*

Gallium Nitride based high electron mobility transistors (HEMTs) are attractive for use in high power and high frequency applications, with higher breakdown voltages and two dimensional electron gas (2DEG) density compared to their GaAs counterparts. Specific applications for nitride HEMTs include air, land and satellite based communications and phased array radar. Highly efficient GaN-based blue light emitting diodes (LEDs) employ AlGaN and InGaN alloys with different compositions integrated into heterojunctions and quantum wells. The realization of these blue LEDs has led to white light sources, in which a blue LED is used to excite a phosphor material; light is then emitted in the yellow spectral range, which, combined with the blue light, appears as white. Alternatively, multiple LEDs of red, green and blue can be used together. Both of these technologies are used in high-efficiency white electroluminescent light sources. These light sources are efficient and long-lived and are therefore replacing incandescent and fluorescent lamps for general lighting purposes. Since lighting represents 20–30% of electrical energy consumption, and because GaN white light LEDs require ten times less energy than ordinary light bulbs, the use of efficient blue LEDs leads to significant energy savings. GaN-based devices are more radiation hard than their Si and GaAs counterparts due to the high bond strength in III-nitride materials. The response of GaN to radiation damage is a function of radiation type, dose and energy, as well as the carrier density, impurity content and dislocation density in the GaN. The latter can act as sinks for created defects and parameters such as the carrier removal rate due to trapping of carriers into radiation-induced defects depends on the crystal growth method used to grow the GaN layers. The growth method has a clear effect on radiation response beyond the carrier type and radiation source. We review data on the radiation resistance of AlGaN/GaN and InAlN/GaN HEMTs and GaN–based LEDs to different types of ionizing radiation, and discuss ion stopping mechanisms. The primary energy levels introduced by different forms of radiation, carrier removal rates and role of existing defects in GaN are discussed. The carrier removal rates are a function of initial carrier concentration and dose but not of dose rate or hydrogen concentration in the nitride material grown by Metal Organic Chemical Vapor Deposition. Proton and electron irradiation damage in HEMTs creates positive threshold voltage shifts due to a decrease in the two dimensional electron gas concentration resulting from electron trapping at defect sites, as well as a decrease in carrier mobility and degradation of drain current and transconductance. State-of-art simulators now provide accurate predictions for the observed changes in radiation-damaged HEMT performance. Neutron irradiation creates more extended damage regions and at high doses leads to Fermi level pinning while ^{60}Co γ-ray irradiation leads to much smaller changes in HEMT drain current relative to the other forms of radiation. In InGaN/GaN blue LEDs irradiated with protons at fluences near 10^{14} cm^{-2} or electrons at fluences near 10^{16} cm^{-2}, both current-voltage and light output-current characteristics are degraded with increasing proton dose. The optical performance of the LEDs is more sensitive to the proton or electron irradiation than that of the corresponding electrical performances.
© The Author(s) 2015. Published by ECS. This is an open access article distributed under the terms of the Creative Commons Attribution 4.0 License (CC BY, http://creativecommons.org/licenses/by/4.0/), which permits unrestricted reuse of the work in any medium, provided the original work is properly cited. [DOI: 10.1149/2.0251602jss] All rights reserved.

Manuscript submitted October 15, 2015; revised manuscript received November 16, 2015. Published November 24, 2015.

Wide-bandgap III-Nitrides have become one of the most important semiconductor materials systems, with applications in visible-UV light emitting devices (LEDs) and laser diodes (LDs), high-power/high frequency transistors and power rectifiers.[1–4] The strong bonding in binary and ternary nitrides gives them an intrinsically high radiation resistance.[5–26] The fluence of ionizing radiation at which GaN materials and devices such as transistors and light-emitting diodes start to show degradation is about two orders of magnitude higher than in their GaAs equivalents.[27–80] This difference is attributed to the stronger bonding of GaN.[4,6,8,9] A measure of this bond strength is the energy required to displace an atom from its lattice position or simply the atomic displacement energy, denoted by E_d. This parameter has been measured in several semiconductors and empirically determined to be inversely proportional to the volume of the unit cell.[4,6,9,33,63–67] Analysis of the transport properties of electron-irradiated GaN show that E_d (Ga) is 20.5 eV and E_d (N) 10.8 eV.[4] In the case of GaAs, E_d is 9.8 eV.[4,5,9] Figure 1 shows a plot of experimentally determined displacement energies in semiconductors as a function of inverse lattice constant.[4] The latter is a measure of how strongly bonded the component atoms are and should correlate with difficulty in creating lattice displacements and hence the relative radiation resistance of the semiconductor. The high displacement energy for GaN relative to Si and GaAs means it will be more resistant to creation of point defects during irradiation. The displacement energy varies inversely as the volume of the unit cell for many semiconductors.

*Electrochemical Society Fellow.
**Electrochemical Society Active Member.
[z]E-mail: spear@mse.ufl.edu

The response of GaN to radiation damage is a function of radiation type, dose, energy as well as the carrier density, impurity content and dislocation density in the GaN.[12,22,27,35,38,56,57] The latter can act as sinks for created defects and parameters such as the carrier removal rate due to trapping of carriers into radiation-induced defects and is also found to depend on the crystal growth method used to grow the GaN layers. There are three common techniques used to grow GaN layers, namely Metal Organic Chemical Vapor Deposition (MOCVD), Hydride Vapor Phase Epitaxy (HVPE) and Epitaxial Lateral Overgrowth (ELOG), each with its own characteristics in terms of defect density and distribution. The growth method has a clear effect on radiation response beyond the carrier type and radiation source.[12,56]

There are three main GaN-based heterostructures used for electronics, namely AlGaN/ GaN, which is the most common nitride-based heterostructure; AlN/GaN which produces the highest two dimensional electron gas density, but has issues with stability of the AlN and finally, InAlN/GaN, an emerging system with high thermal and chemical stability and lattice matching to GaN at an In mole fraction of 0.17.[1] The InAlN/GaN material system offers an attractive alternative to AlGaN/GaN for high power, high frequency applications.[1]

Given the applications for GaN HEMTs, they will commonly be subject to fluxes of high energy protons and electrons if used in low earth orbit satellites as well as neutrons or gamma rays if used in radiation-hard electronics for nuclear or military systems. Each of these forms of radiation produces different types of damage. In addition, primary defects may recombine, form complexes with each other, with dopants and with extended defects; at high energies the energy of the primary recoils becomes so high that they produce collision cascades and form heavily disordered regions with a very high

Downloaded on 2019-08-31 to IP 128.227.169.164 address. Redistribution subject to ECS terms of use (see ecsdl.org/site/terms_use) unless CC License in place (see abstract).

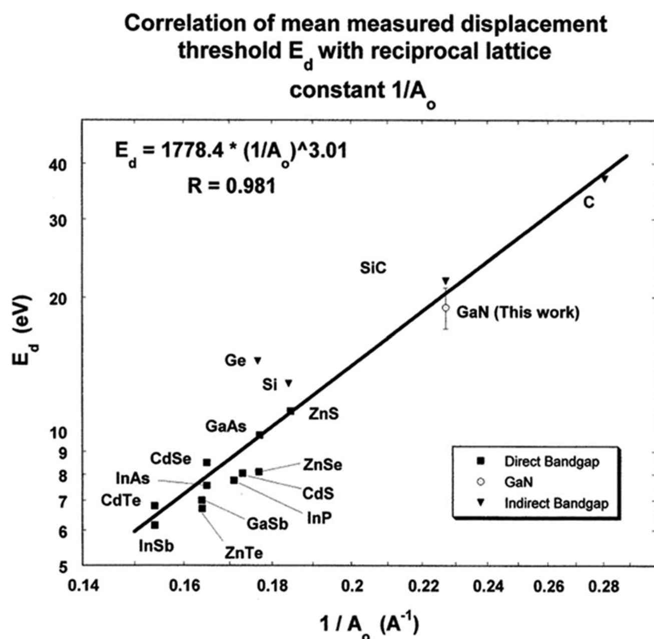

Figure 1. Empirical relationship between mean displacement energy Ed and inverse lattice parameter for various semiconductors. Note the high threshold for GaN, which corresponds to an expected high degree of radiation hardness. (from Ionescu et al.[4]).

defect density in the core. In general, proton and electron irradiation produces simple point defects in the nitride lattice,[10,12,57] while neutron irradiation creates extended defects called Gossick zones, which are heavily disordered core regions surrounded by a space charge region with strong band bending.[11,12,57,64,70,79] The response to gamma irradiation is quite complicated. Compton electrons induced from γ-radiation create electron-hole pairs, thus changing occupancy of traps. Unlike proton irradiation, some studies claim that these defects produced by gamma irradiation can improve device performance such as increasing drain saturation current.[60,61] In some cases, low dose γ-irradiation leads to partial relaxation of the elastic strain in AlGaN/GaN heterostructures and enhances the electron mobility by 5–10%. This improvement of the electron mobility increases the drain current. By contrast, others reported the drain current was reduced about 60% after γ-irradiation at around 7×10^4 rad.[14,15,52] These defects in that case must reduce the carrier concentration in the irradiated devices,[81–84] and there was more degradation with increasing γ-irradiation dose.[15,42] The defects produced by γ-irradiation may be structure sensitive which would be one reason for the discrepancies between different reports.[12,57,60,61] Also, dose clearly plays a role in the performance of the devices after irradiation.[85–109] For proton and electron damage, the device degradation scales with dose and is correlated with the nuclear or non-ionizing energy loss component of the ions traversing the active regions of the device which creates lattice displacements. Similar comments apply to neutron-induced damage, but the carrier removal rates for neutron irradiation are much lower than for protons. It is instructive to summarize the effect of γ-ray exposure on simple nickel/n-GaN Schottky barrier diodes. Current-voltage (I–V), capacitance-voltage (C-V), and deep-level transient spectroscopy (DLTS) measurements show an increase in effective Schottky barrier height, a degradation of the reverse leakage current, but minimal effect on the forward I–V characteristics.[14,15] Low temperature (≤50°C) post-irradiation annealing after a cumulative irradiation dose of 21 Mrad (Si) was found to restore the reverse I-V characteristics to pre-irradiation levels without significantly affecting the radiation-induced changes in C-V and forward I-V characteristics.[14,15] Three shallow radiation-induced defect centers with thermal activation energies of 88, 104 and 144 meV were detected by DLTS[14,15] with a combined production rate of 2.12×10^{-3} cm^{-1}. These centers are likely to be related to nitrogen-vacancies. The effect of high-energy γ-rays on device performance was suggested to be dependent on dislocation and interfacial defect density. These results indicated that GaN has an intrinsically low susceptibility to radiation-induced material degradation, but that that the total-dose radiation hardness may be limited by damage to the metal-GaN interface. This case study shows some of the important issues in radiation-induced GaN device degradation, namely the dependence of the final outcome on the details of the device structure, such as the contact metallurgy, thickness of component layers, the post-irradiation thermal history, the polarity of the GaN material and the type of radiation involved.

GaN Materials and Device Technology

GaN is a direct bandgap (3.4 eV) semiconductor which is typically synthesized in the hexagonal wurtzite crystal structure with lattice constants a = 3.189Å and c = 5.185Å, generally on lattice mismatched substrates. There is a significant iconicity component to the bonding, with a strong charge transfer between the very electronegative nitrogen atoms and the less electronegative metal atoms (Ga in the case of GaN, or Al and In in the case of AlGaN and InAlN ternary alloys). The exciton binding energy is 23.4 meV, the refractive index is 2.43 and the thermal conductivity is 1.3 W/cm · K at 300 K. GaN has a lattice polarity along the c-axis direction due to the lack of inversion symmetry. Due to the presence of the polar axis, GaN-based materials grown on a lattice mismatched substrate can have two inequivalent orientations as shown in Figure 2 (top).[38] These orientations are the

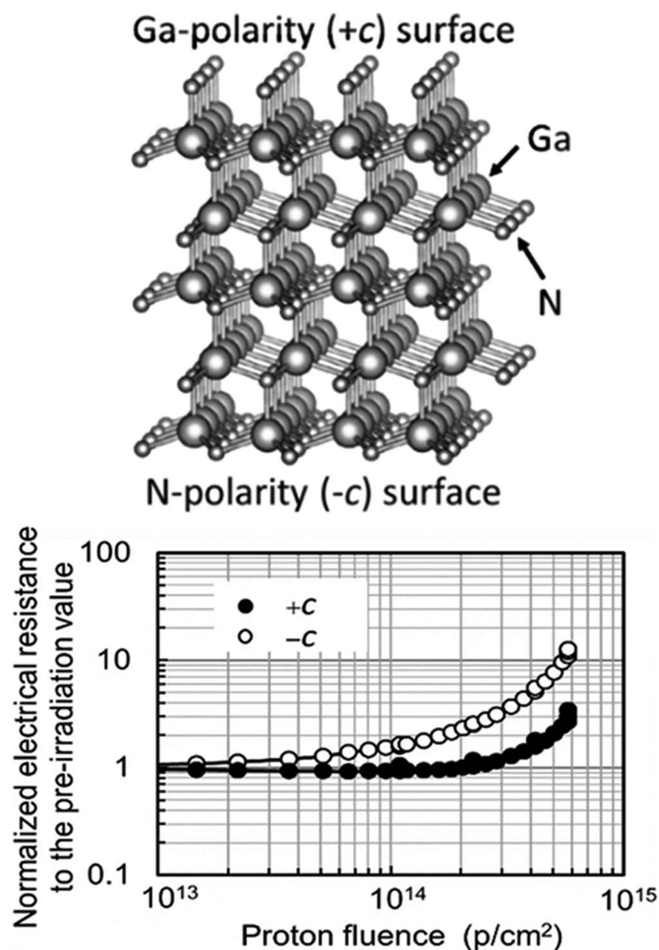

Figure 2. (top) Crystal structure and polarity of GaN showing the Ga and N-polar faces (bottom) normalized change in electrical resistance of different polarity GaN samples as a function of proton dose. The Ga polar surface shows less change due to radiation exposure (after Matsuo et al.[38]).

Downloaded on 2019-08-31 to IP 128.227.169.164 address. Redistribution subject to ECS terms of use (see ecsdl.org/site/terms_use) unless CC License in place (see abstract).

Ga-face and N-face polarities, depending on whether the Ga atoms or N atoms are facing toward the sample surface.[38] For Ga-face layers, the crystallographic c-axis and the internal electric field are both directed away from the substrate toward the surface, while the polarization-induced fixed lattice charges are in the opposite direction and are negative at the surface and positive at the substrate interface. For N-face layers, these charges and directions are inverted. The choice of Ga-face or N-face has been found to affect a number of device-related issues, including the radiation hardness. As shown in Figure 2 (bottom),[38] the Ga-face orientation shows a higher degree of resistance to changes in electrical resistance normalized to the pre-irradiation values as a function of 8 MeV proton fluence up to 5.8×10^{14} cm^{-2}.

Due to the lack of uniform, large area, low-cost GaN substrates, the GaN epitaxial process has benefited greatly from the viability of heteroepitaxy and the commercial success of GaN HEMTs is directly attributable to the ability to deposit high quality epitaxy on non-GaN substrates and the ability to integrate GaN HEMT device fabrication in standard GaAs processing lines. Historically, there have been three substrates used for heteroepitaxial GaN-based devices: sapphire (Al_2O_3), silicon carbide (SiC), and silicon (Si). In addition, long-lifetime GaN laser diodes have been achieved by homoepitaxy on GaN substrates. Many other materials have been used as substrates to deposit GaN, many with good crystalline quality, but the majority of research and development efforts have focused on sapphire, silicon carbide, silicon or gallium nitride substrates.

GaN blue, green and white LEDs initially drove the development and production of Al_2O_3 as a substrate material. This industry has pushed demand for Al_2O_3 wafer scaling up to 150 mm while reducing the price per unit area. The approaches originally developed for nucleating and growing GaN LED structures have been applied to the growth of GaN HEMT structures. These nucleation schemes very effectively mitigate the lattice incongruity between GaN and Al_2O_3 while the coefficient of thermal expansion (CTE) mismatch favors compression of the epi, in contrast with the tension typically exhibited by GaN-on-SiC and GaN-on-Si. While compressive stress may manifest itself in wafer bow, it does not result in epilayer cracking as when growing on SiC or Si.

While much of the early GaN HEMT research utilized Al_2O_3 substrates, the low thermal conductivity of this material has essentially removed its widespread application today. The extremely high power densities achieved with GaN HEMTs is achieved with high current densities that produces significant heating within the 2DEG channel of the HEMT and this self-heating will result in reduced current at high voltage. For this reason, HEMTs are now mainly fabricated from GaN-on-Si or GaN-on-SiC structures. These heteroepitaxial devices contain dislocation densities from 10^8 to 10^9 cm^{-2}. By comparison, a typical Si or GaAs-based semiconductor device will have fewer than 10^4 cm^{-2} dislocations since densities significantly degrade device lifetime and performance. The epitaxial growth of GaN HEMT structures can be carried out by MOCVD or MBE, with the majority done with the former due to the lower cost. Whereas in other material systems, most notably GaAs, MBE typically provides higher purity sources resulting in 'cleaner' epi, in GaN the MBE process often uses metallorganic sources for the column III elements and/or gas source (i.e., ammonia) for the nitrogen (column V) element. The use of these source materials substantially reduces the higher purity advantage in the as-grown film realized in GaAs.

Typically, HEMT structures are grown with a nucleation AlN layer that mitigates lattice mismatch and stress, followed by a buffer layer structure that also reduces dislocation density and provides electrical isolation to minimize leakage current. In a typical AlGaN/GaN HEMT, the AlGaN barrier layer Al content typically is in the range of 15–30% mole fraction with a thickness of nominally 15–30 nm. The structure may terminate with a GaN cap to planarize the surface and to increase the effective Schottky barrier height due to piezoelectric polarization effects. Figure 3 (top) shows the structure of a typical GaN-based HEMT.[4]

GaN-based optical emitters (LEDs and laser diodes) have been a tremendous success story and although their applications are less

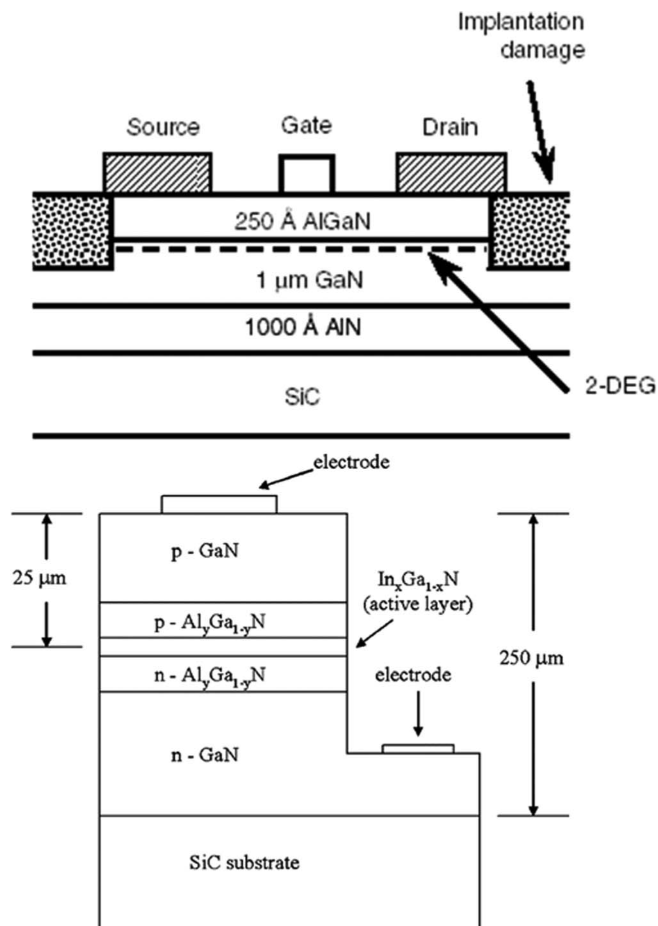

Figure 3. The two most common GaN-based devices device structures for which radiation damage studies have been performed. A schematic of an AlGaN/GaN HEMT is shown at top, while a schematic diagram of an AlGaN/InGaN QW LED is shown at bottom (after Ionescu et al.[4] and Khanna et al.[171]).

likely to involve radiation damage, there is still interest in their radiation hardness. These applications are in displays and lighting that are based on InGaN/AlGaN/GaN blue LEDs that excite a yellow-emitting phosphor, often Y_3 Al_5O_{12}:Ce. This combination of the blue light with the phosphor-generated yellow light leads to white light. The LEDs exhibit excellent reliability with lifetimes >100, 000 hours and are used in general lighting applications and for back-illumination in liquid crystal displays in mobile phones, tablets, laptops, computer monitors and TV screens, There is much progress on use of three-colour LEDs for dynamic control of color composition. The replacement of light bulbs and fluorescent tubes by LEDs leads to enormous energy savings. There is also emerging work on the use of UV-emitting AlGaN/GaN LEDs for water purification since their UV light destroys the DNA of bacteria, viruses and microorganisms. A typical GaN-based LED structure is shown in Figure 3 (bottom).

Blue and UV-emitting GaN diode lasers are employed in high-density DVDs for information storage and are under development for laser lighting because of their superior efficiency relative to LEDs at high powers. These laser lights are already used in some high-end automotive applications. Future work will include optimizing the orientation of the nitride layers with the discovery that the nonpolar plane is not efficient for emission wavelengths beyond blue and this has led to a focus on use of semipolar planes such as (20-2-1), (10-1-1) and (20–21) for blue, green, yellow, and red emitting devices.

In this review, we will focus on the effects of radiation damage in the two most common GaN devices, namely HEMTs and LEDs,

Downloaded on 2019-08-31 to IP 128.227.169.164 address. Redistribution subject to ECS terms of use (see ecsdl.org/site/terms_use) unless CC License in place (see abstract).

although the results are relevant to other GaN-based devices such as lasers, solar-blind UV detectors, heterojunction bipolar transistors, diode rectifiers and various types of gas and biomedical sensors.

Stopping of Ions and Related Lattice Damage in GaN

As they traverse the GaN device, the irradiating ions lose energy by two main mechanisms, known as nuclear and electronic stopping.[110–129] These mechanisms are due to interactions with the nuclei and the electrons of the target material, respectively.[126] If the ions collide with atoms in the GaN, the positively charged ions are Coulombically repelled by the positive cores of the lattice atoms. This Coulombic repulsion is "screened" by the cloud of electrons surrounding each atom. Nuclear stopping is more important at higher atomic number (heavier elements) and lower ion velocities (low acceleration energy/voltage).[111,113,114] Electronic stopping dominates at lower atomic number (lighter elements) and higher ion energies.[118–121] The rate of energy loss to nuclear collisions per unit path length can be calculated by summing the energy loss multiplied by the probability of that collision occurring.[121–124] Nuclear stopping is elastic, and so energy lost by the incoming ion is transferred to the target atom that is subsequently recoiled away from its lattice site, creating a damage or defect site.[111,114] Electronic stopping is inelastic since energy is lost during the process. The collisions may result both in excitations of bound electrons of the medium, and in excitations of the electron cloud of the ion as well as thermal vibrations of the target.[111,114,121] The lost energy eventually dissipates as heat, and does not create atomic displacements in the materials. The electronic stopping cross section is proportional to the velocity of the implanted ion and therefore to the square root of its energy. Its contribution dominates in the high-energy regime.

Nuclear stopping power refers to the elastic collisions between the projectile ion and atoms in the GaN. The conventional term "nuclear" is somewhat imprecise since nuclear stopping is not due to nuclear forces, but it is meant to note that this type of stopping involves the interaction of the ion with the nuclei in the target. These displaced nuclei may also have enough energy to displace other nuclei, leading to a cascade of recoiled atoms.[115] Nuclear energy loss dominates at low to intermediate energies, and leads to the creation of deep-level compensating defects.[117,118] At high energies, the contribution from this process tends to be small because fast ions have only a short time to interact with a target nucleus, and cannot transfer energy efficiently.[125–127] Figure 4 shows a schematic of the relative energy loss due to electronic and nuclear stopping processes as a function of ion energy. The relative importance of these two stopping mechanisms

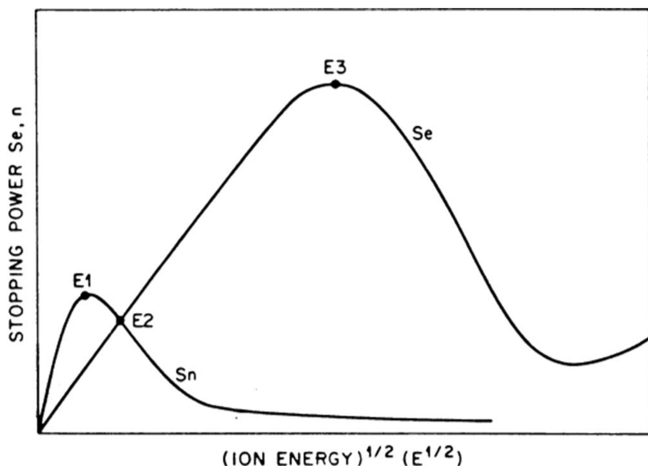

Figure 4. Schematic of the cross section S (proportional to the energy loss per unit distance) for electronic (S_e) and nuclear (S_n) stopping processes as a function of ion energy. Typical values for the parameters E_1, E_2 and E_3 for N ions irradiating GaN are: $E_1 = 20$ keV, $E_2 = 40$ keV, $E_3 = 8$ MeV.

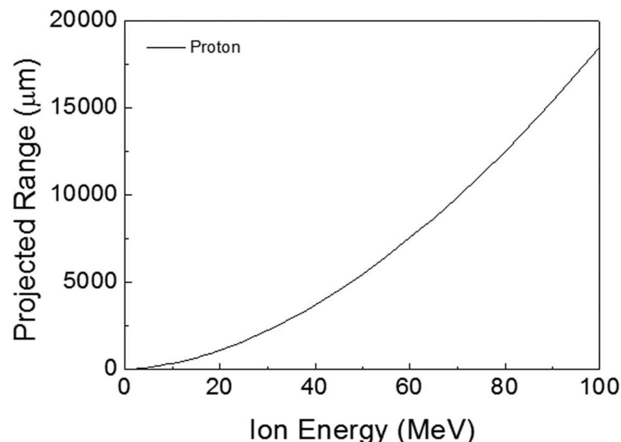

Figure 5. Range of protons in GaN over the range of energies from 1–100 MeV.

also depends on the mass of the implanted ions, the mass and atomic density of the target.[111] Both the stopping effects produce an energy loss rate of some tens of eV per angstrom in semiconductors.

At the ion energies typically encountered in space applications, the ions pass through the entire GaN device, as well as the substrate. Figure 5 shows a Transport of Ions in Matter (TRIM) simulation[111] of the range of protons in GaN over the energy range 1–100 MeV. Even a 2 MeV proton has a range of 43 μm in GaN, much larger than the thickness of the epi films used in HEMTs or LEDs.

One can calculate the energy loss using the well-established treatments in the literature, originally developed for ion implantation in solids. There are a number of codes available to do this, including TRIM/SRIM (a Monte-Carlo approach),[111] Marlowe (developed at Oak Ridge National Labs)[126] and a number of commercial programs. We briefly summarize the physics behind these simulators.

The interaction potential V(r) between the ion and the GaN is a repulsive coulomb potential due to the positive charges of the core atoms.[111,124] This coulomb potential is screened by the surrounding electrons. The effect of the electrons can be described by adding a dimensionless screening function Φ (r) to the coulomb potential.

$$V(r) = \left[\left(Z_1.Z_2.e^2\right)/r\right].\Phi(r)$$

where Z_1 is the atomic number of the ion and Z_2 is the average atomic number of the Ga and N, e is the electronic charge and r is the distance of closest approach of the ions and nuclei.

The average nuclear stopping power $S_n(E_O)$ provides the average energy transferred by each nuclear collision between the ions and the Ga and N atoms if the particle energy is E_O. The nuclear stopping power in units of eV/(atom/cm^2) is given by[111]

$$\begin{aligned} S_N(E_O) &= [(\pi.a_u.\gamma.E_O)/\varepsilon].S_N(\varepsilon) \\ &= \left[8.462\times10^{-15}.Z_1.Z_2.M_1\right].S_N(\varepsilon)/(M_1+M_2). \\ &\quad\cdot\left(Z_1^{0.23}+Z_2^{0.23}\right) \end{aligned}$$

The universal screening potential is a function of the dimensionless reduced radius *x* which is related to the real radius by the scaling length $a_{u,}$ given by[111]

$$a_u = 0.8854\left[a_o/Z_1^{0.23}+Z_2^{0.23}\right]$$

where a_o is the Bohr radius (0.53 Å). M_1 is the mass of the incoming ion and M_2 the mass of the Ga and N atoms and $\gamma = 4M_1M_2/(M_1^2+M_2^2)$.

The electronic stopping power or energy loss per unit length of the ion path involves excitation or ionization of the atoms in the target can be calculated according to the Bethe-Bloch theory for high ion velocities[111]

$$S_{eb} = [8\pi.Z_1^2.e^4]/I_O\cdot\varepsilon_b\times\ln(\varepsilon_b+1+5/\varepsilon_b)$$

Downloaded on 2019-08-31 to IP 128.227.169.164 address. Redistribution subject to ECS terms of use (see ecsdl.org/site/terms_use) unless CC License in place (see abstract).

where $\varepsilon_b = [4E\,(m_e/M_1 m_o)]/Z_2 I_O$ and m_e is the electron mass, m_o the atomic mass unit, M_O the relative atom mass of the ion, and I_O the Bloch constant in units of eV.

The radiation hardness of any semiconductor device is determined by its response to various types of radiation exposure. These include total ionizing dose (TID), which is the degradation induced by a cumulative dose of radiation, enhanced low dose rate effects (ELDRS), in which low doses produce a disproportionately large amount of damage compared to that of higher doses, neutron and proton displacement damage, and single event effects (SEE), in which the passage of a single ion or short burst of radiation can disrupt the operation of the device. This creates an ionized track which may cause a highly localized effect similar to a transient dose and lead to a change in output, a bit flip in memory or a register or in extreme cases, a destructive latchup and burnout. TID is typically caused by lattice displacement damage caused by ionizing radiation over the integrated exposure time and may be caused by high energy X-rays, γ-rays, or charged particles such as protons and heavy ions.[125–129] In Si CMOS devices, this damage is typically detected as trapped charge in an oxide layer, surface, or interface as the electrons created are removed by the electric fields present in the device, leaving a net positive charge in the oxide or interface. These effects may cause shifts in threshold voltage and increase leakage current of the device. In GaN devices, MOS technology is not yet established and metal gates are more commonly used for charge control in transistors. In that case, the TID is more typically detected as a change in the carrier density and mobility in the channel of transistors or a decrease in optical output from LEDs. All of these types of radiation, ie. charged particles, X-rays and γ-rays, deposit energy and create electron-hole pairs in the GaN. This dose is measured in units of Rads (an acronym for radiation absorbed dose) or the SI unit which is the gray (Gy); 1 Gy = 100 rads = 1 J/kg. TID generally results in gradual degradation of the device performance.

In addition to the protons and heavy ions in the space environment, neutrons occur naturally in the terrestrial environment, and nuclear reactors emit both neutrons and γ-rays. Neutrons cause non-ionizing damage to semiconductor materials, and may cause nuclear collisions which create secondary ionizing particles. The behavior of charged particles such as protons, electrons and alpha particles) on the semiconductor through which they pass is quite different from that of neutrons and gamma rays. As discussed earlier, the charged particles are directly ionizing as they strongly interact with the orbital electrons of the semiconductor as they pass through.

Displacement Damage

Displacement damage is the most important effect observed in irradiated GaN devices and is the result of nuclear interactions which cause lattice defects. Displacement damage is due to cumulative long-term non-ionizing radiation damage in the GaN. The collision between an incoming ion and a lattice atom displaces the atom from its original lattice position, leaving vacancies, interstitials and complexes of both, sometimes with impurities in the GaN. If an incident energetic particle such as a neutron or proton collides with the nucleus of a lattice atom, the primary knock-on atom may be displaced from the lattice if the incident particle has sufficient energy (E > Ed), where Ed is the lattice displacement energy. The lattice displacement energy is inversely proportional to the lattice constant. If a lattice atom is displaced, it may result in a stable defect or trap, which will affect the performance of the HEMT by removing carriers from the 2DEG and decreasing the mobility. The defects may also result in threshold voltage shift, decrease in transconductance, and decrease in drain saturation current.

Displacement damage can be quantified using the non-ionizing energy loss (NIEL) due to the nuclear stopping component. The NIEL is energy lost to non-ionizing events per unit length, in units of MeV/cm or $MeV \cdot cm^2$ /g. The NIEL is a useful concept for devices because it is commonly observed that displacement damage effects are proportional to the non-ionizing particle's energy loss and the nuclear recoils produced.[125,126] A displacement damage dose (Dd) can be computed from the relation Dd is equal to the NIEL times the dose (Φ). The production of vacancies and interstitials involves a transfer of particle kinetic energy to potential energy stored in the crystal lattice. Both vacancies and interstitials (especially the latter) are mobile at fairly modest temperatures and thermal annealing causes a significant fraction of them to recombine. At these temperatures, the vibration of the atoms in the lattice increases, and this additional energy provides a mechanism by which an interstitial can migrate to a nearby vacancy and eliminate both defects by recombination.[125–128]

Table I. Calculated Ionizing and Non-Ionizing Energy Losses and Total Ionizing Dose for protons of different energy in GaN at a fixed fluence of 10^{13} cm^{-2}(after Weaver et al.[33]).

Energy Loss	2 MeV	15 MeV	40 MeV	100 MeV
IEL(keV/ion)	105	26	12	6
NIEL (eV/ion)	3	0.3	0.1	0.05
Total Ionizing Dose (Rads)	10^7	3.4×10^6	1.6×10^6	8×10^5

The NIEL discussed earlier is used to describe the rate of energy loss due to atomic displacements as a particle traverses the GaN layers. The product of the NIEL and the particle fluence (time-integrated flux) gives the displacement damage energy deposition per unit mass of material. NIEL plays the same role to the displacement damage energy deposition as the stopping power to the TID. The concept of NIEL has been very useful for correlating particle-induced displacement damage effects in semiconductor and optical devices.[125–127] Many studies have successfully demonstrated that the degradation of semiconductor devices upon exposure to radiation fluxes can be linearly correlated to the displacement damage energy, and subsequently to the NIEL deposited in the semiconductor devices. The Monte Carlo code TRIM (Transport of Ions in Matter)/SRIM (Stopping and Range of Ions in Matter) is widely used to obtain information about vacancy production rates.[111] With some manipulation of the output files, TRIM can also be employed to calculate NIEL.[125–127] The TRIM output gives the vacancy production rate as a function of position as the incident proton slows down in the target material. Combining these data with the total energy loss data, the vacancy production rate as a function of proton energy can be found.[111–115] The vacancy concentration can be converted to damage energy using the modified Kinchin-Pease approximation[118] which then yields the NIEL as a function of proton energy. As an example, Table I shows calculated Ionizing and Non-Ionizing Energy Losses and Total Ionizing Dose for protons of different energy in GaN at a fixed fluence of 10^{13} cm^{-2}. Notice how all of these quantities actually decrease at higher energy due to the increased electronic stopping component. This also means that NIEL in the active regions of HEMTs or LEDs is lower for higher ion energies, with a consequently lower amount of device degradation.

In the case of lower ion energies where the particles actually stop in the active region of the device, the projected range Rp is then essentially proportional to the initial incident ion energy. With an amorphous target material, the ion profile follows purely Gaussian stopping distribution, which is related to the projected range Rp, standard deviation ΔRp and implant dose[111]

$$\Phi N(x) = \Phi / \left(\sqrt{2\pi}\Delta R_p\right) / \exp\left[-\left(x - R_p\right)^2 / 2\Delta {R_p}^2\right]$$

The peak concentration $Np = \Phi/\sqrt{2\pi}\Delta Rp$ occurs at Rp, and N(x) $= N_p/\sqrt{e}$ at $x = R_p \pm \Delta R_p$. Considering the single crystal nature of the GaN, the channeling effect must be taken into account. Channeling takes place when implanted ions enter regions between rows of atoms, so that few nuclear collisions occur. In the beginning of the slowing-down process at high energies, the ion is slowed down mainly by electronic stopping, and it moves almost in a straight path. When the ion has slowed down sufficiently, the collisions with nuclei (the nuclear stopping) become more and more probable, finally dominating the slowing down. When atoms of the solid receive significant recoil energies when struck by the ion, they will be removed from their lattice positions, and produce a cascade of further collisions in the material.

Downloaded on 2019-08-31 to IP 128.227.169.164 address. Redistribution subject to ECS terms of use (see ecsdl.org/site/terms_use) unless CC License in place (see abstract).

These collision cascades are the main cause of damage production during ion implantation in semiconductors.

When the energies of all atoms in the system have fallen below the threshold displacement energy, the production of new damage ceases, and the concept of nuclear stopping is no longer meaningful. The total amount of energy deposited by the nuclear collisions to atoms in the materials is called the nuclear deposited energy. Light ions slow down initially primarily by electronic stopping with little displacement damage until eventually nuclear stopping becomes dominant at the end of this range. By contrast, heavy ions undergo a relatively higher degree of nuclear stopping, displacing target atoms right from the surface inwards, producing collision cascades, leading to considerable lattice damage within a small volume. Depending on the ion, the dose, and the implant temperature, the implant damage can consist of either amorphous layers or extended crystalline defects (dislocations and stacking faults). In GaN, damage accumulation and possible amorphization are modeled by either a heterogeneous mechanism, in which individual damage clusters are considered to be amorphous and overlapping of these regions results in complete amorphization (heavy ions), or a homogeneous mechanism in which the crystal becomes unstable and collapses to an amorphous state when the defect density reaches a critical value (light ions). Since ions require certain threshold energy for the production of damage, the maximum of damage distribution is always closer to the surface than that of the ion profile. Note that for a particular ion to completely penetrate a doped semiconductor layer and render it semi-insulating, it is the ion damage profile that is important, not the ion profiles itself. Both the damage profile and dopant profile can be simulated by Monte Carlo calculations of energy deposition given up in atomic stopping processes.

To summarize the above, a successful displacement damage model for GaN devices must account for various experimental observations, including dynamic and injection annealing effects, the role of impurities, differences in carrier removal rates by different types of radiation and the observed scaling of degraded parameters with the nonionizing energy loss in many cases.

Early radiation damage studies included the development of the Gossick cluster model,[112] which has given a qualitative understanding of the functional dependence of displacement damage effects. This was enhanced by the discovery of the correlation of displacement damage with nonionizing energy loss. It must be emphasized that there are still gaps in the understanding of the microstructure of radiation-induced defects and how the type of radiation influences both their stability and production. For example, in Si, the well-known E-centers (vacancy-phosphorus defects) produced by 1-MeV electrons anneal at a significantly lower temperature than those produced by protons. The situation in GaN is at an even more preliminary stage in terms of understanding the main defects created by radiation other than protons.

The nonionizing energy loss rate can be calculated analytically from first principles based on differential cross sections and interaction kinematics. NIEL is that part of the energy introduced by elastic (both Coulombic and nuclear) and nuclear inelastic interactions that produces the initial vacancy-interstitial pairs and phonons (e.g., vibrational energy). NIEL can be calculated for any type of radiation using the following analytic expression that sums the elastic and inelastic contributions: $\mathrm{NIEL} = (\mathrm{N/A})\,[\sigma_e T_c + \sigma_i T_i]$, where σ_e and σ_i are total elastic and inelastic cross sections, respectively, T_e and T_i are elastic and inelastic effective average recoil energies corrected for ionization loss, respectively, N is Avogadro's number, and A is the gram atomic weight of the target material. Note that the units for NIEL, typically MeV-cm^2/g, are the same as those for stopping power or linear energy transfer (LET) that describe energy transfer by ionization and excitation per unit length. Since nuclear stopping power does not involve electronic excitations, NIEL and nuclear stopping can be considered to be the same quantity in the absence of nuclear reactions. The total non-relativistic stopping power is therefore

$$F(E) = F_e(E) + F_n(E)$$

The model given by Ziegler, Biersack and Littmark[111] (the so-called "ZBL" stopping) in the different versions of the TRIM/SRIM codes, is used most often today.

Summary of Radiation Effects in GaN

Harsh environments involving high radiation fluences present a severe challenge for designers of GaN electronic and photonic devices for use in space, critical systems for nuclear reactors, and position sensitive detectors for particle beams and advanced light sources.[5] In space-based applications, the radiation doses encountered are up to 40 Mrad, although in the most extreme conditions envisaged may reach 400–1000 Mrad depending on radiation type.[130–143]

Radiation induced defects within the semiconductor lead to enhanced generation /recombination currents, reduced charge collection signals in detector structures, and a drift in the operating point, to the extent that stable operation is not possible beyond fluences of roughly mid-10^{14} fast hadrons/cm^2 in silicon detector technology.[5]. Newer technologies such as GaN would reduce the need for replacing Si detectors in applications like the CERN Large Hadron Collider (LHC) in which the detectors operate at beam peak luminosities of roughly 10^{35} cm^{-2} s^{-1} and would require replacement of the detectors more than once a year.[5]

For particle tracker applications in accelerators, the requirement for large total radiation length in order to minimize effects of multiple scattering currently limits interest to diamond or SiC. However, for space applications GaN offers the prospect of making high-speed power handling devices that are highly radiation hard.[5] The changes of AlGaN/GaN parameters start at doses far exceeding the ones expected in space applications. The main bulk of experimental device results refers to proton irradiation because of the practical importance of protons of (1–100) MeV for space applications and because high energy protons are convenient when studying the radiation effects on GaN-based heterostructures.[130–133] With neutron irradiation problems with induced radioactivity are a serious concern, while, for gamma-irradiation very high radiation doses have proved to be necessary to observe detectable changes. Electron irradiation has been widely used for defect studies aimed at determining fundamental material characteristics, but has not been so popular in device degradation work.

Proton damage.— With proton irradiation, the main effects in GaN are a reduction in carrier concentration due to trapping into radiation-induced defect levels and a reduction in carrier mobility, while in HEMTs one observes a shift of the threshold voltage toward more positive values, the decrease of the saturation current I_{Dmax} caused by the decrease of the 2DEG density and 2DEG mobility, and the decrease of devices transconductance (gm). Carrier scattering from radiation-induced defects in or near the 2DEG decreases mobility while induced defects elsewhere act as charged traps that screen the 2DEG and decrease the carrier concentration. There is also an increase in gate lag after proton irradiation.[25] Gate-lag can significantly limit the RF performance and long-term reliability of GaN HEMTs and in unirradiated GaN devices is attributed to two mechanisms, namely trapping in the GaN buffer region of the device and trapping at the AlGaN surface. Gate-lag due to surface traps originates from temporary variations in the occupancy of donor traps in the access regions next to the gate. Gate-lag due to bulk traps in the GaN buffer region may also occur due to the trapping of hot electrons generated in the 2DEG under the gate edges. This depletes the 2DEG and causes a reduction in the drain current. The magnitude of the reduction in drain current depends on trap density and distribution, trap energy, and the presence or absence of a passivation layer on the surface. These effects are illustrated by Figures 6–8 for 1.8 MeV proton irradiation at room temperature.[12,17,22,24,27–32]

The rate of parameter changes was found to decrease with increasing the proton energy which correlates with the amount of energy deposited by the given particle into atomic displacements in the AlGaN barrier and the 2DEG region.[33] The normalized drain current

Downloaded on 2019-08-31 to IP 128.227.169.164 address. Redistribution subject to ECS terms of use (see ecsdl.org/site/terms_use) unless CC License in place (see abstract).

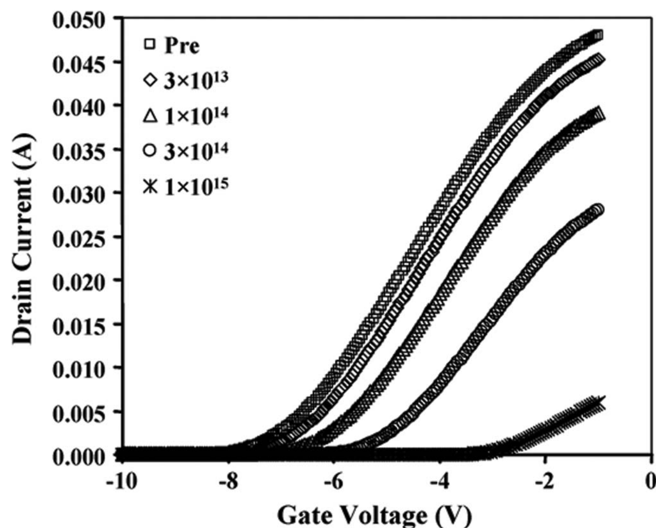

Figure 6. Drain current before and after 1.8 MeV proton irradiation as a function of gate voltage at a drain-source voltage of 2 V in GaN (cap)/AlGaN/AlN/GaN transistors on sapphire (after Karmarkar et al.[22]).

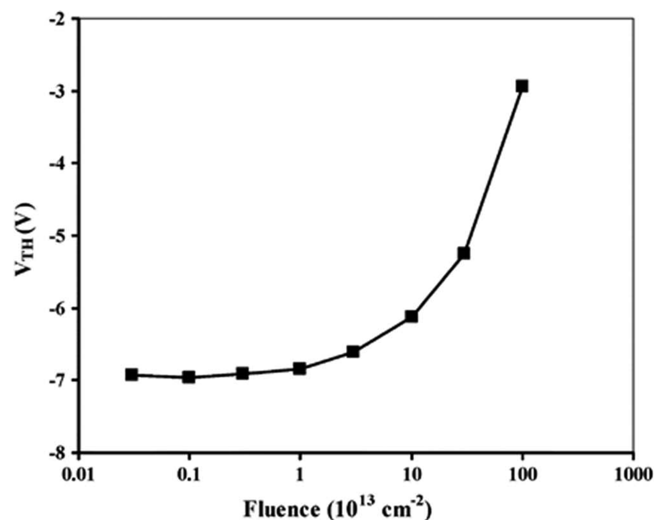

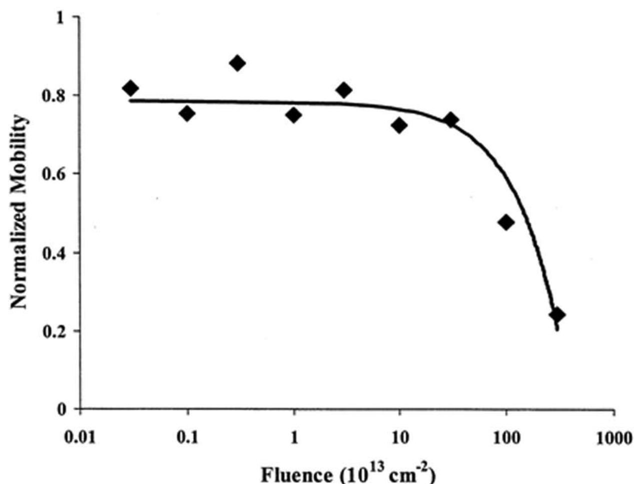

Figure 7. (top)Threshold voltage variations in AlGaN/GaN HEMTs as a function of 1.8 MeV proton fluence (after Karmarkar et al.[22] (bottom) Normalized mobility as a function of 1.8-MeV proton fluence (after X. Hu et al.[28]).

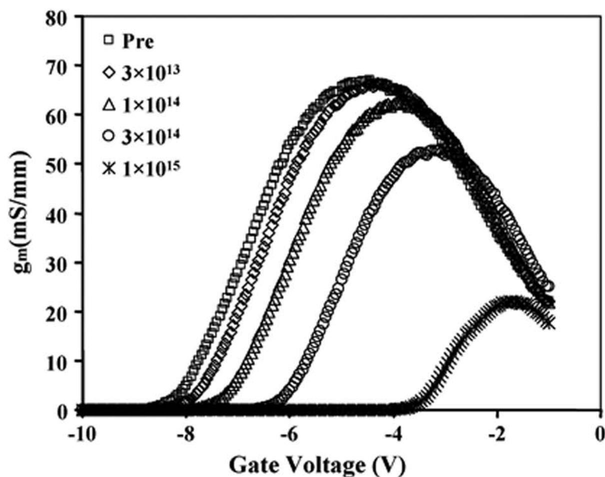

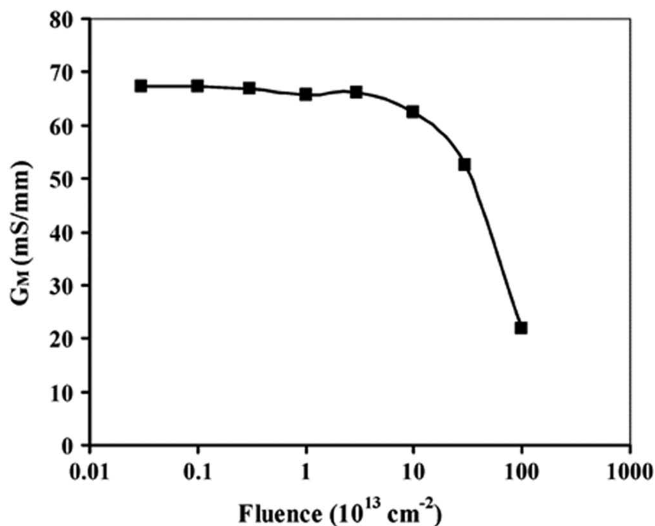

Figure 8. (top) Transconductance-gate voltage curves from AlGaN/GaN HEMTs as a function of 1.8 MeV proton fluence and (bottom) variation of peak transconductance with proton fluence (after Karmarkar et al.[22]).

decreases almost linearly with fluence according to the relation[3]

$$\left[I_{DMax(irradiated)}\right) / I_{DMax(unirradiated)}] = 1 - m\Phi,$$

where $I_{DMax(irradiated)}$ and $I_{DMax(unirradiated)}$ are the drain currents after and before irradiation, respectively, m is a constant with value 1.63×10^{15} cm^2 and Φ is the fluence to which the HEMTs were exposed.[33] Figure 9 shows the decrease in drain current of AlGaN/GaN HEMTs irradiated with protons, electrons, He^+ or C^+ ions over a range of energies and doses.[33] The non-ionizing energy loss varies from 0.03 for 2 MeV protons to 13.4 MeVcm^2/g for 1.5 MeV C^+ ions irradiating the HEMTs, or equivalently, the carbon ions are about 450 times more damaging than the protons at these energies.[33] As expected, the HEMTs exhibit a high radiation tolerance on the order of 100 Megarads and this is independent of the aluminum mole fraction in the AlGaN, which was varied from 0.15 to 0.36 in these experiments.[33]

The role of background impurities in the GaN is also of interest, particularly hydrogen, which is a common component of the precursors used to grow all MOCVD material. We have not seen any effect of hydrogen content on the removal rate of carriers in either proton or electron irradiated GaN when the hydrogen was injected post-growth by exposure to a plasma. However, in material grown by MBE using NH_3-rich conditions, there were differences noted in the rate of positive threshold voltage shift and transconductance of HEMTs upon 1.8 MeV proton irradiation.[30,35,36] The threshold voltage shifts were found to be the highest for N-rich MBE growth,

Downloaded on 2019-08-31 to IP 128.227.169.164 address. Redistribution subject to ECS terms of use (see ecsdl.org/site/terms_use) unless CC License in place (see abstract).

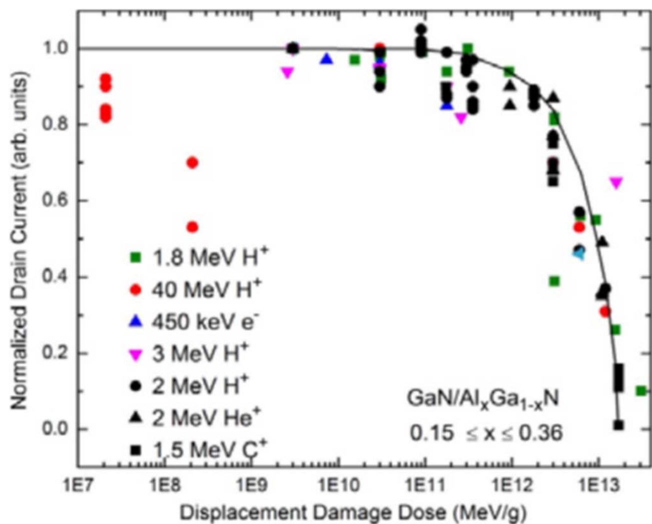

Figure 9. Normalized drain current as a function of calculated displacement damage dose for different AlGaN/GaN HEMTs with Al mole fraction in the AlGaN barrier varying from 0.15 to 0.36, irradiated with different ionizing species at different energies in the range 0.45–40 MeV (after Weaver et al.[33]).

considerably lower for Ga-rich MBE growth, and the lowest for NH_3-MBE and MOCVD growth (both characterized by N-rich conditions and the abundance of hydrogen). In a comparison of HEMTs grown only by MBE under Ga-rich or ammonia –rich conditions, while there was no difference in pinch-off voltage change with proton fluence,[45] there were significant differences in transconductance as shown in Figure 10.[45] The NH_3-rich devices showed lower degrees of degradation in transconductance with increasing proton fluence and the 1/ f noise of the devices increased with increasing fluence. Density functional theory calculations showed that N vacancies and Ga-N divacancies lead to enhanced noise in these devices.[35,37] Density functional theory calculations show these changes were consistent with the reconfiguration and/or dehydrogenation of oxygen-related defects in Ga-rich devices.[45,85]

It is widely accepted that the positive shifts of the threshold voltage are caused by the introduction of negatively charged traps in the AlGaN barrier or in the GaN buffer, while negative shifts are due to the increase of the positive charge in the barrier. Calculations of the defects formation energies and defects concentrations in AlGaN by protons showed that the type of defects formed by irradiation depends on the density and type of starting defects.[98,108,128] If, for example, in the initial state the dominant defects are V_{Ga} acceptors, as it should be for n-type material, particularly under N-rich growth conditions, proton irradiation can transform them into negatively charged nitrogen interstitials Ni and negatively charged V_{Ga}-V_N divacancies (the latter with the −2/−3 charge transition level near E_c-1 eV in AlGaN). The result is the buildup of the negative charge in the barrier and the shift of the threshold voltage to more positive values. Since the ionization level of divacancies is close to the Fermi level in the barrier, one can expect the increase in the low-frequency noise of the devices which indeed is observed.[37,54] The density of V_{Ga} should be higher under the N-rich conditions in MBE and therefore the value of the positive shift in the threshold voltage should be the more pronounced than for MBE growth under Ga-rich conditions. For MOCVD and NH_3-MBE grown HEMTs, additional hydrogen passivation of defects was needed to explain the relatively lower shifts of the threshold voltage.[37,54,98,108] This hydrogenation of defects was proposed as the cause of the negative threshold voltage shifts upon the application of off-state-stress to the HEMTs, with the dominant hydrogenated defects proposed to be C acceptors and nitrogen antisite donors.[37,54,98,108]

GaN Schottky diodes offer a simplified platform to understand the effects of proton damage. Figure 11 shows the normalized carrier concentration in n-GaN diodes as a function of 1.0- and 1.8-MeV proton fluence (top) and Schottky barrier height in these diodes (bottom) as

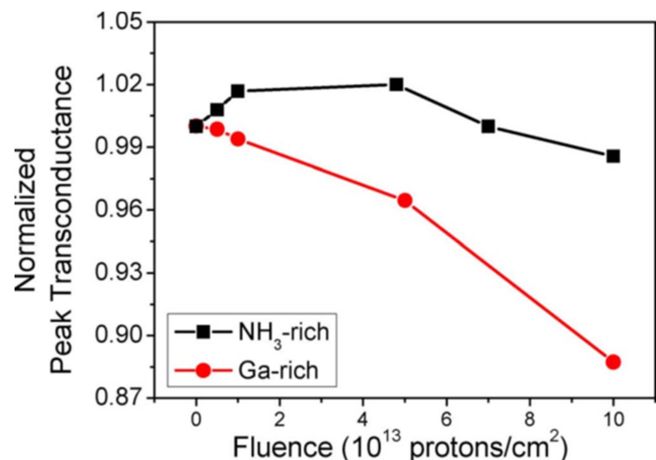

Figure 10. Normalized peak transconductance as a function of 1.8 MeVproton fluence for AlGaN/GaN HEMTs grown under either Ga-rich or ammonia-rich conditions (after J. Chen et al.[45]).

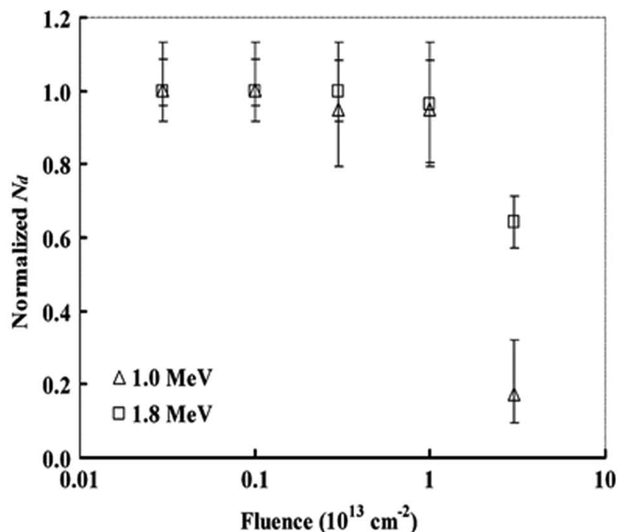

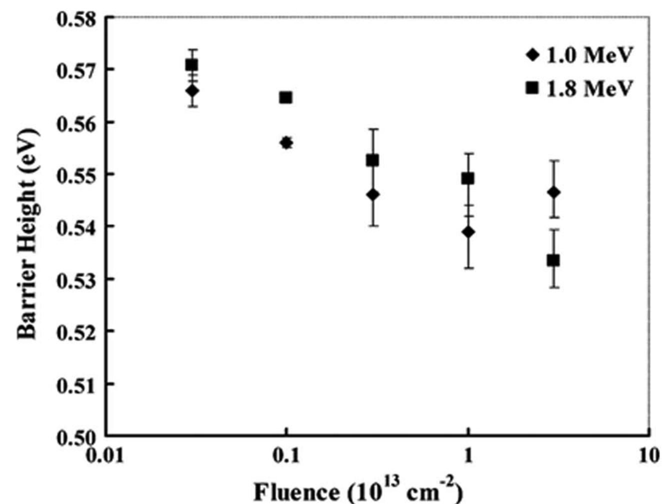

Figure 11. (top) Normalized carrier concentration in n-GaN diodes as a function of 1.0- and 1.8-MeV proton fluence (bottom) Schottky barrier height in n-GaN diodes as a function of proton fluence (after Kamarkar et al.[24]).

Downloaded on 2019-08-31 to IP 128.227.169.164 address. Redistribution subject to ECS terms of use (see ecsdl.org/site/terms_use) unless CC License in place (see abstract).

a function of proton fluence.[24] Note the reduction in carrier density due to trapping of conduction electrons in deep level states created by radiation exposure and the reduction in barrier height.[24]

Electron damage.— Electron irradiation of GaN has been much less studied than proton damage. Electron irradiation with various energies creates 0.16–0.18 eV traps in GaN due to N vacancies with ionization energy of 0.07 eV and a high barrier for capture of electrons. Other traps are tentatively ascribed to Ga vacancy complexes with nitrogen interstitials. These defects can be annealed at ~300°C. Electron irradiation produces strong compensation of the conductivity in GaN/AlGaN multiple quantum wells and introduces interface traps with ionization energies of 100 meV and 190 meV, in addition to a broad band of interface traps closer to the middle of the bandgap, acceptor traps near $E_c-1.1$ eV and hole traps near $E_v+0.9$ eV in the GaN barriers and at the GaN/InGaN interfaces in the QWs. Electron irradiation creates much higher densities of defects than gamma- radiation but lower than protons. Under electron irradiation of HEMT structures, one observes negative-voltage threshold shifts at lower fluences similarly to the case of gamma-radiation, but positive shifts for higher fluences, similarly to the case of protons. The rate of electron irradiation induced parameter changes of the AlN/GaN HEMTs was found to be about an order of magnitude slower than that of AlGaN/GaN HEMTs.[91] This was explained by the much thinner barrier in the AlN case and, hence, the lower energy impacted into lattice defects formation by irradiating electrons in such a barrier. The main effect of electron irradiation of AlGaN/AlN/GaN, AlGaN/GaN, and InAlN/GaN heterojunctions (HJs) grown by MOCVD on sapphire and of AlGaN/GaN heterojunctions grown by MOCVD on Si(111) is the decrease of 2DEG mobility of heterojunctions with consequent increase of the sheet resistivity, while the 2DEG concentration was effected only slightly.[91] The decrease in threshold voltage of AlGaN/GaN/Si HJs and HEMTs can be explained by an increase of the density of deep acceptor traps. DLTS and admittance measurements on AlGaN/GaN/Si HEMTs and admittance spectra measurements on AlGaN/GaN/Si HJs show that the traps involved have activation energies of 0.3, 0.45, 0.55, and 0.8 eV. The radiation tolerance of AlGaN/GaN on Si HEMTs is similar to that of more established AlGaN/GaN and AlGaN/AlN/GaN structures on sapphire, while the radiation tolerance of InAlN/GaN structures is considerably lower.

Gamma ray damage.— Previous reports on the effects of gamma-ray irradiation on GaN, especially device structures, exhibited some conflicting results.[14,15,31,40,42,48,59,61,62,134] In general, HEMTS that are irradiated with gamma rays exhibit negative threshold voltage shifts and in some cases an increase in 2DEG sheet concentration, in contrast to the results for proton-irradiated HEMTs. Compton electrons induced from γ-radiation create electron-hole pairs, thus changing occupancy of traps. Unlike proton irradiation, some studies claim that these defects can improve device performance such as increasing drain saturation current.[59,60] These defects are believed to be nitrogen vacancies that have electrical activation energies about 216 meV from the conduction band. Nitrogen vacancies act as donors and increase the effective channel doping and thus increase drain-source current in HEMTs. These types of defects have been reported after low-energy proton, electron, and γ-irradiation. It was also reported that low dose γ-irradiations partially relaxed the AlGaN/GaN heterostructure elastic strains and enhanced the electron mobility by around 7–8%.[61,62] This improvement of the electron mobility could also increase the drain current.

In contrast to these results, Schwartz et al.[42] showed that the drain current was reduced by about 60% after γ-irradiation at around 700 Gy. These defects in that case must reduce the carrier concentration in the irradiated devices, and there was more degradation with increasing γ-irradiation dose. The defects produced by γ-irradiation may be structure sensitive, which would be one reason for the discrepancies between different reports.[40,42] Also, dose clearly plays a role in the performance of the devices after irradiation. Vintusevich et al.[61] found out that at 10^5 rad, the Ids increased but started to deteriorate

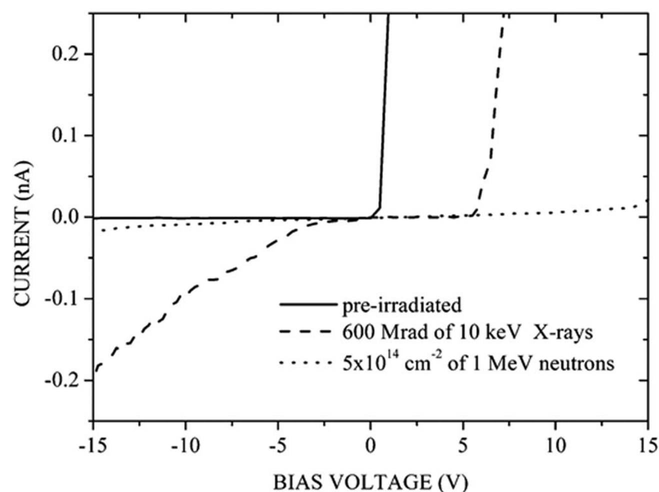

Figure 12. I-V characteristics for epitaxial n- GaN diodes after either X-ray or 1 MeV neutron irradiation (after Rahman et al.[5]).

after higher doses of 10^6 rad. Some of the important factors that could affect the electrical characteristics after the gamma-ray irradiations include the presence of a passivation layer, the metals used in the gate and Ohmic contacts, the native defect density in the barrier and GaN layers, and the gate length and gate width. The passivation layer affects the transport in the channel in HEMTs, and can reduce current fluctuations after irradiation. In some cases, the type of metallization on semiconductors also affects the electrical characteristics under high dose gamma-ray irradiation. Gamma rays can cause reactions at the interface between the metal and semiconductor, resulting in high ideality factors and increased on-state resistance, as well as reordering of native defects and impurities. For ^{60}Co gamma-irradiation with a very high dose of 600 MRad, the threshold voltage shifted to more negative values, the saturation current slightly increased, while the slope of the drain-source I-V characteristics in the linear region markedly decreased signifying a slightly higher 2DEG concentration, but a lower 2DEG mobility.

Neutron damage.— In the study of Rahman et al.,[5] Schottky diode GaN detectors were irradiated with 1 MeV neutrons to fluences of 5 $\times$ 10^{14} cm^{-2} and with 10-keV X-rays to doses of 600 Mrad. Neutrons have a significantly higher damage factor than X-rays and the neutron irradiation reduced charge collection efficiencies values to about 75% whereas the X-ray irradiation had almost no impact on this parameter since the carrier transit times across the depletion region of the detectors remained comparable to the defect capture times. The I-V characteristics in Figure 12 also show only a slight degradation in the reverse characteristics with X-ray irradiation,[5] but the neutron irradiation basically destroyed the diode behavior of the detectors.[5]

In terms of the defects responsible for the positive shift of the threshold voltage of HEMTs after irradiation, the literature suggests that these are the same defects as present in the material rather than new types of defects created during the irradiation. For example, it was shown that neutron and electron irradiations produce defects similar to the defects causing metastabilities and low threshold voltages in AlGaN/GaN, AlGaN/AlN/GaN, and InAlN heterostructures. Neutron irradiation effects were studied for a group of AlGaN/AlN/GaN heterostructures with Al composition in the barrier of 20, 30, 40, and 50%.[94] The neutron irradiation increased the density of the acceptor states in the barrier layers and these acceptors were shown to be the same ones that caused metastable decrease of the threshold voltage upon cooling down at high reverse bias and persistent increase of the threshold voltage after low temperature illumination. The threshold voltages necessary for 2DEG depletion in Ni Schottky diodes fabricated on the heterostructures were found to shift toward more positive values with increasing the neutron fluence in the (1–5) $\times$

Downloaded on 2019-08-31 to IP 128.227.169.164 address. Redistribution subject to ECS terms of use (see ecsdl.org/site/terms_use) unless CC License in place (see abstract).

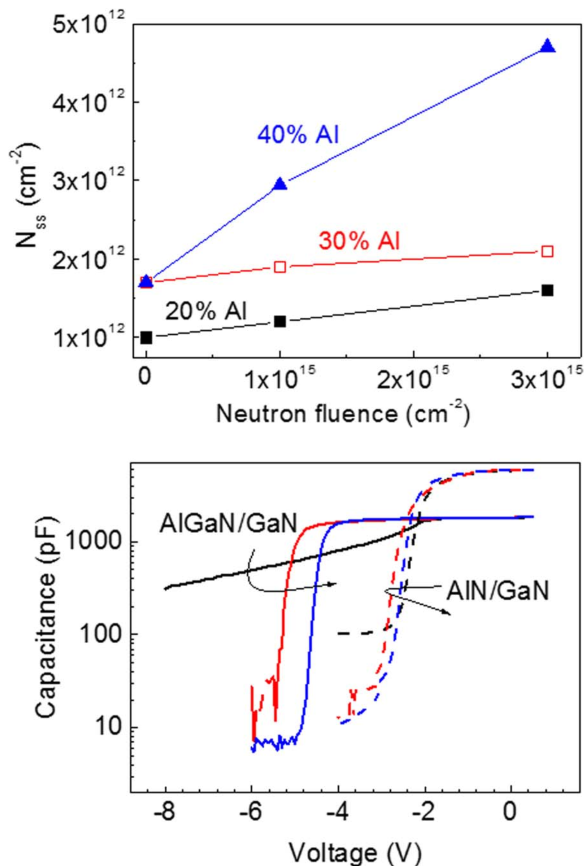

Figure 13. (top) The areal density of deep acceptor traps in the barrier of AlGaN/AlN/GaN heterostructures as a function of neutron fluence, for different Al composition in the AlGaN sub-barrier (bottom) C-V characteristics of AlGaN/GaN (solid lines) and AlN/GaN (dashed lines) measured at 10 kHz before 10 MeV irradiation (black curves) and after irradiation with the fluences of 5×10^{15} cm^{-2} (red curves), and 10^{16} cm^{-2} (blue curves).

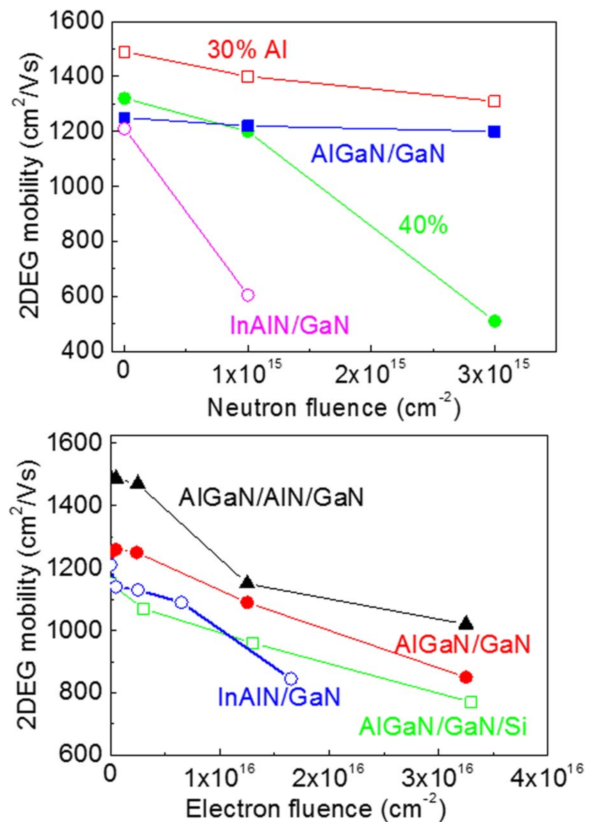

Figure 14. (top) 2DEG electron mobility as a function of neutron fluence for AlGaN/AlN/GaN heterostuctures with Al concentration in the AlGaN barrier of 30% and 40%; also shown are the data for the AlGaN/GaN heterostructures (30% Al) and for InAlN/GaN heterostructures. (bottom) 2DEG electron mobility as a function of10 MeV electrons fluence for AlGaN/AlN/ GaN, AlGaN/GaN, and InAlN/GaN heterostructures grown on sapphire, also shown are the results for AlGaN/GaN/Si heterostructures grown on Si substrate.

10^{15} cm^{-2} range. DLTS and the optical ionization spectra of acceptors before and after irradiation were very similar to these characteristics in the starting films. Thus, it was concluded that the neutron irradiation increases the density of pre-existing barrier traps rather than creates new traps.[94] The trap concentrations at various neutron fluences could be estimated from observed changes of the threshold voltage and increased approximately linearly with the neutron fluence (see Figures 13 and 14). The introduction rate of these acceptors were similar to the introduction rate of compensating acceptors measured for undoped AlGaN single films. The introduction rate of acceptors increased for AlGaN films with high Al composition (40% or higher) for which the starting concentrations of deep barrier acceptor traps were high. Most likely, this increased starting concentration reflected higher density of native defects and impurities (see above). The lower radiation tolerance of these more defective and less pure materials is, however, in line with the results of calculations suggesting that the effective radiation defects formation energies should decrease for material with a higher starting density of defects.[94]

The second effect of neutron irradiation is the decrease of the 2DEG mobility measured by Hall effect.[20,56,135] The characteristic feature of these results was that the mobility started to rapidly decrease at a certain threshold fluence, and the value of this fluence was the lower the higher the starting density of the barrier traps. Simultaneously with the strong decrease of 2DEG mobility measurable decreases of the Schottky diodes capacitance in accumulation are reported. For fluences greatly exceeding the threshold fluence the 2DEG conductivity could no longer be observed. In the sample with the highest Al composition of 50% in the AlGaN barrier and the highest density of deep barrier acceptors this loss of 2DEG mobility occurred after irradiation with the lowest neutron fluence used (10^{15} cm^{-2}). The mobility changes observed were explained in the following way. The Fermi level at the surface of AlGaN/GaN heterostructures is pinned somewhere around Ec−1 eV. Thus, at 0 V surface potential the 2DEG density should be at its maximum at the AlGaN/GaN interface. However, the presence of a high density of deep charged acceptors in the barrier causes local fluctuations of the threshold voltage and hence nonuniform 2DEG concentration and additional scattering that affect the 2DEG mobility.[20,56] The magnitude of the effect is higher for higher density of the barrier acceptors. As the density of these acceptors increases with irradiation the magnitude of the threshold voltage fluctuations increases causing the gradual decrease of mobility. When the magnitude of local fluctuations of the threshold voltage becomes so high that in parts of the structure the voltage locally exceeds the threshold voltage, local areas where no 2DEG is present appear. This results in the current flow in the 2DEG region acquiring the percolation character thus pulling down the effective 2DEG mobility. The Schottky diodes capacitance in accumulation also decreases because only part of the area is occupied by the 2DEG electrons.[135]

The behavior of AlGaN/GaN heterostructures with Al composition of 30% was also compared with the behavior of the AlGaN/AlN/GaN heterostructures for the case of neutron irradiation.[137,140] The presence of deep acceptors causing the same metastability as for the AlGaN/AlN/GaN structures was observed and the characteristics of acceptors as determined by the spectral dependence of the threshold voltage shift and the signatures of defects in reverse DLTS were similar for AlGaN/AlN/GaN and AlGaN/GaN structures. The behavior of mobility with irradiation and the changes of the threshold voltage

Downloaded on 2019-08-31 to IP 128.227.169.164 address. Redistribution subject to ECS terms of use (see ecsdl.org/site/terms_use) unless CC License in place (see abstract).

with neutron fluence were also similar for the same concentration of Al in the barrier indicating that the main event occurred either in the AlGaN barrier or in the GaN buffer, not at the AlN/GaN interface.[137]

For InAlN/GaN heterostructures, the neutron irradiation effects again were similar to those observed in AlGaN/AlN/GaN, AlGaN/GaN heterostructures, but the density of deep compensating acceptors before irradiation was quite high, on the level of AlGaN barriers with high Al mole fraction (3.4×10^{12} cm^{-2} in InAlN versus 1.8×10^{12} cm^{-2} for AlGaN (40% Al) and 3.2×10^{12} cm^{-2} for AlGaN (50% Al)). This could be related to the presence of higher impurity (particularly, oxygen) concentration in InAlN. The starting 2DEG mobility value in InAlN/GaN heterostructures was quite comparable with the 2DEG mobility in AlGaN/GaN structures, but the threshold neutron fluence for the onset of strong mobility degradation was much lower than for AlGaN.[79,140]

Similar effects were observed for AlGaN (30% Al)/GaN/sapphire, AlGaN (30% Al)/AlN/GaN/sapphire, AlGaN (30% Al)/GaN/Si, and InAlN/GaN/sapphire structures grown by MOCVD either on sapphire or Si substrates and irradiated at room temperature with 10 MeV electrons with fluences in the $2 \times 10^{15}-3 \times 10^{16}$ cm^{-2} range.[91,105,132–140] Figure 14 shows the 2DEG mobility evolution with electron irradiation for the studied heterostructures. The positive shifts of the threshold voltage of C-V characteristics and the metastable changes in the threshold voltage upon cooling down and illumination had the same nature as for neutron irradiation. The mobility degradation occurred in a similar fashion for all the AlGaN heterostructures and was not strongly affected by the presence of AlN inset layer or changing of the substrate from sapphire to Si. But, as for the case of neutron irradiation, the decrease of mobility with electron fluence was the fastest for the InAlN/GaN/sapphire heterostructure, obviously, for the same reasons as discussed above for the case of neutrons.[79] Figure 15 shows gate lag measurements on the AlGaN/GaN/Si HEMT before irradiation (top) and gate lag measured on the AlGaN/GaN/Si HEMT after irradiation with 1.3×10^{16} cm^{-2} 10 MeV electrons (bottom).[91] After irradiation the pulsed signal compared to DC signal decreased by about two times pointing to a much more prominent contribution of deep traps. From DLTS and admittance spectra results it seems reasonable to associate this decrease with the increased density of barrier/interface traps with activation energy 0.3, 0.45, 0.55, and 0.8 eV introduced by irradiation.[91]

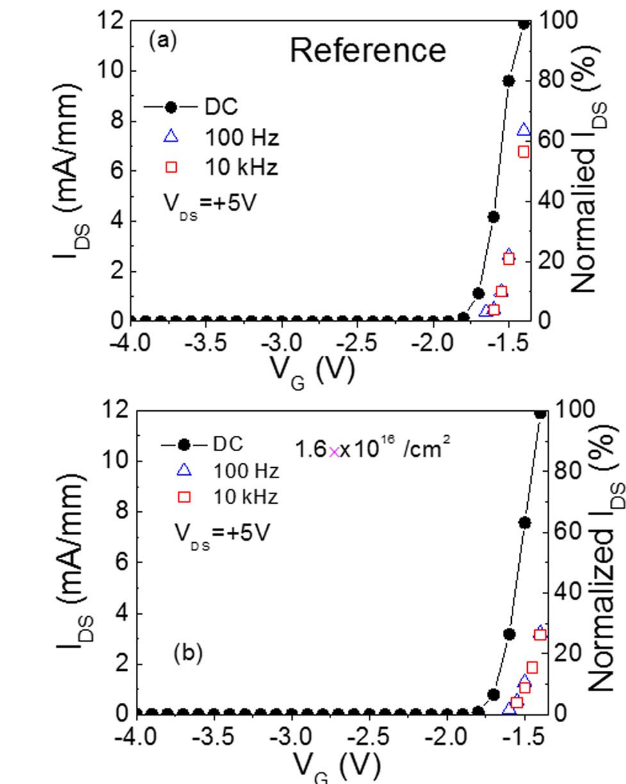

Figure 15. (top) DC and AC measurements of the drain current as a function of gate voltage for the AlGaN/GaN/Si HEMTs before electron irradiation; (bottom) the same after irradiation with 1.3×10^{16} cm^{-2} 10 MeV electrons.

Coming back to the point that radiation exposure increases the concentration of defects already present in the GaN, Figure 16 shows a schematic representation of energy levels in the gap of both n-and p-type GaN before and after proton irradiation.[71,78] Note how many of the defects already present in the material increase after proton irradiation.

Figure 17 provides a summary of the carrier removal rates in n-and p-GaN films, and InAlN/GaN and AlGaN/GaN HEMT structures exposed to proton, electron, neutron or gamma-ray fluences at different energies. The carrier removal rate relates the removal of carriers as deep traps are introduced by the radiation. The carrier removal rate R_c can be related to the radiation fluence, Φ, initial carrier concentration, n_o, and final carrier concentration after irradiation, n, through the equation $n-n_o = R_c\Phi$. These results provide a practical guide for estimating how much degradation will occur in GaN-based materials or devices for a given dose of any of these types of radiation. These are found to be a strong function of initial carrier concentration, dose rate and dislocation density in the material. For example, high dose rates may lead to more extensive defect complexing, or sample self-heating with consequent higher rates of self-annealing of defects. It is important to ensure that carrier removal rates are being measured in a regime in which saturation of the carrier trapping has not already occurred, leading to artificially low extracted carrier removal rates. This will obviously occur at lower doses for lightly doped samples.

Proton irradiation leads to carrier removal rate in proton irradiated n-GaN$\sim 10^2$–10^3 cm^{-1} depending on the proton energy and increases for higher donor concentrations. In p-GaN implanted with 100 keV protons, degradation of luminescent and properties starts at doses $\sim 10^{12}$ cm^{-2}, while decreases in hole concentration were evident for

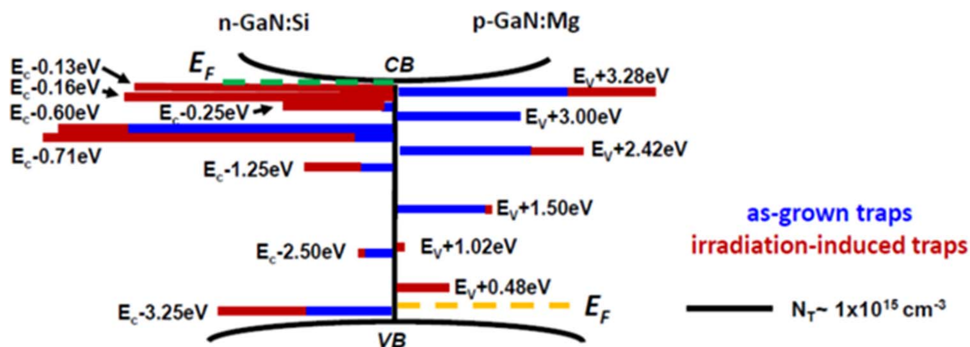

Figure 16. Schematic of position in the bandgap of defects in n- and p-GaN before and after proton irradiation (after Sasikumar et al.[71,78]).

Downloaded on 2019-08-31 to IP 128.227.169.164 address. Redistribution subject to ECS terms of use (see ecsdl.org/site/terms_use) unless CC License in place (see abstract).

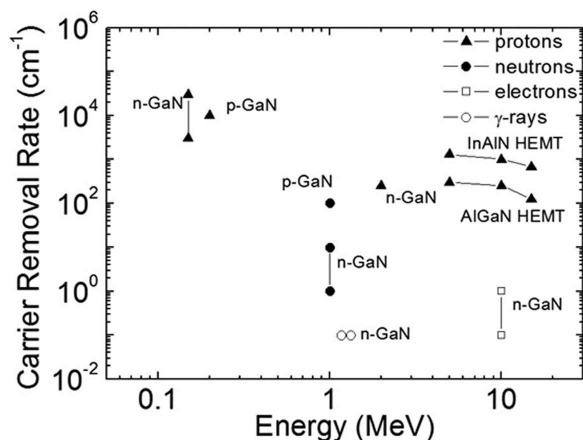

Figure 17. Carrier removal rate in single layer GaN or HEMT structures as a function of energy for different types of radiation.

doses beginning at 10^{13} cm^{-2}.[2,56,57,79] Both threshold doses are more than an order of magnitude lower than in proton implanted n-GaN and may involve complex formation between the radiation defects and Mg acceptors. The main deep centers introduced by proton damage in p-GaN have activation energies 0.3 eV, 0.6 eV and 0.9 eV. It is important to understand the limitations of applying these numbers-if the dose used is high enough to create a trap density that removes all carriers, then obviously any further increase in dose has no effect on carrier removal other than to create hopping conduction. Thus it is imperative that the carrier removal rates be measured at low enough doses or in material with a high enough carrier density that the removal rate scales in a linear fashion with fluence.[56,57] This is one of the reasons that literature values of carrier removal rates for each of the radiation types show a significant variation, even for nominally similar energies and fluences.

Changes in GaN-Based HEMT Performance after Irradiation

Proton damage.— A wide range of studies have been performed on proton damaged HEMTs in different proton energy regimes.[5,12,16,21–25,27–37,42–47,49–58,79] For the high energy protons encountered in space-based applications, AlGaN/GaN HEMTs show decreases in tranconductance (g_m), drain-source current (I_{DS}), shifts in threshold voltage (V_T) and gate current (I_G) after irradiation with 40 MeV protons at doses equivalent to decades in low-earth orbit. These protons create deep electron traps that increase the HEMT channel resistance and decrease carrier mobility. The effects of radiation-induced displacement damage on device properties are usually described using models based on an approximately linear relationship between the calculated NIEL and the damage factor. AlGaN/GaN HEMTs are relatively robust when exposed to particle irradiation due to the high threshold energy, over 20 eV, required for stable defect creation in a perfect crystal. Because of this high threshold energy, they have a much higher threshold for damage.

A number of factors can influence the relationship between NIEL and damage in semiconductor structures.[33,34,42,50] For example, in AlGaN/GaN HEMTs at low proton fluences, the degradation is dominated by changes in device regions other than the two-dimensional electron gas (2DEG), such as the electrical contacts, while at higher fluences, displacement damage in the region of the 2DEG and surrounding layers becomes a more significant contributing factor. In the case of high-fluence proton irradiation (at an energy of 1.8 MeV), the vast majority of recoil atoms have energy less than 20 eV. However, theoretical studies of atomic recoils in GaN using classical molecular dynamics indicate that average displacement threshold energies are 45 eV and 100 eV for Ga and N atoms, respectively. These high average displacement thresholds suggest that post-irradiation material degradation is difficult to explain solely by the displacement of atoms in a perfect crystal lattice, since the average recoil energy is significantly less than the threshold energy for atomic displacement, and because high-energy transfer collision events are relatively rare. The calculations suggest that, while low energy recoils do not create defects in a perfect lattice, these particles can interact with pre-existing defects, formed during processing, and with radiation-generated defect complexes in the end-of-track regions.[29,36,107,108] The end-of-track regions have high concentrations of vacancies. Threshold-voltage shifts and increases in 1/f noise are observed in proton-irradiated AlGaN/GaN high-electron-mobility transistors, indicating defect-mediated device degradation.

In AlGaN/GaN HEMTs, the drain-source currents decreased 15–20% for irradiation with 40 MeV protons at a dose of 5×10^9 cm^{-2} and 30–50% decrease at a dose of 5×10^{10} cm^{-2}.[32] Post-irradiation annealing at 300°C restored 70% of initial gm and Ids in such HEMTs receiving doses of 5×10^{10} cm^{-2}. For proton-irradiation at 1.8 MeV, both AlGaN/GaN and AlGaN/AlN/GaN HEMTs showed significant degradation, around 40% drain current reduction,[22,24] after the devices were exposed to protons at a dose of 10^{14} cm^{-2}. Sasikumar et al.[71] have identified two main levels as being responsible for the threshold voltage shifts in irradiated AlGaN/GaN HEMTs, namely at $E_C-0.3.25$ eV and at $E_C-0.1.25$ eV. The latter is possibly the nitrogen interstitial defect, while the former is not firmly identified.

The functional dependence of HEMT degradation on proton energy is interesting because of the fact that the active layers of the device are so close to the surface.[86,106,131] For this reason, higher energy protons actually create less displacement damage or non-ionizing energy loss in the active regions and create less degradation of the HEMT electrical performance. For example, drain-source current- voltage (I_{DS}-V_{DS}) characteristics at various gate-source voltage (V_{GS}) obtained before and after irradiation at various proton energies (5, 10 and 15 MeV) at a fixed dose 5×10^{15} cm^{-2} shown in Figure 18 display more degradation of current at lower energies because of the higher NIEL.[86,106,131] The change of knee voltage was nominal after proton irradiation. The reduction of the drain current level was observed from all of the proton–irradiated AlGaN/GaN HEMTs. As expected from SRIM results, there was less damage from higher proton energies since most protons will penetrate the samples including the shallow two dimensional electron gas (2DEG) layer and cause less damage. The drain-source voltage at 6 V and zero gate voltage was reduced by 9% for 15 MeV irradiation, 15% for 10 MeV irradiation and 47% for 5 MeV irradiation.

Chen et al.[45] have reported that degradation due to proton irradiation has a more measurable impact on the RF performance in comparison to the DC performance. In particular, gate lag and increases in both channel resistance and device capacitance due to fast bulk and surface traps contribute more notably to RF degradation than to DC degradation.[45]

Similar effects have been reported for InAlN/GaN HEMTs.[51] Displacement-damage induced degradation was studied for proton fluences from 10^{14} p/cm^2 to 4×10^{14} p/cm^2, at 3 MeV. As is usual, a positive V_{TH} shift and an increase of the on-state resistance (R_{ON}) that followed a linear trend with the proton radiation fluence was observed. Increases of both the diode gate current and current collapse also accompanied the degradation of drain-source current.

Electron damage.— For 10 MeV electron irradiation of HEMTs, the observed carrier removal rates are lower than for protons of comparable energy.[56,57] The 50% degradation of the 2 DEG conductivity happens at several times higher doses (close to 3×10^{16} cm^{-2} versus 6.5×10^{15} cm^{-2}) for AlN/GaN than for AlGaN/GaN structures, while an even lower fluence of 1.3×10^{16} cm^{-2} was needed for InAlN/GaN HEMTs, in line with previous observations for neutron irradiated heterojunctions.[79] The shift of C-V characteristics was due to an increased concentration of deep acceptor traps in the barrier/interface region. In AlGaN/GaN/Si transistors there an increase in concentration of deep barrier/interface traps with activation energy of 0.3 eV and 0.55 eV. This increase in trap density correlates with an increase in gate lag of HEMTs after electron irradiation. Electron irradiation at

Downloaded on 2019-08-31 to IP 128.227.169.164 address. Redistribution subject to ECS terms of use (see ecsdl.org/site/terms_use) unless CC License in place (see abstract).

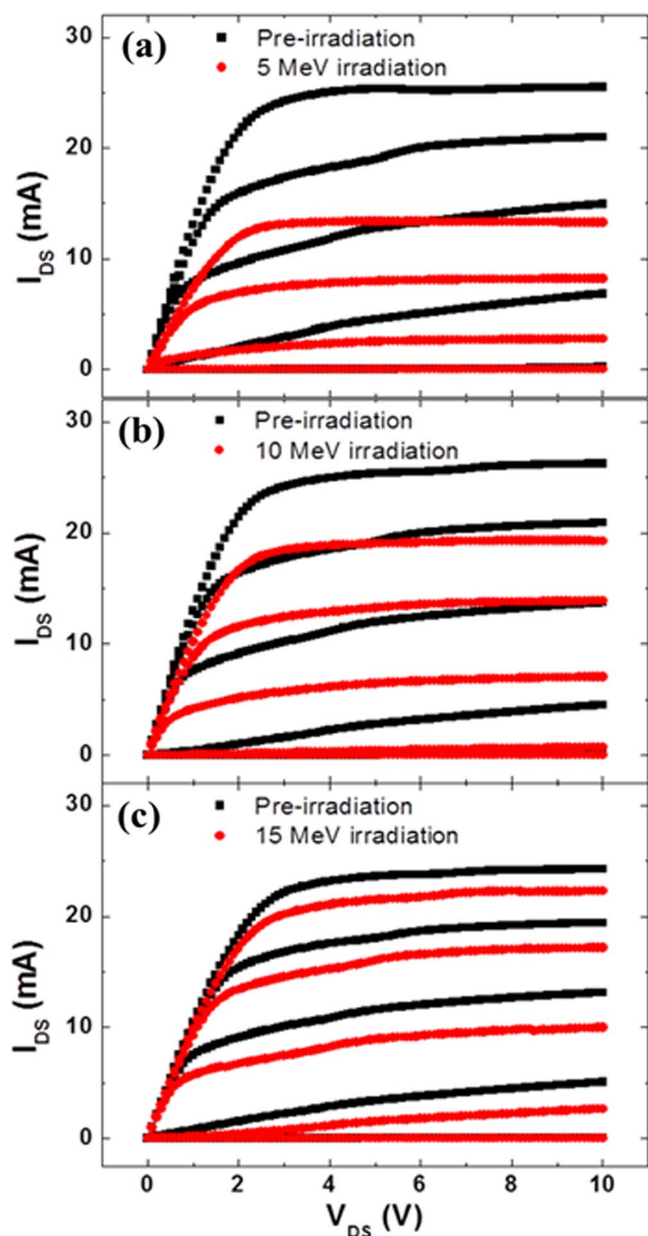

Figure 18. I_{DS}-V_{DS} before and after proton irradiation at energies of (a) 5 MeV (b) 10 MeV (c) 15 MeV. The dose was fixed at 5×10^{15} cm^{-2}, while $V_{GS} = 0$ V ~ -4 V.

an energy of 10 MeV of n-GaN grown by both MOCVD and ELOG led to compensation of n-type conductivity and carrier removal rate increased substantially with starting donor concentration. The main compensating defect created was an electron trap at EC$-$0.15 eV. Once the dose is high enough and the Fermi level crossed this level, two centers at 0.2 eV and 1 eV contribute to compensation. After very high doses, the Fermi level in moderately doped GaN is pinned near Ec$-$1 eV, which again appears to be due to the nitrogen interstitial. The carrier removal rate in ELOG n-GaN was lower than MOCVD samples with similar doping levels. As with proton irradiation, AlN/GaN heterostructures were more resistant to electron irradiation damage hard than AlGaN/GaN or InAlN/GaN.

Experiments on the amount of trapping introduced in high-power AlGaN/GaN/Si HEMTs by electron irradiation show the changes in the gate lag produced by irradiation with electron fluence of 1.3×10^{16} cm^{-3}.[2,56,57] The difference between the drain-source current I_{DS} measured as a function of gate voltage V_G at DC and AC conditions was taken as a measure of gate lag magnitude (the measurements were done at the drain-source voltage of 5 V and the pulsing frequency in AC of 100 Hz and 10 kHz). The AC current in accumulation constituted about 60% of the DC current before irradiation, but only about 30% after irradiation. Electron irradiation introduced a high concentration of electron traps with activation energies 0.17, 0.3, 0.45 eV not observed in this particular transistor before irradiation. It also measurably increased the density of electron traps with activation energies 0.55 eV and 0.8 eV detected before irradiation.

Neutron damage.— For fast neutrons which create large recoil cascades, carrier removal in HEMTs is by disordered regions in which the Fermi level in the core is pinned between the Ga interstitial donor level and the N interstitial acceptor level,[132–140] ie between $E_C-0.8$ eV and $E_C-1.0$ eV, surrounded by a space charge region with a high potential barrier for electrons. Carrier removal rate is experimentally found to be related to the threading dislocation distribution. The major electron traps created have levels at $E_C-0.45$ eV, 0.85 eV (Ga_I^{++}), E_C-1 eV (N_I^-). The carrier removal rate is found to be the sum of contributions from these disordered regions and from traps whose introduction rate increases with doping and decreases in the order MOCVD/ELOG/ HVPE GaN.[56,57]

Recent experiments using Electron Paramagnetic Resonance (EPR) have found strong evidence of a nitrogen sublattice defect produced with high introduction rates in GaN created by proton, electron or ion irradiation at room temperature.[70] The defect configuration is actually that of a $(N\text{-}N)_N$ split interstitial which is electrically active and pins the Fermi level at $E_C-1.0$ eV below the conduction band. This N split interstitial is removed by annealing at 400°C. As pointed out above, this defect must be considered along with the N vacancy donors, N interstitial acceptors, and Ga vacancy acceptors. The new experimental data suggest the N split interstitial is ambipolar, i.e., a deep acceptor defect with a level at Ec$-$1:0 eV in n-type material and a deep donor in p-type material. As its introduction rate is close to the theoretical value for primary N interstitials, the transformation in the split interstitial is apparently complete in n-type and semi insulating.[70]

Gamma ray damage.— AlGaN/GaN HEMTs irradiated with 60 Co gamma-ray doses up to 600 Mrad of ^{60}Co γ-rays showed an increase in reverse breakdown voltage (V_{RB}) by a factor of two, a negative shift in V_T and a decrease in gm by 25%.[96,103] These results are consistent with the gamma-irradiation causing a decrease in the effective channel doping through introduction of deep electron traps. The irradiated devices were annealed at 200°C for 25 minutes and these HEMTs showed partial recovery of device performance. The impact of irradiation and annealing on minority carrier diffusion length and activation energy were monitored through the use of the Electron Beam Induced Current (EBIC). The level of recovery of gamma irradiated devices after annealing treatment depended on the dose of irradiation. Recovery of devices was evident from the significant increase in the diffusion length after annealing. Gamma-irradiation induced nitrogen vacancy defects created additional traps in AlGaN/GaN HEMTs, which decrease the carrier concentration and mobility and increase the activation energy related to carrier recombination. These defects act as scattering centers which result in degradation of both device performance and reliability.[96,103] After annealing the device at 200 °C, the defects were reduced, resulting in an increase of both diffusion length and performance.

Deep states in irradiated HEMTs.— In many cases one observes similar defects upon electrical stressing of HEMTs and LEDs with the changes induced by high energy particle irradiation, and many of these are already present in the material and their concentration increases with radiation fluence.[2,136–154] The majority of deep electron traps in GaN are most likely dislocation-related and that probably explains the prominent role of dislocations in the trapping, gate leakage, subthreshold current leakage, and degradation in AlGaN/GaN HEMTs. The gate leakage in AlGaN/GaN HEMTs seems to be promoted by open-core screw dislocations and, in InAlN/GaN

Downloaded on 2019-08-31 to IP 128.227.169.164 address. Redistribution subject to ECS terms of use (see ecsdl.org/site/terms_use) unless CC License in place (see abstract).

HEMTs, by dislocations decorated by In. Some major hole traps in n-GaN and n-AlGaN are most likely related to gallium vacancies complexes with Si or oxygen and to C.[2]

To give an example of the defects observed in HEMTs after proton irradiation, 3 MeV proton irradiation of AlGaN/GaN HEMTs prepared on SiC substrates with a fluence of 10^{14} cm^{-2} caused a marked increase of the trapping impact on drain current was observed with pulsed measurements. The time-domain analysis of the transients produced two distinct peaks E2 and E4 corresponding to the centers responsible for the gate and drain-lag phenomena. The density of both traps increased after proton irradiation. Measurement of the effect at various temperatures gave the activation energies and the capture cross sections of the E2 and E4 electron traps as 0.6 eV, 3.9×10^{-15} cm^2 (E2) and 0.8 eV, 4×10^{-15} cm^2 (E4). The results are very similar to those observed in electron irradiation of AlGaN/GaN/Si HEMTs, and the E2 and E4 traps parameters are very reasonably close to the ETB4 and ETB5 electron traps parameters determined in DLTS measurements on AlGaN/GaN/Si HEMTs. Both types of traps increase in concentration under high energy particle bombardment. The E2 and E4 traps are believed to be located in the region below the gate which seems to be in agreement with conclusions of DLTS-based measurements. The E2 (ETB4) traps role in changing the trapping in AC transistor parameters and their degradation with electrical stressing has already been discussed in the previous section, where the traps in question were assigned to defects in the GaN buffer at the AlGaN/GaN interface.

The changes in the threshold voltage and in the channel mobility of AlGaN/GaN transistors can be to some extent explained by the introduction of deep acceptors in the barrier layer of the structures. However, deep traps are also introduced in the GaN buffer layer of HEMTs and can lead to similar effects. Thus, modeling of proton damage in AlGaN/GaN HEMTs based on assuming the introduction of deep traps contributing to partial 2DEG depletion and to 2DEG electrons scattering was successful in predicting the devices performance with radiation. These studies are very important, particularly for understanding the nature of current collapse in various AlGaN/GaN HEMTs structures and more research is definitely necessary on that front.

Deep traps contribution to the AlGaN/GaN HEMTs degradation after bombardment with high energy particles is important, but not the sole problem that may occur in devices subject to radiation fluxes. Issues such as changes in surface passivation and Schottky and Ohmic contacts performance are also factors. For example, it has been shown that SiN passivation of the surface of the AlGaN/GaN HEMTs seriously improves the tolerance to the ^{60}Co gamma-irradiation, dielectric passivation was also observed to be beneficial in proton irradiated HEMTs.[144] For the proton fluences used, the defects in the passivating dielectric were not causing new problems. Radiation induced variations in Schottky diodes quality can seriously impact the trapping phenomena via changing the reverse current leakage. The general trend seems to be that low radiation doses adversely affect the reverse current, while high doses decrease it.

Proton irradiation decreases the doping concentration and increases the ideality factor and series resistance, but has little effect on the Schottky barrier height in n-GaN Schottky diodes. Comparison between Schottky diodes and high electron-mobility transistors suggests that the degradation in both types of devices is predominantly due to carrier removal and mobility degradation caused by radiation-induced defect centers in the crystal lattice, with interface disorder playing a relatively insignificant part in overall device degradation.[145–155]

In summary, the main effects of radiation damage in GaN-based HEMTs can be noted as follows:

1. Total dose proton and electron damage leads to decreases in drain current, mobility, transconductance, positive threshold voltage shifts and an increase in gate lag and 1/f noise in the devices. This occurs by introducing trap states that remove carriers and degrade mobility.
2. Degradation due to proton irradiation has a more measurable impact on the RF performance in comparison to the DC performance. Gate lag and increases in both channel resistance and device capacitance due to fast bulk and surface traps contribute more notably to RF degradation than to DC degradation. The amount of degradation scales with dose and is dependent on the growth technique for the component epitaxial layers which influences the dislocation density and distribution and the concentration of background impurities. Ga-polar GaN grown MOCVD appears more radiation hard than N-polar GaN, while growth by MBE under NH_3-rich or Ga-rich conditions subtly affects the noise and transconductance performance after irradiation.
3. The carrier removal rates are a function of initial carrier concentration, dose and dose rate but not of hydrogen concentration in the nitride material grown by Metal Organic Chemical Vapor Deposition.
4. Neutron irradiation created more extended damage regions and at high doses leads to Fermi level pinning while 60Co γ-ray irradiation leads to much smaller changes in HEMT drain current relative to the other forms of radiation.
5. The carrier removal rate by protons, electrons and neutrons in nitride heterostructures increases in the following sequence AlN/GaN> AlGaN/GaN> InAlN/GaN. This is consistent with their average bond strengths.

Annealing of Radiation Damaged HEMTs

The negative effects of displacement damage can be improved by a process of thermal annealing at room temperature or at elevated temperatures. In some cases there is a significant recovery of device characteristics after storage for several weeks at room temperature. Cai et al.[30] showed that a rapid thermal anneal (RTA) at 800°C removes most of the defects created by 1.8 MeV proton irradiation at doses of 1014 cm^{-2} and drastically improved the device performance post-irradiation. Annealing of defects introduced in single layers of n-GaN by 2 MeV protons or 0.2–2.4 MeV electrons showed that some of the defects started annealing around 250°C and was complete by 350°C.[2,145,146] Electron traps associated with N interstitials annealed out at 380°C.[70,145,146] The Ga interstitial-related deep donors started annealing even at room temperature, while the 1 eV Ga vacancy states were stable up to 500°C.[2] When the proton or electron doses are increased or neutrons are used for the irradiation and the density of defects is increased, the thermal stability of radiation damage becomes higher.[2] For example, in n-GaN irradiated with high doses of protons, the bandedge luminescence intensity could not be restored even after annealing at 800°C. Similarly, the evolution of the sheet resistivity of n- GaN irradiated with fast and thermal neutrons to high fluences ($\sim 10^{17}$ cm^{-2}) showed a number of recovery stages. The as-irradiated resistivity decreased at the 150–250°C stage, increased strongly from 250–450°C and then gradually decreased in a broad stage between 500–1000°C.[57] The first stage corresponds to reconstruction of common deep acceptors which explains the decrease in resistivity. The reverse annealing stage at 250–450°C is most likely due to movement of the N_i, Ga_i centers forming new deep compensating centers. The onset of the third stage of recovery at 500°C correlates with the V_{Ga} acceptors annealing stage which explains the decrease of the resistivity. The Fermi level was pinned at deep centers with activation energy 0.45 eV. The most prominent electron traps were at 0.9 eV and 1 eV, likely related to the Ga_i donors and the N_i acceptors, but with a high binding energy, possibly trapped within disordered regions.[2,57] After 1000°C annealing the Fermi level was pinned near Ec–0.2 eV and DLTS spectra were dominated by the 0.6 eV and 0.9 eV traps in high concentration. The total concentrations of the 0.45 eV traps pinning the Fermi level after 800°C annealing and of the 0.2 eV traps dominant in the 1000°C annealing are close to each other and equal to the number of donor Ge atoms converted from Ga by interaction with thermal neutrons (2×10^{16} cm^{-3}). Hence, these relatively deep traps could be complexes of radiation defects with donor atoms. Even after moderate neutron doses, removal of the disordered regions was incomplete and the initial conductivity was not restored.[2,57]

Downloaded on 2019-08-31 to IP 128.227.169.164 address. Redistribution subject to ECS terms of use (see ecsdl.org/site/terms_use) unless CC License in place (see abstract).

For very high neutron fluences the resistivity of GaN passes through a maximum related to the onset of hopping conductivity. The activation energy for the temperature dependence of resistivity for doses before the maximum resistivity showed the usual value of 0.9-1 eV. After a fluence corresponding to maximum resistivity, the temperature dependence was weaker and annealing showed a strong reverse annealing stage up to 300°C where the density of radiation defects decreased and the activation energy returned to the 0.9 eV value. Complete recovery could not be attained even after annealing at 1000°C.[2,57]

For AlGaN/GaN HEMTs irradiated with 40 MeV protons at doses equivalent to decades in low-earth orbit, post-irradiation annealing at 300°C restored 70% of initial gm and I_{DS} in HEMTs receiving doses of 5×10^{10} cm^{-2}. In AlN/GaN HEMTs irradiated with 5 MeV protons at fluences from 2×10^{11} to 2×10^{15} protons/cm^2, there was less degradation in drain current as a result of the more radiation-hard heterostructure compared to AlGaN/GaN. Annealing of these devices at 250–350°C from 5 minutes to 3 hours showed that the forward and reverse gate current decreased 10% under these conditions, moving back toward their pre-irradiation values, but there was no obvious drain current improvement obtained.[32,131] Proton irradiation of Sc_2O_3/GaN and Sc_2O_3/MgO/GaN MOS diodes at two energies, 10 and 40 MeV, and total fluences of 5×10^9 cm^{-2} caused a decrease in forward breakdown voltage and a flatband voltage shift in the capacitance-voltage characteristics, indicating a change in fixed oxide charge and damage to the dielectric. The interface state densities after irradiation increased from 5.9×10^{11} cm^{-2} to 1.03×10^{12} cm^{-2} in Sc_2O_3/GaN diodes and from 2.33×10^{11} to 5.3×10^{11} cm^{-2} in Sc_2O_3/MgO/ GaN diodes. Post-annealing at 400°C in forming gas recovered most of the original characteristics but did increase the oxide/GaN interfacial roughness.[32,131,156] These results were not dependent on the proton energy, but the radiation did enhance roughening of the interface compared to unirradiated diodes annealed in the same fashion, where no significant change in interface roughness was observed until annealing at 800°C.

Defects in GaN before Irradiation

Native defects are present in high concentrations in GaN and strongly influence its electrical and optical properties and as summarized for heterostructures in Table II.[2] They are often formed as compensation sources when dopants are introduced, or as a result of nonstoichiometric growth or annealing. Additional sources of contamination include the gas precursors for crystal growth. The isolated native defects are Ga or N vacancies, interstitials, and antisites (ie. GaN or N^{Ga}) but these may interact or form combinations with impurities or dopants to form more complex defects. Both types of vacancies (V_{Ga} and V_N) in GaN are multiply charged defects with several energy levels in the gap.[2] Some studies indicate that the gallium vacancy is the most common native defect in n-type material, while the nitrogen vacancy is the most common in p -type GaN. Due to their larger formation energies, self-interstitials and antisites are less likely to be present in as-grown material.[82–84] There is a strong tendency to self-compensation in nitrides and thus acceptors such as gallium vacancies are favored in n-type material, with donors such as nitrogen vacancies in p-type material.[82] Undoped GaN is usually n-type due to the presence of common impurities such as silicon or oxygen as well as nitrogen vacancies. Based on energetics, the main defects in p-type GaN are predicted theoretically to be V_N, V_{Ga} and N_I, while in n-type material, the most common defects are predicted to be V_N, GaN, Ga_I and V_{Ga}.[82–84]

The structure of most intrinsic defects in GaN is still not well established with the exception of the Ga interstitial, the Ga monovacancy[70] and the N split interstitial.[70,83] Based on simulations, a model for the N split-interstitial defects was proposed as the stable configuration of

Table II. Trap parameters detected from deep traps studies on AlGaN/GaN heterostructures (adapted from Ref. 2).

Trap name	Type (e, n)	E_a (eV), E_c-E_d for e-traps; E_v+E_a for h-traps	σ (cm^2)	Comments
E1	e	0.6	6.8×10^{-15}	DLTS, ODLTS, buffer/interface
E2	e	0.59	3.3×10^{-13}	DLTS, ODLTS, buffer/interface
E3	e	0.7	3×10^{-15}	DLTS, ODLTS, buffer/interface
E4	e	0.33	1.3×10^{-15}	DLTS, ODLTS, buffer/interface
H1	p	1.1	4.2×10^{-12}	ODLTS, barrier
H2	p	0.41	2.3×10^{-15}	ODLTS, barrier
H3	p	0.28	2.3×10^{-16}	ODLTS, barrier
E1	e	0.6	1.8×10^{-16}	PICTS, buffer
H1	p?	0.82	7.8×10^{-15}	PICTS, buffer
A_1	e	1	2×10^{-12}	DLTS, buffer, defect on dislocation
A_2	e	1.2		DLTS, buffer, N_i defect on dislocation?
A_3	e	1.3		DLTS, buffer, defect on dislocation, high C in the buffer
A_x	e	0.9		DLTS, buffer, defect on dislocation, low C in the buffer
H_1**	p	1.24	5×10^{-12}	DLTS, barrier, low C in the buffer
H_2**	p	1.3		DLTS, barrier, high C in the buffer
A	e	0.15	8.9×10^{-19}	DLTS, buffer/interface
B	e	0.21	1.1×10^{-18}	DLTS, buffer/interface
C	e	0.12	1.8×10^{-18}	DLTS
D	e	0.42	1.3×10^{-19}	DLTS
E	e	0.49	2.4×10^{-14}	DLTS
F	e	0.94	1.1×10^{-12}	DLTS
E1	e	0.3	3.6×10^{-19}	DLTS, buffer
Hx	p	0.82	2.9×10^{-14}	DLTS
ETB1	e	0.15	5×10^{-18}	admittance, barrier
ETB2	e	0.29	1.6×10^{-13}	admittance, barrier
ETB3	e	0.4	6×10^{-15}	admittance, barrier
ETS1	e	0.18	3×10^{-15}	admittance, buffer
ETS2	e	0.27	4.9×10^{-13}	admittance, buffer
ETS3	e	0.45	3×10^{-13}	admittance, buffer

Downloaded on 2019-08-31 to IP 128.227.169.164 address. Redistribution subject to ECS terms of use (see ecsdl.org/site/terms_use) unless CC License in place (see abstract).

the N interstitial, and only recently has experimental evidence for this defect been reported.[70]

The gallium vacancy is an acceptor with relatively low formation energy in n -type GaN and compensates the n-type conductivity.[2,82–84] In n -type GaN the Ga vacancy is filled with electrons, and capture of holes during optical injection may lead to radiative transitions of electrons from the conduction band or from a shallow donor to the negatively charged Ga vacancies. These vacancies can easily migrate even at low temperatures and form stable defect complexes.[2] The nitrogen vacancy was long suspected to be responsible for the majority of the native n-type conductivity in GaN to be close to or inside the conduction band, but the concentration of the these vacancies likely depends heavily on growth conditions.[2,82] The energy level of nitrogen vacancies is reported to be between 0.06–0.13 eV and it is widely accepted that this defect also migrates easily in GaN to form stable defect complexes.[83,84] However, these probably do not include divacancies such as ($V_{Ga}V_N$) because of the predicted high formation energy. This defect would be a double acceptor in n -type GaN and a double donor in p-type GaN. Similarly, antisite defects should have a fairly low probability of formation in as-grown crystals because of the large size mismatch between Ga and N atoms.[82]

Ga interstitials are also expected to be present only at low concentrations in most as-grown GaN layers because of the high formation energy, but we should point out that during exposure to radiation fluxes, the formation may be significant. Ga_I is a double donor with an energy level in the gap at around E_C-0.8 eV. Chow et al.[63,64,84] reported the observation of mobile Ga_I in irradiated GaN below room temperature and this high mobility suggests it likely becomes trapped by other defects and is not present as an isolated defect in as-grown layers under equilibrium conditions.

Similarly, the nitrogen interstitial has a high formation energy in as-grown material and may exhibit a number of charge states in the gap.[2,70] The singly ionized interstitial is an acceptor in n-type GaN with an energy level at around $E_C-1.0$ eV and will compensate the n-type doping.[2,70,83] The migration barrier has been calculated to be low ($\sim$1.5 eV) and therefore diffusion of the nitrogen interstitials will occur even near room temperature.[70,83] Recent experimental reports using a combination of electron paramagnetic resonance, density functional theory, and positron annihilation spectroscopy (PAS) have identified the stable nitrogen interstitial defect in irradiated GaN.[70] As expected, the isolated interstitial is unstable and transforms into a split interstitial configuration $(N\text{-}N)_N$. It is generated by particle irradiation with an introduction rate of a primary defect, pinning the Fermi level at the expected value of $E_C-1.0$ eV for high fluences, and anneals out at 400°C.[70] The associated defect, the nitrogen vacancy, was observed by PAS only in the initial stage of irradiation.[70]

Antisite defects on both the Ga and N sub-lattice may also be present. From theoretical considerations, the gallium antisite (GaN) is suggested to produce a level at $E_V + 0.9$ and may be a significant contributor to compensation in p-type material. The nitrogen antisite (N_{Ga}) can behave as a compensating double donor in p -type GaN or an acceptor in n -type GaN but the formation energy is expected to be high.[2,81–84]

In addition to native point defects, impurities may be present in the as-grown GaN as contamination from precursor gases or the growth reactor itself. The donor impurities include Si, C or Ge when incorporated on Ga sites and O, S, and Se on N sites. The most common of these will obviously be Si and O. It is less common to have acceptor impurities, which could potentially be Be, Mg, Ca, Zn, and Cd on Ga sites or C, Si, and Ge on the N sites.

Defects in GaN after Irradiation

A simple first–order model for the defects created by ionizing radiation such as protons and electrons involves creation of four levels in the gap, namely, V_{Ga}- with an acceptor level at $E_V+1.0$ eV, N_I- with an acceptor level at $E_C-1.0$ eV, Ga_I^{++} with a double donor level at E_C-0.8 eV and V_N^+ with a donor level at $E_C-0.06$ eV.[56,57] It is important to note that literature reports often cite slightly different energies for these defects, or state them in a different convention. For example, the V_N defect may also be quoted as having an energy level of E_V+ 3.28 eV in p-type GaN, which corresponds to the $E_C-0.06$ eV value quoted above, although others suggest $E_C-0.13$ eV as the energy level. Similarly, the V_{Ga} defect may be listed as having an energy level of $E_C-2.5$ eV, which is equivalent to the $E_V+1.0$ eV value discussed earlier.[56,57,71]

Most of the changes in GaN due to proton or electron damage can be understood in terms of introduction of these primary point defects and for example, the carrier removal rate in GaN for light particles is well accounted for by the introduction of these simple defects. At higher doses or when the GaN contains high levels of dopants or other impurities, complexes involving the primary radiation damage defects and these other impurities can occur and the situation becomes more complicated. In addition, differences in electric fields, defect concentrations and experimental precision of the defect spectroscopy techniques can all lead to differences in the experimentally reported values for energy levels in irradiation GaN structures.

Experimentally, a large number of levels are observed to be introduced into both n- and p-type GaN after proton irradiation, as was shown earlier in Figure 16.[71] These were obtained from a combination of Deep Level Transient Spectroscopy (DLTS) and Deep Level Optical Spectroscopy (DLOS), with the latter allowing measurement in a wider range of the gap. In some cases, the levels are already present in the as-grown material and increase in concentration as a result of the additional defects introduced by the irradiation. Obviously, one would expect that variations in levels observed will occur from different groups because of variations in the starting material and growth technique employed. At this stage there is a still a significant variation in irradiated GaN because of these differences in the quality and purity of material from different sources.

Movement of Dislocations in GaN during Electron Beam Irradiation

The radiation enhanced dislocation glide (REDG) effect for basal plane dislocations in GaN can be observed at rather low excitation by E-beam. Yakimov et al.[157] demonstrated dislocation movement upon irradiation by the probing electron beam of a scanning electron microscope. The effect was registered only for the segments of dislocations lying in the basal plane. However, the presence of a large number of pinning sites hampers the long distance displacement and multiplication of basal plane dislocations. The majority of dislocations are immobile due to strong pinning. The effective pinning site density decreases with the increase of the beam current. The movement of basal plane segments of dislocations in low-dislocation-density GaN films grown by epitaxial lateral overgrowth as a result of irradiation with the probing beam of an SEM detected by means of EBIC. Only a small fraction of the basal plane dislocations were susceptible to such changes and the movement was limited to relatively short distances.[157]

The effect is explained by the REDG for dislocations pinned by two different types of pinning sites, a low-activation-energy site and a high-activation-energy site. Only dislocation segments pinned by the former sites can be moved by irradiation and only until they meet the latter pinning sites. Epitaxial lateral overgrowth (ELOG) technique is one of the approaches allowing a dislocation density reduction. In this method, a GaN template is grown by standard metallorganic chemical vapor deposition. Then, a mask of SiO_2 stripes is prepared by photolithography and finally, a thick GaN layer is grown by MOCVD over the masked surface. The material above the mask grows predominantly in the lateral direction and has a dislocation density from two to three orders of magnitude lower than that in the material grown in the windows of SiO_2 mask, for which the dislocation density is the same as for standard MOCVD layers. The density of extended and point defects is very different in these two regions and therefore a lateral inhomogeneity in their electrical properties is expected. These regions have width in the micron range, therefore some special microscopic techniques should be used for characterization of such structures. Similar problems are also encountered in characterization of densely

Downloaded on 2019-08-31 to IP 128.227.169.164 address. Redistribution subject to ECS terms of use (see ecsdl.org/site/terms_use) unless CC License in place (see abstract).

packed integrated circuits. The application of scanning electron microscopy in the Electron Beam Induced Current (EBIC) mode for characterization of such structures is discussed in this presentation. Some examples that demonstrate the possibilities of this method are presented. It is shown that in ELOG films, the EBIC method allows not only to reconstruct the diffusion length distribution, i.e. the distribution of recombination centers, but also the donor distribution. The accuracy of these measurements was checked by a comparison of EBIC results obtained on homogeneous GaN films with those obtained on the same films by the C-V method. We observed a factor of about three times difference between the donor concentration in the laterally grown and window regions of the ELOG films. This difference was similar for films with different average donor concentration, which allowed for a possible explanation of the effect.[157] Similar investigations of neutron irradiated films showed that this method can reveal inhomogeneous radiation defect accumulation.

Usually it has been assumed that REDG does not take place in GaN or that the dislocation mobility is too low for gliding at low temperatures. However, this effect for basal dislocations in GaN was observed under irradiation in a Transmission Electron Microscope (TEM) at beam current densities of 1–100 A/cm^2, i.e. comparable with that used in high-power LEDs. Importantly, the REDG effect is more pronounced for basal plane dislocations than for prismatic plane ones. Usually, in GaN films grown in the [0001] direction, the majority of dislocations are of the threading type normal to the basal plane. However, in GaN grown by Epitaxial Lateral Overgrowth (ELOG) films with stripes parallel to the [1–100] direction and the thickness in the 6–9 micron range, the large proportion of dislocations in the low-dislocation-density wing regions have long segments located in the basal plane. This happens because of the threading dislocations bending out of the [0001] direction.

Role of Growth Technique and Extended Defect Density

At this stage, GaN heterostructures for transistors are usually grown on lattice mismatched substrates and contains a high density of dislocations. In GaN HEMTs grown on sapphire substrates, the dislocation density is $\sim 10^8-10^9$ cm^{-2}. Figure 19 shows a TEM cross-section of an AlGaN/GaN HEMT structure grown on a SiC substrate showing the high dislocation density, still typically $>10^7$ cm^{-2}. The dislocation density can be decreased to $\sim 10^6$ cm^{-2} for epitaxially laterally overgrown ELOG GaN, while thick ($>$200 μm) GaN films grown on sapphire by hydride vapor phase epitaxy HVPE have dislocation densities $< 10^7$ cm^{-2}. Interaction of radiation defects with dislocations is a factor in all these approaches.

One of these effects is spatial correlation of electron capture by deep traps decorating dislocations,[2,56,57] including the 1 eV N_I-related acceptors, 0.8 eV Ga_I and 0.95 eV V_{Ga} electron traps introduced by 2 MeV proton irradiation. During irradiation some of the interstitial defects can migrate to dislocation boundaries. Another effect is the impact of dislocations on mobility of charge carriers. With increasing radiation dose, the electron concentration within the grains becomes lower and the potential barrier is higher. For p-GaN, tunneling of holes is difficult even at high acceptor densities and hole mobility seldom shows the expected theoretical temperature or concentration dependence. The theory predicts a strong increase of the electron mobility with decreasing dislocation density and increasing electron concentration, the latter due to enhanced screening of dislocations.[2,56] However, the effect of dislocations on the carrier mobility is not reduced to the sum of contributions from individual dislocations. For dislocation densities exceeding $\sim 10^8$ cm^{-2} in GaN, dislocations form a cellular structure with dislocation boundaries formed mostly by the threading edge dislocations and characteristic grain size determined by the dislocation density. For carriers to travel over the grain boundaries involves overcoming a high potential barrier. When the electron concentration is high, tunneling through the barriers is efficient and the material behaves as though electrical nonuniformities were not present.

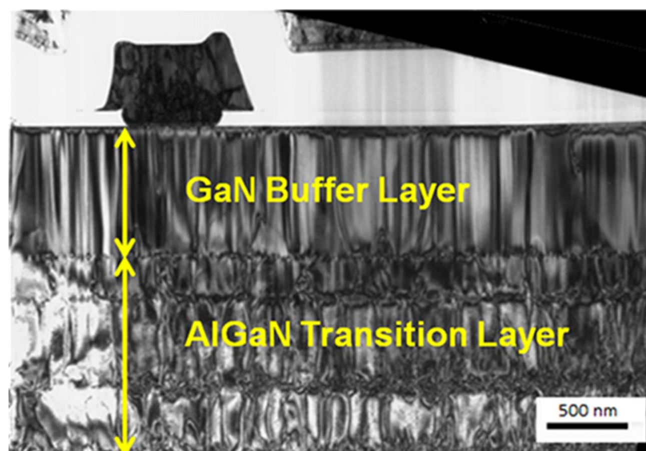

Figure 19. Cross section TEM image of AlGaN/GaN HEMT structure grown on a SiC substrate showing the high dislocation density.

As an example, neutron irradiation of undoped ELOG GaN resulted in a five times lower effective removal rate than for standard MOCVD GaN.[56] The carrier removal rates for thick HVPE-grown GaN were lower than for either the MOCVD or ELOG grown material and the dependence of the removal rate on starting concentration was stronger. This is not a consequence of dislocation density changes, because the dislocation density in the low-dislocation-density wing of ELOG samples is similar to the dislocation density in bulk HVPE samples but appears to be related to the uniformity of dislocation distribution. For MOCVD GaN the dislocations form a clear cellular pattern, with the typical size of dislocation cell of 0.3–0.5 μm. In ELOG GaN, wing regions with randomly distributed dislocations with density $\sim 5\times 10^6$ cm^{-2} are adjacent to the high dislocation-density window regions, whereas in HVPE samples the dislocation density is uniformly low at the level of $\sim 10^7$ cm^{-2}. This could be important for the probability of primary radiation defects to escape to the dislocations. It is well known that Ga vacancies (V_{Ga}) and Ga interstitials (Ga_I) are mobile at room temperature in GaN. We also note that it has been discovered by electron beam induced current (EBIC) profiling in neutron irradiated ELOG n-GaN that the decrease of the charge collection efficiency in EBIC occurs much more rapidly in the parts of ELOG wing region close to the window region than in the bulk of the ELOG wing where the radiation induced changes are the lowest. Carrier removal rates in neutron irradiated n-GaN increase with doping and decrease in the sequence MOCVD/ ELOG/ HVPE. The former were associated with disordered regions in GaN and determine the carrier removal rate in undoped films. The latter were attributed to radiation defect complexes with shallow donors.

Radiation Damage in InGaN/GaN Light Emitting Diodes

The development of GaN-based solid-state lighting holds promise for various applications such as traffic signals, automotive lighting, color display, indoor/outdoor lighting, mobile phones and televisions InGaN/GaN quantum wells (QWs) have been widely used in light-emitting diodes (LEDs) and laser diodes (LDs) due to their high luminescence efficiency in the near UV, blue and green regions.[158–171] Recently, the application of GaN-based LEDs has been extended to satellite communication systems for weather forecasting or broadband data transmission due to their high radiation hardness. The materials used in GaN-based LEDs have small lattice constants (a = 3.189 Å, c = 5.186 Å for wurtzite GaN structure) due to their strong bond energies and therefore show superior resistance to damage under radiation environments due to the higher displacement energies compared with other semiconductor systems such as the GaAs used in red LEDs (a = 5.653 Å). As we discussed for the electronic devices, it has been experimentally shown that the displacement energy is inversely

Downloaded on 2019-08-31 to IP 128.227.169.164 address. Redistribution subject to ECS terms of use (see ecsdl.org/site/terms_use) unless CC License in place (see abstract).

proportional to lattice constant.[172–178] The minority carrier lifetime, τ, in LEDs is sensitive to the presence of displacement damage and is related to the particle flux Φ by

$$(1/\tau) - (1/\tau_o) = \Phi/K$$

where τ_o is the initial lifetime, τ the lifetime after irradiation and K is known as the lifetime damage constant. For GaN, K is $\sim10^{-7}$ cm^2 s per particle for 40 MeV protons.[176]

Proton damage.— Displacement damage has a strong dependence on particle energy particularly for protons.[176–186] For energies below 30 MeV, protons interact with the nucleus through Rutherford scattering. Low-energy protons, which travel more slowly, transfer more energy than protons with higher energy due to their reduced velocity, increasing the cross section. As a result, the effectiveness of protons in producing displacement effects in LEDs depends on 1/E for energies below about 8 MeV.[176] This is important in radiation testing of LEDs, where high-energy protons are often used because they can penetrate package materials with only slight energy corrections.[176]

Osiński et al.[166] first reported the superior radiation hardness of group-III nitride based LEDs compared with that of GaAs-based LEDs. In their work, the output power of AlGaN/InGaN/GaN green LEDs after 2 MeV proton irradiation at a dose of 1.68×10^{12} /cm^2 was found to decrease by 40%.[166] Gaudreau et al.[167] reported that 2 MeV proton irradiation at higher fluences above 3×10^{12} /cm^2 significantly reduced the electrical and optical performance of AlGaN/InGaN /AlGaN blue LEDs, and the light output after 9.36×10^{14} /cm^2 proton irradiation decreased by 99.95%. They also observed that the optical properties degraded faster than the electrical properties due to an increase in non-radiative transitions through radiation-induced defect states. Khanna et al.[168] reported on the proton energy dependence of light output degradation of AlGaN/InGaN/AlGaN blue LEDs over the energy range of 2–115 MeV.

Khanna et al.[171] showed that the radiation hardness for light emission in GaN LEDs is substantially better at low temperatures, as determined by measurements of light emission at room and low temperatures from GaN LEDs following proton irradiation at room and low temperatures. The enhanced low-temperature radiation hardness for light emission in these LEDs was explained in terms of an improvement in radiative efficiency due to a reduction of nonradiative transition probability at low temperatures. Further, lattice displacement damage in these devices due to irradiation at room temperature was compared with the corresponding damage at low temperatures and was found to be dependent on irradiation temperature.[168,171] They also examined the proton energy dependence of emission intensity for blue GaN LEDs after proton irradiation with energies from 2–115 MeV at fluences varying from 10^{11} to 10^{15} cm^{-2}. There was more lattice displacement damage in GaAs LEDs following irradiation at low temperatures due to reduced annealing during irradiation. The light output data for both GaAs QW and GaN QW LEDs, and the I–V data for GaAs QW LEDs suggested that there is less lattice damage following low temperature irradiation than for irradiation at room temperature.[171]

The proton energy dependence of light output degradation in GaN LEDs was also examined for energies from 2–115 MeV[168] and modeled according to the theory of Rose and Barnes.[172] The normalized light output I_{irr}/I_o at different energies from these LEDs taken at a fixed dc current of 0.3 mA versus the fluence ϕ is shown in Figure 20.[168] Here I_{irr} is the light output after irradiation at a given fluence value ϕ and I_o is the value for the unirradiated device. For each energy, the normalized light output decreases as the fluence increases because the irradiation introduces defects which may act as either radiative or nonradiative recombination centers. As the proton energy is increased, the degradation curves shift to the right, as expected since the higher energies do less damage for the same proton fluence according to NIEL calculations.

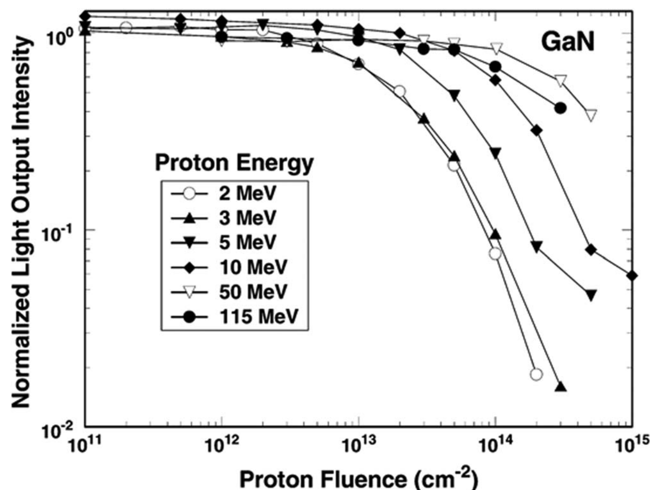

Figure 20. GaN LED light output as a function of fluence normalized to the preirradiation value (after Khanna et al.[168]).

The LED degradation due to particle irradiation at any given particle energy was fitted to the relationship due to Rose and Barnes[172]

$$I_{irr(\phi)}/I_o = (1 + A\phi)^{-1/n}$$

where $I_{irr(\phi)}$ is the LED light output measured after irradiation, I_o is the pre-irradiation value, A is a fitting parameter defined as the damage constant, ϕ is the particle fluence in units of particles/cm^2, and n is another fitting parameter. The data was consistent with the recombination mechanism being space charge limited.

Figure 21 presents a comparison of the light output degradation with proton fluence for GaN QW LEDs with both quantum well and bulk GaAs LEDs irradiated under the same conditions.[168] Note the much higher radiation tolerance of the GaN LEDs. The QW GaN-based diodes are about two orders of magnitude harder than QW GaAs diodes. One would expect AlGaN UV LEDs to be even more radiation hard because of the higher average bond strength relative to GaN and InGaN. One important consideration with radiation studies is whether the measurements are made on unpackaged die or completed LEDs in standard packages. It is known that the polymers in the lenses may degrade during irradiation, changing the opacity of the package and thus the light output may appear to degrade even though the Led die itself has had no change in optical output.

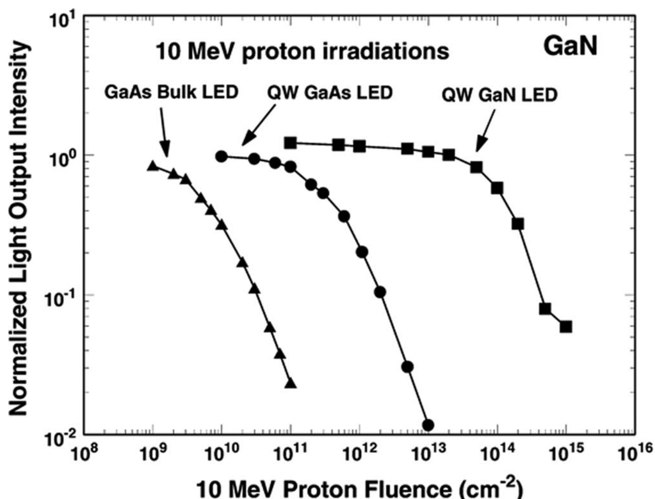

Figure 21. A comparison of LED light output radiation response from 10 MeV protons of GaAs and GaN LEDs. (after Khanna et al.[168]).

Downloaded on 2019-08-31 to IP 128.227.169.164 address. Redistribution subject to ECS terms of use (see ecsdl.org/site/terms_use) unless CC License in place (see abstract).

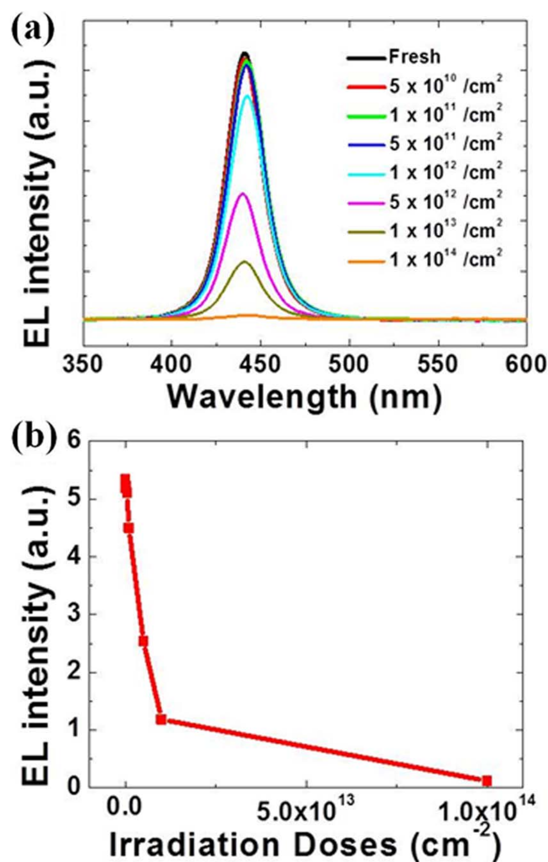

Figure 22. (a) The electroluminescence (EL) spectra, which measured at an injection current of 100 mA, of InGaN/GaN blue LEDs prior to and after 340 keV proton irradiations with different doses. (b) The change of EL intensity as a function of irradiation doses.

The effects of proton irradiation on the optical and electrical performance of InGaN/GaN blue light-emitting diodes (LEDs) irradiated with protons at a fixed energy of 340 keV and doses ranging from 5 $\times$ 10^{10} to 1 $\times$ 10^{14} /cm^2 were also investigated.[170] The forward operating voltages at an injection current of 100 mA before and after proton irradiation with doses from 5 $\times$ 10^{10} to 5 $\times$ 10^{11}/cm^2 were almost the same, around 4.4 V. However, the forward operating voltages at an injection current of 100 mA after higher doses of 10^{12}, 5 $\times$ 10^{12}, 10^{13} and 10^{14} /cm^2 were progressively higher, with values of 4.37, 4.39, 4.5 and 8.11 V, respectively. The light output at an injection current of 100 mA after low dose proton irradiations from 5 $\times$ 10^{10} to 5 $\times$ 10^{11} /cm^2 slightly decreased by 2∼4%, compared with the unirradiated reference LEDs. At higher doses, the light output at an injection current of 100 mA after 10^{12}, 5 $\times$ 10^{12}, 10^{13} and 10^{14} /cm^2 proton dose drastically decreased by 15.3, 55.7, 75.6 and 98.9%, respectively. The degradation of light output was much faster than that of I–V characteristics. The device conductivity is related to both radiative and non-radiative recombination, however, most of the light output is involved in near-band-edge emission caused by only radiative recombination. Therefore, the faster degradation of light output indicates that defects generated by energetic protons can act as non-radiative recombination centers.

Figure 22 (top) shows typical electroluminescence (EL) spectra at an injection current of 100 mA before and after 340 keV proton irradiations with various doses from 5 $\times$ 10^{10} to 10^{14} cm^{-2}. The EL intensity gradually decreased with increasing proton dose, as shown in Figure 22 (bottom) and the EL spectra after 10^{14} cm^{-2} proton irradiation had almost no emission due to the high level of displacement damage caused by the high dose proton irradiation. The trends of the changes in EL intensity were similar to that of the light output. This

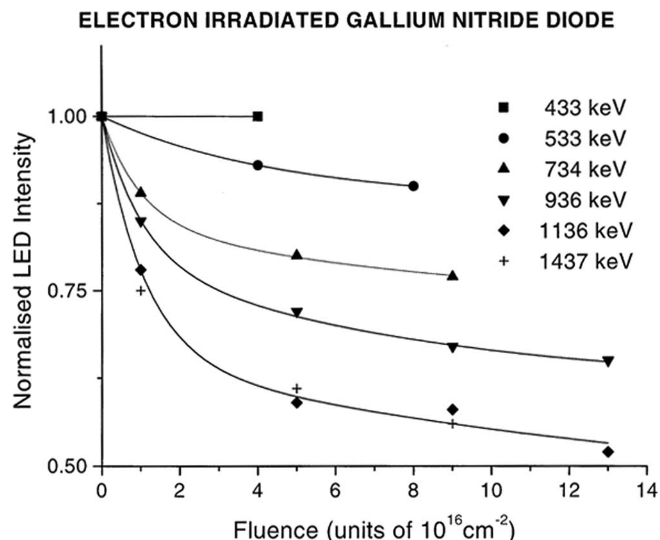

Figure 23. Normalized LED light intensity versus electron irradiation fluence. The data can be reproduced by the exponentially decreasing function (after Ionascut-Nedelcescu et al.[4]).

degradation after proton irradiation was caused by the trapping of carriers in proton irradiation-induced deep levels which may act as either radiative or non-radiative recombination centers. However, there was almost no increase in yellow-green emission, which is originated in GaN defect sites such as vacancies, impurities and deep levels,[173–180] after proton irradiation. The EL peak position before and after proton irradiations had no significant changes.

Electron damage.— Electrons, with their much lower mass than protons, require energies that are nearly relativistic to produce atomic displacements in GaN LEDs.[176] Consequently, there is a minimum energy threshold for displacements from electrons. Above that energy, the effectiveness of electrons in producing displacement damage continues to increase with energy, unlike protons, where damage decreases with increasing energy.[176]

GaN LEDs irradiated at room temperature with electrons in the range 300–1400 keV showed that a threshold energy of 440 keV was needed to create detectable damage, corresponding to a gallium atom displacement energy of 19± 2 eV[4]. This value of the displacement energy is comparable to that of SiC but is smaller than that of diamond and larger than that of GaAs. No threshold energy for the nitrogen atom was observed. It was concluded that the nitrogen sublattice repairs itself through annealing.[4] Figure 23 shows the normalized LED light intensity versus electron irradiation fluence for different electron energies.[4] The data can be reproduced by the exponentially decreasing function[4] given earlier by Rose and Barnes.[172]

Gamma ray damage.— The luminescence intensities of InGaN MQW LEDs (460 nm peak emission) irradiated by γ-rays decreased as the radiation dose becomes higher.[177] InGaN MQW LEDs in the form of unpackaged die with emission wavelengths from 410–510 nm were irradiated with $^{Co}60$ γ-rays with doses in the range 150–2000 Mrad (Si). The forward turn-on voltage for all the irradiated LEDs was increased slightly (by ∼0.1–0.15 V for 500 MRad dose irradiation) while the reverse breakdown voltage was unchanged within experimental error. The light output intensity for the 410 nm devices was decreased by 20% after a dose of 150 MRad and 75% after ∼2 GRad. The current transport in the LEDs was dominated by generation-recombination (ideality factor ∼2) both before and after irradiation. Their electroluminescence characteristics were more affected by the irradiation (losing about a factor of 4 intensity at extremely high doses), suggesting that the main degradation

Downloaded on 2019-08-31 to IP 128.227.169.164 address. Redistribution subject to ECS terms of use (see ecsdl.org/site/terms_use) unless CC License in place (see abstract).

mechanism is creation of recombination centers. The morphology and appearance of the p and n-Ohmic metallization did not show any detectable change as a result of even the highest γ-ray dose. There was no post-irradiation recovery at room temperature noted in these devices.

Small redshifts (∼54 meV) of the (PL peak energy of blue InGaN/GaN light-emitting diodes exposed to ^{60}Co γ-rays was reported after doses of 200 MRad.[178] Time-resolved PL indicated that the PL radiative time increased with fluence and there was a higher carrier localization energy and larger Stokes' shift, respectively, in the irradiated LEDs. This suggests the redshifts of the PL peak emission introduced by γ-ray irradiance mainly originated from the enhancement of indium fluctuation.[178] Transient capacitance measurements of Schottky diodes fabricated on undoped n-type GaN exposed to ^{60}Co gamma irradiation indicate the introduction of two defect levels with thermal activation energies of 89 and 132 meV.[179] The defect peaks showed significant broadening, but were consistent with electron-irradiation-induced nitrogen-vacancy related centers.[179]

Neutron damage.— Fast neutron irradiation with fluxes > 10^{15} cm^{-2} caused degradation in the I–V characteristics as well as light output of blue GaN LEDs emitting at 476 nm.[174] Atomic displacements were reported as responsible for both of the electrical and optical degradations. The decreasing slope (α) of the ln(I) versus V plots after irradiation was attributed to the neutron radiation-induced carrier removal effect. The increasing value of saturation current I_0 after irradiation was attributed to increasing trap concentration.[174] The light output at a bias current of 2.5 mA degraded almost completely (99%) after 1.6 × 10^{15} n/cm^2 neutron irradiation. Some optical and electrical recovery due to an injection-enhanced annealing effect was observed in the irradiated LEDs.[174]

Another study examined InGaN/GaN multiquantum well LEDs with emission wavelength of 450 nm irradiated with average energy of 9.8 MeV and dose of 5.5 × 10^{11} cm^{-2} neutrons.[163] Immediately after irradiation, the forward current of the irradiated LEDs was decreased as a result of the creation of deep levels by the neutron-induced lattice displacement. However, unstable lattice damages resulting from the collisions with the incoming neutrons were removed at room temperature 6 days after the irradiation.[163] The diode turn-on voltage, ideality factor, and optical emission intensity were recovered to the pre-irradiated state by self-annealing process at room temperature.[163]

Alpha particles.— InGaN quantum well structures (470 and 510 nm) on GaN epilayers exposed to 500 keV alpha particles to fluences >10^{14} cm^{-2} showed only small wavelength shifts were observed even with the highest fluences.[175] Cathodoluminescence experiments showed that luminescence in the quantum wells was strongly influenced by charges injected deep into the GaN epilayer. The 500 keV alpha penetration depth was ∼ 1 μm, so that defects were created at a faster rate in GaN compared to InGaN as alpha particles slowed and stopped within a minority carrier diffusion length of the quantum wells. The rate of luminescent decay was similar for both materials and the quantum well luminescence decay rate was dominated by radiation-induced defects in the GaN epilayer. InGaN quantum wells were found to be somewhat more radiation sensitive than GaN.[175]

In summary, the effect of radiation damage on GaN-based LEDs is as follows:

1. There is a decrease in light output that scales with proton dose.
2. The optical output decreases faster than the degradation in electrical parameters of the LEDs.
3. Electron damage requires a threshold energy of at least 440 keV to create damage in GaN LEDs.
4. Neutron-irradiated LEDs can show a significant amount of recovery after storage at room temperature.
5. Deep UV LEDs which contain high concentration AlGaN alloys are expected to be more radiation hard than visible LEDs based on InGaN/GaN quantum wells.

Single Event Upsets in GaN HEMTs

Single-event upsets (SEU) or transient radiation effects in electronics are defined as state changes of memory or register bits caused by a single ion interacting with the chip.[187–193] SEU do not necessarily cause permanent damage to the device, but may cause lasting problems to a system which cannot recover from such an error. In very sensitive devices, a single ion can cause a multiple-bit upset (MBU) in several adjacent memory cells. SEUs can become Single-event functional interrupts (SEFI) when they upset control circuits, placing the device into an undefined state, which would then need a reset or a power cycle to recover.

Single-event latchup (SEL) can occur in any chip with a parasitic PNPN structure and since thyristors are not yet available in GaN, these are not an issue for GaN electronics. A heavy ion or a high-energy proton passing through one of the two inner-transistor junctions can turn on the thyristor structure, which goes into latchup until the device is power-cycled.[187–189] Single-event transient (SET) occurs when the charge collected from an ionization event discharges in the form of a spurious signal traveling through the circuit. This has the same effect as an electrostatic discharge. In Si CMOS circuits, single-event snapback, basically similar to SEL but not requiring the PNPN structure, can be induced in N-channel MOS transistors switching large currents when an ion hits near the drain junction and causes avalanche multiplication of the charge carriers.[188–193] Single-event induced burnout (SEB) may occur in power MOSFETs when the substrate right under the source region gets forward-biased and the drain-source voltage is higher than the breakdown voltage of the parasitic structures. The resulting high current and local overheating then may destroy the device. Single-event gate rupture (SEGR) can be observed in power MOSFETs when a heavy ion hits the gate region while a high voltage is applied to the gate. This creates local breakdown in the SiO_2 with overheating of the gate. SEGR can also occur even in memory cells during write or erase, when the cells are subjected to a comparatively high voltage.

The effects of single event particle strikes in GaN HEMTs have only begun to be investigated.[187–193] Single event upsets include both soft errors and hard errors. A soft error occurs when a heavy ion strikes a semiconductor substrate, creating electron-hole pairs, and charge collects at nodes in the circuit, resulting in transient signals. Sometimes catastrophic failures (or hard errors) occur when a heavy ion strikes a sensitive region in the device and permanently cause increased leakage current or rendesr the device inoperable. There is limited SEE data for AlGaN/GaN HEMT devices[189,190] and some initial data on single event gate rupture.[189]

Bazzoli et al.[189] were the first to study SEEs in GaN HEMTs. They reported soft errors using heavy ions (Fe, Br, Xe) with linear energy transfer (LET) up to 39 $MeVmg^{-1}$ cm^2 which temporarily increased gate leakage current and would be classed as soft damage. They also reported catastrophic failures using Xe ions at a LET of 60 $MeVmg^{-1}$ cm^2, ie. the component can be destroyed with only one interaction with an ion. These phenomena appear to be similar to single event gate rupture (SEGR), despite a lack of gate oxide.[189] No single event burnout (SEB) could be induced. The same HEMTs were unaffected by 14 MeV neutron irradiation and heavy ions with LETs of 1.8 and 18.5 $MeV.mg^{-1}.cm^2$.

Kuboyama et al.[190] reported several different types of permanent damage in AlGaN/GaN HEMT devices irradiated with Kr, Ne or Ar heavy ions from an accelerator at fluences up to ∼10^8 cm^{-2} GaN HEMTs using heavy ions. They observed enhanced charge collection with Ne ions and increased leakage current with Ar and Kr ions. A new damage mode, which introduced the leakage paths between the drain and source, was observed with Kr ions at high drain voltages[190] and also new leakage paths emerged between the drain and source terminals without any damage signature to the gate.

Rostewitz et al.[188] evaluated the Single Event Burnout (SEB) and SEE of HEMTs under dc and rf operations during high energy Ar, Xe or Kr ion irradiation. They found that SEBs are correlated to enhanced Single Event Transients (SETs) close to the gate region and

Downloaded on 2019-08-31 to IP 128.227.169.164 address. Redistribution subject to ECS terms of use (see ecsdl.org/site/terms_use) unless CC License in place (see abstract).

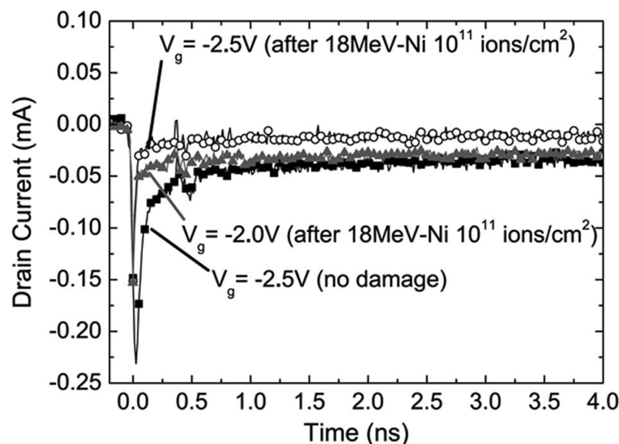

Figure 24. Typical transient drain currents at drain bias of V 10 V when 18 MeV-Ni ion strikes the center of gate electrode (after Onoda et al.[183]).

that no SEBs occurred under rf operation. Onoda et al.[187] showed the drain currents increased when thigh energy Ni ions impacted the gate electrode and demonstrated that 18 MeV-Ni ions can cause positive charge buildup in the AlGaN layer even at room temperature.[187] Figure 24 shows typical transient drain currents at drain bias of V 10 V when a 18 MeV-Ni ion struck the center of gate electrode.[183] The drain current did not increase when ions struck the HEMT other than at the gate electrode. Since there was no charge buildup in the AlGaN layer when ions traversed any region other than the gate electrode, only back-channel effect contributed to the enhanced charge collection. The largest charge enhancement was found when 18 MeV-Ni ions impacted the center of the gate electrode in the pinch-off bias condition due to an enhanced charge collection.[183,187] The key point of the back-channel effect is the positive charge accumulation in the GaN layer under the gate. The positive charges reduce the potential barrier between the source and the channel, resulting in the current from the source to the drain. A decrease in the saturation drain current and a positive shift of the threshold voltage were observed as a result of the high energy Ni irradiation[187] and the transient drain and source currents were strongly affected by the change in I–V characteristics caused by displacement damage. There were two different failure modes, namely increased drain and gate leakage at high drain voltage, and SEB using drain voltage of 155 V and particle LET of 48 $MeVmg^{-1}$ cm^2.[187,188]

Scheick[192] examined the susceptibility of enhancement mode GaN HEMTs to heavy ion induced SEE. This study noted that the susceptibility to SEE was dependent on ion type, angle, circuit capacitance and manufacturing lot. These preliminary results suggest GaN transistors are less vulnerable to single event burnout than Si MOSFETs. In AlGaN/GaN MOSHEMTs,[193] simultaneous charge collection was observed at the gate and the drain or the source, depending on strike location. Heavy ion data coupled with device simulations show that the introduction of a thin HfO_2 layer in the gate stack introduces only a small valence band barrier, reducing but not preventing collection of holes at the gate in HfO_2-gate devices. Furthermore, using Al_2O_3 gate oxide increases the valence band barrier over that of the HfO_2, to the point where the radiation-induced transient is not detectable. Analysis of the band structure of the HEMT using simulations showed that hole collection at the gate is favorable under off-state conditions, even for devices with an HfO_2 gate dielectric while use of an Al_2O_3 dielectric produced a valence band barrier that reduced hole collection to a level below the resolution of the test setup.[193] This suggest that device design will be important in reducing the susceptibility of GaN-based MOS transistors to SEE.

Simulation of Radiation Effects on AlGaN/GaN HEMT's

Electronic device simulation historically has focused on solving a set of three coupled partial differential equations - one for potential (Poisson) and one each for holes and electrons (continuity).[194] Device scaling pushed the research focus on the transport coefficients in the equations. Mobility expressions became more sophisticated and velocity saturation and high electric field effects needed to be accounted for. In some cases the equation set expanded to include energy conservation of the carrier distribution.

The simulation of damage due to irradiation represents a specific problem in device simulation in which charge trapping, at least, needs to be accounted for. For example, to capture total ionizing dose (TID) effects in oxides of transistor-based technologies, it is necessary to include the addition of deep level traps and the partial ionization of multiple defect levels. All three differential equations require modification to account for charges trapped in deep levels. The FLOODS simulator[50,195] allows the physics to be modified easily using command line expressions, so it is ideally suited for this type of problem.

In general, proton-based radiation damage to AlGaN/GaN HEMTs results in reductions in mobility and increases in the threshold voltage that lead to reductions in peak transconductance, and drain current. The reduction in mobility can be much greater in magnitude than the changes in the other parameters. For example Liu et al.[102] measured 40% reduction in mobility and only a 0.1 V shift (3% change) in threshold voltage and 13% reduction in drain saturation current for a specific case of proton radiation.[102] Gaudreau measured a decrease in carrier concentration by a factor of two and a decrease in mobility by a factor of a thousand.[26]

The simulation incorporates a mobility model that includes ionized impurity scattering as described by Farahmand et al.,[196] who used a Monte Carlo simulation to extract a dependence of mobility on impurity scattering. Their standard approach to describing mobility is seen in the following equation:

$$\mu_0 = \mu_{min} + \frac{\mu_{max} - \mu_{min}}{1 + \left(\frac{N}{N_{ref}}\right)^{\alpha}}$$

in which μ_{min}, μ_{max}, N_{ref} and α are fitting parameters dependent on the material. For GaN, the parameters are 295 cm^2/Vs, 1406 cm^2/Vs, 10^{17}, and 0.66 respectively.[196] N is the term for the ionized impurity concentration. Included in this term are the ionized donor and acceptor trap concentrations and the background doping value. This is a necessary modification from many commercial tools, as they include only doping levels and not the ionized trap concentrations. Included in this term are the ionized donor and acceptor trap concentrations and the background doping value. These are summed together, even though in many materials there is a difference between the effect of a donor and acceptor on mobility of electrons. There is no data indicating a differential in GaN or AlGaN.

Experimental data from quantify the amount of mobility reduction for given amounts of proton irradiation as shown in Figure 25.[22,27,102] We assume that only the acceptor-like Gallium vacancies (V_{Ga}) are ionized near the two-dimensional electron gas (2DEG) since the Fermi level is above the conduction band edge and thus excludes donor ionization. Thus, V_{Ga} concentrations given by the TRIM simulations[197] are plotted against mobility reductions in Figure 25. The experimental data sets show mobility reduction trends that are captured well by the model using ionized traps to account for the observed mobility reduction.

It is known that acceptor-like traps, which leave negative space charge when ionized, explain the positive shift in threshold voltage and degradation in drain current and transconductance as seen in irradiated AlGaN/GaN HEMTS. The experimentally-derived changes in performance used for calibration include a 13% reduction in the drain saturation current and a 0.1 V positive shift in the threshold voltage, both of which correspond to a 5 MeV proton radiation at a fluence of 2×10^{14} cm^{-2}. Initial simulations of these devices indicated that a threshold voltage shift of only 0.1 V required trap concentrations that are orders of magnitude lower than the value predicted by the TRIM simulation and the mobility model ($\sim 1 \times 10^{17}$ cm^{-3}). Therefore, a model that includes only acceptor traps cannot explain experimental results.

Downloaded on 2019-08-31 to IP 128.227.169.164 address. Redistribution subject to ECS terms of use (see ecsdl.org/site/terms_use) unless CC License in place (see abstract).

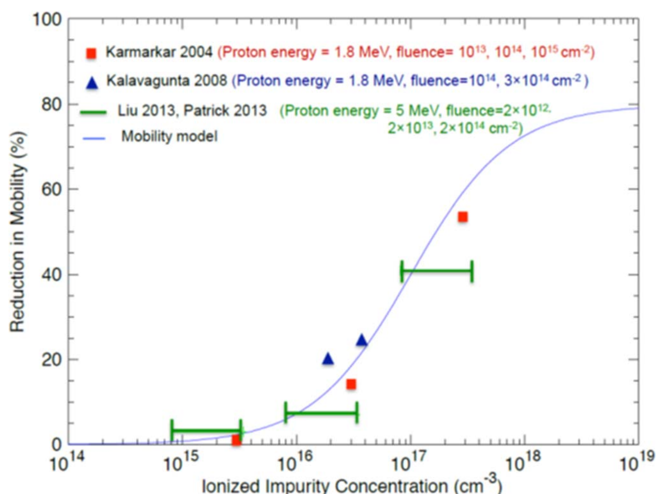

Figure 25. Reduction in mobility as predicted from TRIM damage levels.[197] Data from Refs. 22,27 and 102 (figure from Ref. 184).

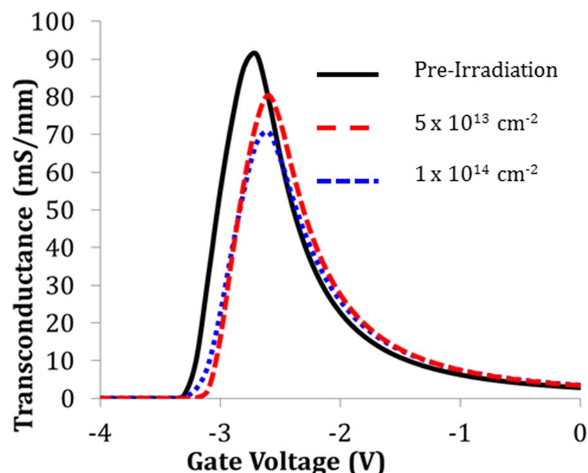

Figure 27. Simulated transconductance of proton irradiated HEMTs as a function of bias for three different fluences.

Thus it can be inferred that donor-like traps are compensating the acceptor-like traps in a manner that lowers the total amount of charge in the GaN layer. Since the concentration of traps are not known precisely, it is useful to simulate the performance degradation for a range of acceptor and donor traps to determine sensitivity. At this point we also choose donor and acceptor trap energies. We assume the dominant traps could be acceptor-like Gallium vacancies with energy level 1.0 eV above the valence band (E_v) and donor-like Nitrogen vacancies 0.1 eV below the conduction band (Ec).[57] Figure 26 show 3-D surface plots of threshold voltage shift as a function of acceptor and donor concentrations. Simulation results having donor concentrations higher than acceptor concentrations are not given due to the inability of the device to turn off. In Figure 26, performance changes are labeled for points of equivalent acceptor and donor concentrations. Trap concentrations near 10^{17} cm^{-3} for acceptors and donors match the experimental results of 0.1 V threshold voltage shift for a proton fluence of 2×10^{14} cm^{-2} at 5 MeV. Since Gallium and Nitrogen vacancies have similar displacement energies (not more than a factor of two), it is plausible that the number of vacancies could be created in approximately equal amounts. Figure 25 shows a concentration near 10^{17} cm^{-3} fits the observed mobility reduction for the radiation case.

These simulation results conclude that compensation by donor traps is very important in determining the amount of performance degradation in the devices. The compensation by ionized donors confines the negative space charge to within a small distance from the AlGaN/GaN interface. This simulation result is supported by experimental results using back-side irradiation and thus localization of radiation defects. Li et al.[186] showed that no performance change to the devices occurred for irradiation cases where the defects did not reach the AlGaN/GaN interface.[186] We also note that the acceptor traps will be fully ionized near the 2DEG for a wide range of trap energies; thus the resultant outcome is insensitive to the acceptor trap energy.

Of course the trap states influence not only DC characteristic but also AC characteristics. We have done small signal analysis along the lines of Laux[198] but expanded it to include a small signal approximation to the trap occupancy to investigate the effect of the trap generation on the RF response. Figure 27 shows a comparison of the peak transconductance as a function of gate bias for several radiation dose exposures. The peak transconductance is lower for irradiated samples but also shows a shift to higher gate voltage. These effects are important to understand for maximizing device behavior over a lifetime of exposure conditions.

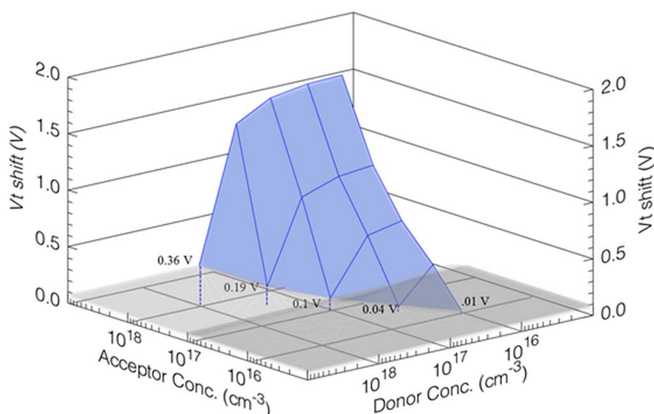

Figure 26. Positive threshold voltage shift (Vt) as a function of acceptor and donor concentrations. The trap types are acceptor-like vacancies at energy level $E_v+1.0$ eV and donor-like vacancies at $E_c-0.1$ eV.

Conclusions

In GaN-based HEMTs, the primary degradation mechanisms after exposure to ionizing radiation are decreased sheet carrier mobility due to increased carrier scattering and decreased sheet carrier density. The device degradation is observed as a decrease in the maximum transconductance, an increase in the threshold voltage, and a decrease in the drain saturation current. The carrier removal rate in nitrides depends on radiation type, growth method and the dislocation density and distribution. The response of GaN to radiation exposure such as protons can be largely understood by a simple model involving creation of point defects. Neutron damage creates more extended damage regions. The carrier removal rate by protons, electrons and neutrons in nitride heterostructures increases in the following sequence AlN/GaN> AlGaN/GaN> InAlN/GaN. This is consistent with their average bond strengths. Proton damage has been the most widely studied and understood. As an example, the drain-source currents of both AlGaN/GaN and InAlN/GaN HEMTs decreased 15–20% for proton irradiation with doses of 5×10^9 cm^{-2} and 30–50% decrease at a dose of 5×10^{10} cm^{-2}. The drain current of proton damaged HEMTs can be partially recovered (40–70%) after annealing at 300°C. We have not seen any significant effect on the carrier loss rate in AlGaN/GaN HEMTs during either 10 MeV electron or 10 MeV proton irradiation to total doses of 10^{13} cm^{-2} (protons) or 10^{15} cm^{-2} (electrons) over a range of almost two orders of magnitude in dose rate for both types of radiation.

Downloaded on 2019-08-31 to IP 128.227.169.164 address. Redistribution subject to ECS terms of use (see ecsdl.org/site/terms_use) unless CC License in place (see abstract).

GaN based HEMTs and LEDs are significantly more radiation hard than their GaAs counterparts to both total ionizing dose and single event upsets. There has been little work on the the influence of electric fields in biased GaN devices on the introduction rate and stability radiation damage, but the initial work on testing proton and electron damage under the presence of electric fields, shows that the typical fields present in HEMTs does not significantly affect the carrier removal rate for either type of radiation. In addition, it is certainly the case that results of zero bias irradiation is still relevant because RF communication circuitry may not always be at operational voltages and in space missions, it is also common to power off electronics in order to conserve power.[199] In this latter case, more damage might actually occur when the device is powered off than happens when it is operating.

There are still a number of issues where additional work is needed,[2,12,56,57,79,200–208] including:

1. The effect of small amounts of radiation damage on GaN device reliability is still not settled and also the role of different contact metals, device geometry or passivation layers on the stability of the devices after irradiation should be understood.
2. The increasing use of thick GaN quasi-bulk substrates grown by HVPE is an area where more work will be needed to understand the effects of charge induced by radiation exposure.
3. There needs to be more work on MOS-HEMTs since the vast majority of studies have used metal-gate HEMTs.
4. In addition, the correlation of radiation damage to changes in rf performance of HEMTs needs additional understanding.
5. Similarly, the understanding of the effects of X-ray irradiation is still at a relatively immature stage.
6. The study of single-event upsets on GaN electronics is still at an early stage.
7. The continued development of GaN radiation simulators to include a broader range of alloys and device structures is needed, along with integration of the full set of the grown-in point defects that increase in concentration with radiation exposure.

Acknowledgments

The work is supported by an U.S. DOD HDTRA grant No. 1-11-1-0020. The work at NUST MISiS was supported in part by the Ministry of Education and Science of the Russian Federation in the framework of Increase Competitiveness Program of NUST «MISiS» (К2-2014-055).

References

1. See, for example, *Nitride Semiconductor Devices-Principles and Simulation*, ed. J. Piprek (Wiley-VCH, Weinheim, 2007); *III-V Compound Semiconductors-Integration with Si-Based Microelectronics*, ed. T. Li, M. Mastro, and A. Dadgar (CRC Press, Boca Raton, 2011); *GaN Processing for Electronics, Sensors and Spintronics* (Springer, London, 2006).
2. A. Y. Polyakov and In-Hwan Lee, *Mat. Sci. Eng. R*, **94**, 1 (2015).
3. S. M. Khanna, J. Webb, H. Tang, A. J. Houdayer, and C. Carlone, *IEEE Trans. Nucl. Sci.*, **47**, 2322 (2000).
4. A. Ionascut-Nedelcescu, C. Carlone, A. Houdayer, H. J. von Bardeleben, J.-L. Cantin, and S. Raymond, *IEEE Trans. Nucl. Sci.*, **49**, 2733 (2002).
5. M. Rahman, A. Al-Ajili, R. Bates, A. Blue, W. Cunningham, F. Doherty, M. Glaser, L. Haddad, M. Horn, J. Melone, M. Mikuz, T. Quinn, P. Roy, V. O'Shea, K. M. Smith, J. Vaitkus, and V. Wright, *IEEE Trans. Nucl. Sci.*, **51**, 2256 (2004).
6. D. C. Look, D. C. Reynolds, J. W. Hemsky, J. R. Sizelove, R. L. Jones, and R. J. Molnar. *Phys. Rev. Lett.* **79**, 2273 (1997).
7. L. Polenta, Z.-Q. Fang, and D. C. Look, *Appl. Phys. Lett.*, **76**, 2086 (2000).
8. J. Nord, K. Nordlund, and J. Keinonen, *Phys. Rev. B*, **68**, 184104 (2003).
9. H. Y. Xiao, F. Gao, X. T. Zu, and W. J. Weber, *J. Appl. Phys.*, **105**, 123527 (2009).
10. M. G. Ganchenkova and R. M. Nieminen, *Phys. Rev. Lett.*, **96**, 196402 (2006).
11. A. Y. Polyakov, D.-W. Jeon, In-Hwan Lee, N. B. Smirnov, A. V. Govorkov, E. A. Kozhukhova, and E. B. Yakimov, *J. Appl. Phys.* **113**, 083712 (2013).
12. S. J. Pearton, Y.- S. Hwang, and F. Ren, *J. Mater.* **67**, 1601 (2015).
13. H. Y. Kim, T. J. Anderson, M. A. Mastro, J. A. Freitas, S. Jang, J. Hite, C. R. Eddy, and J. Kim. *J. Cryst. Growth* **326**, 62 (2011).
14. G. A. Umana-Membreno, J. M. Dell, G. Parish, B. D. Nener, L. Faraone, and U. K. Mishra, *IEEE Trans. Electron. Dev.* **50**, 2326 (2003).
15. G. A. Umana-Membreno, J. M. Dell, G. Parish, B. D. Nener, L. Faraone, S. Keller, and U. K. Mishra, *J. Appl. Phys.*, **101**, 054511 (2007).
16. A. Kumar, A. Hähnel, D. Kanjilal, and R. Singh, *Appl. Phys. Lett.*, **101**, 153508 (2012).
17. X. Hu, B. K. Choi, H. J. Barnaby, D. M. Fleetwood, R. D. Schrimpf, S. Lee, S. Shojah-Ardalan, R. Wilkins, U. K. Mishra, and R. W. Dettmer, *IEEE Trans. Nucl. Sci.* **51**, 293 (2004).
18. C.-H. Lin, E. J. Katz, J. Evan, J. Qiu, Z. Zhang, U. K. Mishra, L. Cao, and L. J. Brillson, *Appl. Phys. Lett.*, **103**, 162106 (2013).
19. J. W. McClory and J. C. Petrosky, *IEEE Trans Nucl. Sci.* **54**, 1969 (2007).
20. A. Y. Polyakov, N. B. Smirnov, A. V. Govorkov, N. G. Kolin, D. I. Merkurisov, V. M. Boiko, A. V. Korulin, and S. J. Pearton, *J. Vac. Sci. Technol. B* **28**, 608 (2010).
21. B. D. White, M. Bataiev, S. H. Gross, X. Hu, A. Karmarkar, D. M. Fleetwood, R. D. Schrimpf, W. J. Schaff, and L. J. Brillson, *IEEE Trans. Nucl. Sci.* **50**, 1934 (2003).
22. A. P. Karmarkar, B. Jun, D. M. Fleetwood, D. D. Schrimpf, R. A. Weller, B. D. White, L. S. Brillson, and U. K. Mishra, *IEEE Trans. Nucl. Sci.* **51**, 3801 (2004).
23. J. W. McClory, J. C. Petrosky, J. M. Sattler, and T. A. Jarzen, *IEEE Trans. Nucl. Sci.*, **54**, 1946 (2007).
24. A. P. Karmarkar, B. D. White, D. Buttari, D. M. Fleetwood, R. D. Schrimpf, R. A. Weller, L. J. Brillson, and U. K. Mishra, *IEEE Trans. Nucl. Sci.*, **52**, 2239 (2005).
25. A. Kalavagunta, M. Silvestri, M. J. Beck, S. K. Dixit, R. D. Schrimpf, R. A. Reed, D. M. Fleetwood, L. Shen, and U. K. Mishra, *IEEE Trans. Nucl. Sci.* **56**, 3192 (2009).
26. F. Gaudreau, P. Fournier, C. Carlone, S. M. Khanna, H. Tang, J. Webb, and A. Houdayer, *IEEE Trans. Nucl. Sci.* **49**, 2702 (2002).
27. A. Kalavagunta, A. Touboul, L. Shen, R. D. Schrimpf, R. A. Reed, D. M. Fleetwood, R. K. Jain, and U. K. Mishra, *IEEE Trans. Nucl. Sci.* **55**, 2106 (2008).
28. X. Hu, A. Karmarkar, J. Bongim, D. M. Fleetwood, R. D. Schrimpf, J. Geil, R. A. Weller, B. D. White, M. Bataiev, L. J. Brillson, and U. K. Mishra, *IEEE Trans. Nucl. Sci.*, **50**, 1791 (2003).
29. X. Hu, B. K. Choi, H. J. Barnaby, D. M. Fleetwood, R. D. Schrimpf, S. Lee, S. Shojah-Ardalan, R. Wilkins, U. K. Mishra, and R. W. Dettmer, *IEEE Trans. Nucl. Sci.*, **51**, 293 (2004).
30. S. J. Cai, Y. S. Tang, R. Li, Y. Y. Wei, L. Wong, Y. L. Chen, K. L. Wang, M. Chen, Y. F. Zhao, R. D. Schrimpf, J. C. Keay, and K. F. Galloway, *IEEE Trans. Electron Dev.*, **47**, 304 (2000).
31. B. Luo, J. W. Johnson, F. Ren, K. K. Alums, C. R. Abernathy, S. J. Pearton, A. M. Dabiran, A. M. Wowchak, C. J. Polley, P. P. Chow, D. Shoenfeld, and A. G. Baca, *Appl. Phys. Lett.* **80**, 604 (2002).
32. B. Luo, J. Kim, F. Ren, J. K. Gillespie, R. C. Fitch, J. Sewell, R. Dettmer, G. D. Via, A. Crespo, T. J. Jenkins, B. P. Gila, A. H. Onstine, K. K. Allums, C. R. Abernathy, S. J. Pearton, R. Dwidevi, T. N. Fogarty, and R. Wilkins, *Appl. Phys. Lett.* **82**, 1428 (2003).
33. B. D. Weaver, P. A. Martin, J. B. Boos, and C. D. Cress, *IEEE Trans. Nucl. Sci.*, **59**, 3077 (2012).
34. B. D. Weaver and E. M. Jackson, *Appl. Phys. Lett.*, **80**, 2791 (2002).
35. T. Roy, E X. Zhang, Y. S. Puzyrev, D. M. Fleetwood, R. D. Schrimpf, B. K. Choi, B. Hmelo, B. Anthony, S. T. Pantelides, and J. Chen, *IEEE Trans Nucl. Sci.* **57**, 3060 (2010).
36. Y. S. Puzyrev, C. X. Zhang, E. X. Zhang, M. W. McCurdy, D. M. Fleetwood, R. D. Schrimpf, S. T. Pantelides, S. W. Kaun, E. C. H. Kyle, and J. S. Speck, *IEEE Trans. Nucl. Sci.*, **60**, 4080 (2013).
37. Y. S. Puzyrev, T. Roy, E. X. Zhang, D. M. Fleetwood, R. D. Schrimpf, and S. T. Pantelides, *IEEE Trans. Nucl. Sci.*, **58**, 2918 (2011).
38. M. Matsuo, T. Murayama, K. Koike, S. Sasa, M. Yano, S. I. Gonda, A. Uedono, R. Ishigami, K. Kume, T. Ohtomo, E. Furukawa, Y. Yamazaki, K. Kojima, and S. Chichibu, *Proc. 2015 IEEE International Meeting Future of Electron Devices, Kansai (IMFEDK)*, pp. 50.
39. S. Stoffels, M. Melotte, M. Haussy, R. Venegas, D. Marcon, M. Van Hove, and S. Decoutere, *IEEE Trans. Nucl. Sci.*, **60**, 2712 (2013).
40. L. Chernyak, A. Yadav, E. Flitsiyan, Y.-H. Hwang, Y.-L. Hsieh, L. Lei, F. Ren, and S. J. Pearton, *Rad. Eff. Defects Solids*, **170**, 377 (2015).
41. H. Y. Kim, J. A. Freitas, and J. Kim, *Electrochem. Solid-State Lett.*, **14**, H5 (2011).
42. C. Schwartz, A. Yadav, M. Shatkin, E. Flitsiyan, L. Chernyak, V. Kasiyan, L. Liu, Y. Xi, F. Ren, and S. J. Pearton, *Appl. Phys. Lett.* **102**, 062102 (2013).
43. L. Ling, X. Ma, J. Zhang, Z. Bi, L. Liu, H. Shan, and Y Hao, *IEEE Trans. Nucl. Sci.*, **62**, 300 (2015).
44. G. Sonia, F. Brunner, A. Denker, R. Lossy, M. Mai, J. Opitz-Coutureau, G. Pensl, D. Richter, J. Schmidt, U. Zeimer, L. Wang, M. Weyers, J. Würfl, and G. Tränkle, *IEEE Trans. Nucl. Sci.*, **53**, 3661 (2006).
45. J. Chen, E. X. Zhang, C. X. Zhang, M. W. Mccurdy, D. M. Fleetwood, R. D. Schrimpf, S. W. Kaun, E. C. H. Kyle, and J. S. Speck, *IEEE Trans. Nucl. Sci.*, **61**, 2959 (2014).
46. X. Sun, O. I. Saadat, J. Chen, E. X. Zhang, S. Cui, T. Palacios, D. M. Fleetwood, and T. P. Ma, *IEEE Trans. Nucl. Sci.*, **60**, 4074 (2013).
47. L. Lv, J. G. Ma, Y. R. Cao, J. C. Zhang, W. Zhang, L. Li, S. R. Xu, X. H. Ma, X. T. Ren, and Y. Hao, *Microelectron. Rel.*, **51**, 2168 (2011).
48. O. Aktas, A. Kuliev, V. Kumar, R. Schwindt, S. Toshkov, D. Costescu, J. Stubbins, and I. Adesida, *Solid. State. Electron.* **48**, 471 (2004).
49. E. A. Douglas, E. Bielejec, P. Frenzer, B. R. Yates, S. J. Pearton, C. F. Lo, L. Liu, T. S. Kang, and F. Ren, *J. Vac. Sci. Technol. B*, **31**, 021205 (2013).
50. E. Patrick, N. Rowsey, and M. E. Law, *IEEE Trans. Nucl. Sci*, **62**, 1650 (2015).
51. I. Rossetto, F. Rampazzo, S. Gerardin, M. Meneghini, M. Bagatin, A. Zanandrea, A. Paccagnella, G. Meneghesso, E. Zanoni, C. Dua, M. A. Di Forte-Poisson,

Downloaded on 2019-08-31 to IP 128.227.169.164 address. Redistribution subject to ECS terms of use (see ecsdl.org/site/terms_use) unless CC License in place (see abstract).

R. Aubry, M. Oualli, and S. L. Delage, *Proc. 44th European Solid State Device Research Conference (ESSDERC)*, (2014), pp. 381.
52. J. T. Moran, J. W. McClory, J. C. Petrosky, and G. C. Farlow, *IEEE Trans. Nucl. Sci.*, **56**, 3223 (2009).
53. J. Grant, R. Bates, W. Cunningham, A. Blue, J. Melone, F. McEwan, J. Vaitkus, E. Gaubas, and V. O'Shea, *Nucl. Instrum. Meth. A.*, **576**, 60 (2007).
54. P. C. Adell and L. Z. Scheick, *IEEE Trans. Nucl. Sci.* **60**, 1929 (2013).
55. C. F. Lo, L. Liu, T. S. Kang, F. Ren, C. Schwarz, E. Flitsiyan, L. Chernyak, H. Y. Kim, J. Kim, S. P. Yun, O. Laboutin, Y. Cao, J. W. Johnson, and S. J. Pearton, *J. Vac. Sci. Technol. B* **30**, 031202 (2012).
56. A. Y. Polyakov, S. J. Pearton, P. Frenzer, F. Ren, L. Liu, and J. Kim, *J. Mater. Chem. C*, **1**, 877 (2013).
57. S. J. Pearton, R. Deist, F. Ren, L. Liu, A. Y. Polyakov, and J. Kim, *J. Vac. Sci. Technol. A* **31**, 050801 (2013).
58. Z. Zhang, A. R. Arehart, E. Cinkilic, J. Chen, E. X. Zhang, D. M. Fleetwood, R. D. Schrimpf, B. McSkimming, J. S. Speck, and S. A. Ringel, *Appl. Phys. Lett.* **103**, 042102 (2013).
59. Y. Berthlet, B. Guhel, H. Boudart, J. L. Gualous, M. Trolet, M. Piccione, and C. Gaquiere, *Electronics Lett.*, **48**,1078 (2012).
60. M. R. Hogsed, Y. K. Yeo, M. Ahoujja, M.-Y. Ryu, J. C. Petrosky, and R. L. Hengehold, *Appl. Phys. Lett.* **86**, 261906 (2005).
61. S. A. Vitusevich, N. Klein, A. E. Belyaev, S. V. Danylyuk, M. V. Petrychuk, R. V. Konakova, A. M. Kurakin, A. E. Rengevich, A. Yu. Avksentyev, B. A. Danilchenko, V. Tilak, J. Smart, A. Vertiatchikh, and L. F. Eastman, *Phys. Stat. Solidi A* **195**, 101 (2003).
62. A. M. Kurakin, S. A. Vitusevich, S. V. Danylyuk, H. Hardtdegen, N. Klein, Z. Bougrioua, B. A. Danilchenko, R. V. Danilchenko, R. V. Konakova, and A. E. Belyaev, *J. Appl. Phys.*, **103**, 083707 (2008).
63. K. H. Chow, L. Vlasenko, P. Johannesen, C. Bozdog, G. Watkins, A. Usui, H. Sunakawa, C. Sasaoka, and M. Mizuta, *Phys. Rev. B* **69**, 045207 (2004).
64. K. H. Chow, G. D. Watkins, A. Usui, and M. Mizuta, *Phys. Rev. Lett.*, **85**, 2761 (2000).
65. M. Linde, S. J. Uftring, and G. D. Watkins, *Phys. Rev. B*, **55**, R10177 (1997).
66. I. A. Buyanova, Mt. Wagner, W. M. Chen, B. Monemar, J. L. Lindström, H. Amano, and I. Akasaki, *Appl. Phys. Lett.*, **73**, 2968 (1998).
67. K. Saarinen, T. Suski, I. Grzegory, and D. C. Look, *Phys. Rev. B* **64**, 233201 (2001).
68. H. Y. Xiao, F. Gao, X. T. Zu, and J. Weber, *J. Appl. Phys.* **105**, 123527 (2009).
69. D. C. Look, G. C. Farlow, P. J. Drevinsky, D. F. Bliss, and J. R. Sizelove, *Appl. Phys. Lett.* **83**, 3525 (2003).
70. H. J. von Bardeleben, J. L. Cantin, U. Gerstmann, A. Scholle, S. Greulich-Weber, E. Rauls, M. Landmann, W. G. Schmidt, A. Gentils, J. Botsoa, and M. F. Barthe, *Phys Rev. Lett.* **109**, 206402 (2012).
71. A. Sasikumar, A. R. Arehart, S. Martin-Horcajo, M. F. Romero, Y. Pei, D. Brown, F. Recht, M. A. di Forte-Poisson, F. Calle, M. J. Tadjer, S. Keller, S. P. DenBaars, U. K. Mishra, and S. A. Ringel, *Appl. Phys. Lett.*, **103**, 0335091 (2013).
72. T. J. Anderson, A. D. Koehler, J. D. Greenlee, B. D. Weaver, M. A. Mastro, J. K. Hite, C. R. Eddy, F. J. Kub, and K. D. Hobart, *IEEE Electron Dev. Lett.*, **35**, 826 (2014).
73. A. D. Koehler, T. J. Anderson, J. K. Hite, B. D. Weaver, M. J. Tadjer, J. D. Greenlee, P. Specht, M. Porter, T. R. Weatherford, K. D. Hobart, and F. J. Kub "Investigation of Proton-Irradiated AlGaN/GaN HEMTs on Sapphire, Si, and SiC Substrates" *56th Electronic Materials Conference*, June 25–27, 2014, Santa Barbara, CA.
74. A. D. Koehler, P. Specht, T. J. Anderson, B. D. Weaver, J. D. Greenlee, M. J. Tadjer, M. Porter, M. Wade, O. C. Dubon, K. D. Hobart, T. R. Weatherford, and F. J. Kub, *IEEE Electron Device Letters* **35**, 1194 (2014).
75. J. D. Greenlee, P. Specht, T. J. Anderson, A. D. Koehler, B. D. Weaver, M. Luysberg, O. D. Dubon, F. J. Kub, T. R. Weatherford, and K. D. Hobart, *Appl. Phys. Lett.*, 083504 (2015).
76. A. D. Koehler, T. J. Anderson, M. J. Tadjer, B. D. Weaver, J. D. Greenlee, D. I. Shahin, K. D. Hobart, and F. J. Kub "Impact of surface passivation on the dynamic ON-resistance in proton irradiated AlGaN/GaN HEMTs" *IEEE Electron Device Letters* (submitted).
77. S. Ahn, C. Dong, W. Zhu, B.-J. Kim, Y.-H. Hwang, F. Ren, S. J. Pearton, G. Yang, J. Kim, E. Patrick, B. Tracy, D. J. Smith, and I. I. Kravchenko, *J. Vac. Sci. Technol. B.* **33**, 051208 (2015).
78. A. Sasikumar, A. R. Arehart, S. W. Kaun, J. Chen, E. X. Zhang, D. M. Fleetwood, R. D. Schrimpf, J. S. Speck, and S. A. Ringel, "Defects in GaN based transistors," *Proc. SPIE 8986, Gallium Nitride Materials and Devices IX 89861C*, 1 (2014).
79. A. Y. Polyakov, *Radiation effects in GaN, in: GaN and ZnO-Based Materials and Devices*, Springer Series in Materials Science, S. J. Pearton (Ed.), Springer, Heidelberg, 2012, pp. 251.
80. H. Y. Xiao, F. Gao, X. T. Zu, and J. Weber, *J. Appl. Phys.* **105**, 123527 (2009).
81. D. C. Look, Z. Q. Fang, and B. Claflin, *J. Cryst. Growth*, **281**, 143 (2005).
82. C. G. van de Walle and J. Neugebauer, *J. Appl. Phys.* **95**, 3851 (2004).
83. M. A. Reschikov and H. Morkoc, *J. Appl. Phys.* **97**, 061301 (2005).
84. K. H. Chow, G. D. Watkins, A. Usui, and M. Mizuta, *Phys. Rev. Lett.* **85**, 2761 (2000).
85. J. Chen, J. S. Speck, E. C. H. Kyle, S. W. Kaun, S. T. Pantelides, R. D. Schrimpf, D. M. Fleetwood, M. W. McCurdy, Cher Xuan Zhang, En Xia Zhang, and Y. S. Puzyrev, *Nuclear Science, IEEE Trans.* **60**, 4080 (2013).
86. H.-Y. Kim, C. F. Lo, L. Liu, F. Ren, J. Kim, and S. J. Pearton, *Appl. Phys. Lett.* **100**, 012107 (2012).
87. B. S. Kang, S. Kim, F. Ren, J. W. Johnson, R. Therrien, P. Rajagopal, J. Roberts, E. Piner, K. J. Linthicum, S. N. G. Chu, K. Baik, B. P. Gila, C. R. Abernathy, and S. J. Pearton, *Appl. Phys. Lett.* **85**, 2962 (2004).
88. R. Mehandru, B. Luo, J. Kim, F. Ren, B. Gila, A. H. Onstine, C. R. Abernathy, S. J. Pearton, D. Gotthold, R. Birkhahn, B. Peres, R. Fitch, J. Gillespie, T. Jenkins, J. Sewell, D. Via, and A. Crespo, *Appl. Phys. Lett.* **82**, 2530 (2003).
89. A. P. Karmarkar, B. D. White, D. Buttari, D. M. Fleetwood, R. D. Schrimpf, R. A. Weller, L. J. Brillson, and U. K. Mishra, *IEEE Trans. Nucl. Sci.* **52**, 2239 (2005).
90. Y. S. Puzyrev, B. R. Tuttle, R. D. Schrimpf, D. M. Fleetwood, and S. T. Pantelides, *Appl. Phys. Lett.* **96**, 053505 (2010).
91. Y.-S. Hwang, L. Liu, F. Ren, A. Y. Polyakov, N. B. Smirnov, A. V. Govorkov, E. A. Kozhukhova, N. G. Kolin, V. M. Boiko, S S Vereyovkin, V Ermakov, C. F. Lo, O. A. Laboutin, Yu Cao, J. W. Johnson, N. I. Kargin, R. V. Ryzhuk, and S. J. Pearton, *J. Vac. Sci. Technol. B* **31**, 022206 (2013).
92. Y.-H. Hwang, S. Li, Y.-L. Hsieh, F. Ren, S. J. Pearton, E. Patrick, M. E. Law, and D. J. Smith, *Appl. Phys. Lett.*, **104**, 082106 (2014).
93. B. D. Weaver, P. A. Martin, J. B. Boos, and C. D. Cress, *IEEE Trans. Nucl. Sci.*, **59**, 3077 (2012).
94. A. Y. Polyakov, N. Smirnov, A. Govorkov, E. Kozhukhova, S. J. Pearton, F. Ren, L. Liu, J. W. Johnson, W. Lim, N. Kolin, S. Veryokin, and V. S. Ermakov, *J. Vac. Sci. Technol. B.* **30**, 061207 (2012).
95. L. Liu, C. F. Lo, Y. Y. Xi, Y. X. Wang, F. Ren, S. J. Pearton, B. P. Gila, H.-Y. Kim, J. Kim, R. C. Fitch, D. E. Walker Jr., K. D. Chabak, J. K. Gillespie, M. Kossler, M. Trejo, D. Via, A. Crespo, and I. I. Kravchenko, *J. Vac. Sci. Technol. B*, **31**, 022201 (2013).
96. O. Lopatiuk-Tirpak, L. Chernyak, Y. L. Wang, F. Ren, S. J. Pearton, K. Gartsman, and Y. Feldman, *Appl. Phys. Lett.* **90**, 172111 (2007).
97. A. Khachatrian, N. J-H. Roche, S. Buchner, A. D. Koehler, T. J. Anderson, V. Ferlet-Cavrois, M. Muschitiello, D. McMorrow, B. Weaver, and K. D. Hobart. "A Comparison of Single-Event Transients in Pristine and Irradiated AlGaN/GaN HEMTs using Two-Photon Absorption and Heavy Ions" *IEEE Transactions on Nuclear Science* (in press).
98. V. Ramachandran, R. A. Reed, R. D. Schrimpf, D. McMorrow, J. B. Boos, M. P. King, E. X. Zhang, G. Vizkelethy, X. Shen, and S. T. Pantelides, *IEEE Trans. Nucl. Sci.*, **59**(6), 2691 (2012).
99. a. L. Selvaraj, T. Suzue, and T. Egawa, *IEEE Electron. Device Lett.*, **30**, 587 (2009). b. L. Bin and T. Palacios, *IEEE Electron Device Lett*. **31**, 9 (2010).
100. M. Kanamura, T. Ohki, T. Kikkawa, K. Imanishi, T. Imada, A. Yamada, and N. Hara, *IEEE Electron Device Lett*. **31**, 189 (2010).
101. H.-Y. Liu, B.-Y. Chou, W.-C. Hsu, C.-S. Lee, J.-K. Sheu, and C.-S. Ho, *IEEE Trans. Electron. Dev.* **60**, 213 (2013).
102. L. Liu, C. V. Cuervo, Y. Xi, F. Ren, S. J. Pearton, H.-Y. Kim, J. Kim, and I. I. Kravchenko, *J. Vac. Sci. Technol. B* **31**, 042202 (2013).
103. H. Y. Kim, J. Kim, L. Liu, C. F. Lo, F. Ren, and S. J. Pearton, *J. Vac. Sci. Technol. B* **31**, 051210 (2013).
104. P. D. Ye, B. Yang, K. Ng, J. Bude, G. Wilk, S. Halder, and J. Hwang, *Appl. Phys. Lett.* **86**, 063501 (2005).
105. A. Y. Polyakov, N. B. Smirnov, A. V. Govorkov, A. V. Markov, S. J. Pearton, N. G. Kolin, D. I. Merkurisov, and V. M. Boiko, *J. Appl. Phys.* **98**, 033529 (2005).
106. Y. Xi, Y.-L. Hsieh, Y.-H. Hwang, S. Li, F. Ren, S. J. Pearton, E. Patrick, M. E. Law, G. Yang, H.-Y. Kim, J. Kim, A. G. Baca, A. A. Allerman, and C. A. Sanchez, *J. Vac. Sci. Technol. B* **32**, 012201 (2014).
107. S. Mukherjee, J. Chen, T. Roy, M. Silvestri, R. D. Schrimpf, D. M. Fleetwood, J. Singh, J. M. Hinckley, A. Paccagnella, and S. T. Pantelides, *IEEE Trans. Nucl. Sci.* **61**, 1316 (2014).
108. M. J. Beck, R. Hatcher, R. D. Schrimpf, D. M. Fleetwood, and S. T. Pantelides, *IEEE Trans. Nucl. Sci.*, **54**, 1906 (2007).
109. Y. Xi, Y.-L. Hsieh, Y.-H. Hwang, and S. Li F. Ren, S. J. Pearton, E. Patrick, M. E. Law, G. Yang, H.-Y. Kim, J. Kim, A. G. Baca, A. A. Allerman, and C. A. Sanchez, *J. Vac. Sci. Technol. B* **32**, 012201 (2014).
110. *Ionizing Radiation in MOS Devices/Circuits*, ed. T. P. Ma and P. V. Dressdorfer (Wiley, NY, 1989).
111. J. F. Ziegler, J. P. Biersack, and U. Littmark, *The Stopping and Range of Ions in Solids*, (Pergamon Press, London, 1996).
112. B. R. Gossick and J. H. Crawford Jr., *Bull. Amer. Phys. Soc.*, **3**, 400 (1958).
113. J. R. Srour and J. M. McGarrity, *Proc. IEEE*, **76**, 1443 (1988).
114. D. Braunig and F. Wulf, *Radiation Physics and Chemistry*, **43**, 105 (1994).
115. J. H. Crawford and F. F. Slifkin, "Defect Creation in Semiconductors", *Point Defects in Solids*, vol. 2 (Plenum Press, NY, 1975).
116. B. R. Gossick, *J. Appl. Phys.*, **30**, 1214 (1959).
117. J. H. Crawford Jr. and J. W. Cleland, *J. Appl. Phys.*, **30**, 1204 (1959).
118. G. H. Kinchin and R. S. Pease, *Rep. Prog. Phys.*, **18**, 1 (1955).
119. W. Harrison and F. Seitz, *Phys. Rev.*, **98**, 1530 (1955).
120. F. Seitz and J. S. Kohler, in *Solid State Physics* vol. **2**, ed. F. Seitz and D. Turnbull (Academic, New York, 1956), pp. 305.
121. S. R. Messenger, E. A. Burke, G. P. Summers, M. A. Xapsos, R. J. Walters, E. M. Jackson, and B. D. Weaver, *IEEE Trans. Nucl. Sci.*, **46**, 1595 (1999).
122. G. P. Summers, E. A. Burke, P. Shapiro, S. R. Messenger, and R. J. Walters, *IEEE Trans. Nucl. Sci.*, **40**, 1372 (1993).
123. F. B. McLean, *IEEE Trans. Nucl. Sci*, **29**, 1651 (1980).
124. G. P. Summers, E. A. Burke, P. Shapiro, S. R. Messenger, and R. J. Waters, *IEEE Trans Nucl. Sci.*, **40**, 1372 (1993).
125. S. R. Messenger, E. A. Burke, M. A. Xapsos, G. P. Summers, R. J. Walters, I. Jun, and T. M. Jordan, *IEEE Trans. Nucl. Sci.*, **50**, 1919 (2003).
126. J. R. Srour, C. J. Marshall, and P. W. Marshall, *IEEE Trans. Nucl. Sci.*, **50**, 653 (2003).
127. J. R. Srour and J. W. Palko, *IEEE Trans. Nucl. Sci.*, **53**, 3610 (2006).

Downloaded on 2019-08-31 to IP **128.227.169.164** address. Redistribution subject to ECS terms of use (see **ecsdl.org/site/terms_use**) unless CC License in place (see abstract).

128. M. J. Beck, R. Hatcher, R. D. Schrimpf, D. M. Fleetwood, and S. T. Pantelides, *IEEE Trans. Nucl. Sci.*, **54**, 1906 (2007).
129. B. R. Tuttle, *Defect Interactions of H_2 in SiO_2*, "Implications for ELDRS and Latent Interface Trap Buildup," *2010 IEEE Nuclear and Space Radiation Effects Conference*, Denver, CO, July 2010.
130. C. F. Lo, C. Y. Chang, B. H. Chu, H. -Y. Ki, J. Kim, and J. David A. Cullen, Lin Zhou, David. J. Smith, I. I. Kravchenko, S. J. Pearton, Amir Dabiran, B. Cui, P. P. Chow, S. Jang, and F. Ren, *J. Vac. Sci. Technol. B.* **28**, L47 (2010).
131. C.-F. Lo, L. Liu, F. Ren, S. J. Pearton, B. P. Gila, H.-Y. Kim, J. Kim, O. Laboutin, Y. Cao, J. W. Johnson, and I. I. Kravchenko, *J. Vac. Sci. Technol. B* **30**, 041206 (2012).
132. C. F. Lo, Fan Ren, S. J. Pearton, A. Y. Polyakov, N. B. Smirnov, A. V. Govorkov, I. A. Belogorokhov, A. I. Belogorokhov, V. Y. Reznik, and J. W. Johnson, *J. Vac. Sci. Technol. B* **29**, 042201 (2011).
133. In-Hwan Lee, A. Y. Polyakov, N. B. Smirnov, A. V. Govorkov, E. A. Kozhukhova, N. G. Kolin, V. M. Boiko, A. V. Korulin, and S. J. Pearton, *J. Vac. Sci. Technol. B* **29**, 041201 (2011).
134. A. Y. Polyakov, N. B. Smirnov, A. V. Govorkov, E. A. Kozhukhova, S. J. Pearton, Fan Ren, L. Lui, J. W. Johnson, N. I. Kargin, and R. V. Ryzhuk, *J. Vac. Sci. Technol. B* **31**, 011211 (2013).
135. A. Y. Polyakov, N. B. Smirnov, A. V. Govorkov, E. A. Kozhukhova, S. J. Pearton, Fan Ren, S. Yu. Karpov, K. D. Shcherbachev, N. G. Kolin, and W. Lim, *J. Vac. Sci. Technol. B* **30**, 041209 (2012).
136. In-Hwan Lee, A. Y. Polyakov, N. B. Smirnov, A. V. Govorkov, E. A. Kozhukhova, N. G. Kolin, V. M. Boiko, A. V. Korulin, and S. J. Pearton, *J. Vac. Sci. Technol. B* **29**, 041201 (2011).
137. A. Y. Polyakov, In-Hwan Lee, N. B. Smirnov, A. V. Govorkov, E. A. Kozhukhova, N. G. Kolin, A. V. Korulin, V. M. Boiko, and S. J. Pearton, *J. Appl. Phys.* **109**, 123703 (2011).
138. In-Hwan Lee, A. Y. Polyakov, N. B. Smirnov, A. V. Govorkov, E. A. Kozhukhova, E. B. Yakimov, N. G. Kolin, V. M. Boiko, A. V. Korulin, and S. J. Pearton, *Appl. Phys. Lett.* **98**, 212107 (2011).
139. A. Y. Polyakov, N. B. Smirnov, A. V. Govorkov, A. V. Markov, N. G. Kolin, D. I. Merkurisov, V. M. Boiko, K. D. Shcherbatchev, V. T. Bublik, M. I. Voronova, I,-H. Lee, C. R. Lee, S. J. Pearton, A. Dabirian, and A. V. Osinsky, *J. Appl. Phys.* **100**, 093715 (2006).
140. A. Y. Polyakov, N. B. Smirnov, A. V. Govorkov, A. V. Markov, S. J. Pearton, A. M. Dabiran, A. M. Wowchak, B. Cui, A. V. Osinsky, P. P. Chow, N. G. Kolin, V. M. Boiko, and D. I. Merkurisov, *Appl. Phys. Lett.* **93**, 152101 (2008).
141. K. K. Allums, M. Hlad, A. P. Gerger, B. P. Gila, C. R. Abernathy, S. J. Pearton, F. Ren, R. Dwivedi, T. N. Fogarty, and R. Wilkins, *J. Electron Mater.*, **36**, 519 (2007).
142. T. Fujii, Y. Gao, R. Sharma, E. L. Hu, S. P. DenBaars, and S. Nakamura, *Appl. Phys. Lett.* **84**, 855 (2004).
143. D.-H. Kim, C.-O. Cho, Y.-G. Roh, H. Jeon, Y. S. Park, J. Cho, J. S. Im, C. Sone, Y. Park, W. J. Choi, and Q.-H. Park, *Appl. Phys. Lett.* **87**, 203508 (2005).
144. J. Kim, F. Ren, G. Y. Chung, M. F. MacMillan, A. G. Baca, R. D. Briggs, D. Schoenfeld, and S. J. Pearton, *Appl. Phys. Lett.* **84**, 371 (2004).
145. A. Y. Polyakov, N. B. Smirnov, A. V. Govorkov, S. J. Pearton, and J. M. Zavada, *J. Appl. Phys.* **94**, 3069 (2003).
146. A. Y. Polyakov, N. B. Smirnov, A. V. Govorkov, N. V. Pashkova, S. J. Pearton, J. M. Zavada, and R. G. Wilson, *J. Vac. Sci. Technol. B* **21**, 2500 (2003).
147. A. Y. Polyakov, N. B. Smirnov, A. V. Govorkov, K. H. Baik, S. J. Pearton, and J. M. Zavada, *J. Vac. Sci. Technol. B* **22**, 2291 (2004).
148. A. Y. Polyakov, N. B. Smirnov, A. V. Govorkov, A. V. Markov, S. J. Pearton, N. G. Kolin, D. I. Merkurisov, and V. M. Boiko, *J. Appl. Phys.* **98**, 033529 (2005).
149. A. Y. Polyakov, N. B. Smirnov, A. V. Govorkov, A. V. Markov, N. G. Kolin, V. M. Boiko, D. I. Merkurisov, and S. J. Pearton, *J. Vac. Sci. Technol. B* **24**, 1094 (2006).
150. A. Y. Polyakov, N. B. Smirnov, A. V. Govorkov, A. V. Markov, N. G. Kolin, D. I. Merkurisov, V. M. Boiko, K. D. Shcherbatchev, V. T. Bublik, M. I. Voronova, S. J. Pearton, A. Dabiran, and A. V. Osinsky, *J. Vac. Sci. Technol. B* **24**, 2256 (2006).
151. A. Y. Polyakov, N. B. Smirnov, A. V. Govorkov, A. V. Markov, S. J. Pearton, N. G. Kolin, D. I. Merkurisov, V. M. Boiko, Cheul-Ro Lee, and In-Hwan Lee, *J. Vac. Sci. Technol. B* **25**, 436 (2007).
152. A. Y. Polyakov, N. B. Smirnov, A. V. Govorkov, A. V. Markov, A. M. Dabiran, A. M. Wowchak, A. V. Osinsky, B. Cui, P. P. Chow, and S. J. Pearton, *Appl. Phys. Lett.* **91**, 232116 (2007).
153. A. Stocco, S. Gerardin, D. Bisi, S. Dalcande, F. Rampazzo, M. Meneghini, G. Meneghesso, J. Gruneputt, B. Lambert, and E. Zanoni, *Microelectron. Rel.* **54**, 2213 (2014).
154. E. J. Katz, C.-H. Lin, J. Qiu, Z. Zhang, U. K. Mishra, L. Cao, and L. J. Brillson, *J. Appl. Phys.* **115**, 123705 (2014).
155. M. G. Weinstein, C. Y. Song, M. Stavola, S. J. Pearton, R. G. Wilson, R. J. Shul, K. P. Killeen, and M. J. Ludowise, *Appl. Phys. Lett.* **72**, 1703 (1998).
156. B. Luo, J. W. Johnson, F. Ren, K. K. Allums, C. R. Abernathy, S. J. Pearton, R. Dwivedi, T. N. Fogarty, R. Wilkins, A. M. Dabiran, A. M. Wowchack, C. J. Polley, P. P. Chow, and A. G. Baca, *Appl. Phys. Lett.* **79**, 2196 (2001).
157. E. B. Yakimov, P. S. Vergeles, A. Y. Polyakov, I.-H. Lee, and S. J. Pearton, *Appl. Phys. Lett.*, **106**, 132101 (2015).
158. S. Nakamura, M. Senoh, N. Iwasa, and S. Nagahama, *Appl. Phys. Lett.* **67**, 1868 (1995).
159. S. Nakamura, S. J. Pearton, and G. Fasol, *The Blue Laser Diode*, (Springer, Berlin 2000).
160. R. Khanna, K. K. Allums, C. R. Abernathy, S. J. Pearton, J. Kim, F. Ren, R. Dwivedi, T. N. Fogarty, and R. Wilkins, *Appl. Phys. Lett.* **85**, 3131 (2004).
161. R. Khanna, S. Y. Han, S. J. Pearton, D. Schoenfeld, W. V. Schoenfeld, and F. Ren, *Appl. Phys Lett*, **87**, 212107 (2005).
162. H. Ohyama, K. Takakura, M. Hanada, T. Nagano, K. Yoshino, T. Nakashima, S. Kuboyama, E. Simoen, and C. Claeys, *Mater. Sci. Eng. B*, **173**, 57 (2010).
163. H.-Y. Kim, J. Kim, F. Ren, and S. Jang, *J. Vac. Sci. Technol. B* **28**, 27 (2010).
164. H. Nykänen, P. Mattila, S. Suihkonen, J. Riikonen, E. Quillet, E. Homeyer, J. Bellessa, and M. Sopanen, *J. Appl. Phys.* **109**, 083105 (2011).
165. H.-Y. Kim, J. Kim, L. Liu, C.-F. Lo, F. Ren, and S. J. Pearton, *J. Vac. Sci. Technol. B* **30**, 012202 (2012).
166. M. Osiński, P. Perlin, H. Schöne, A. H. Paxton, and E. W. Taylor, *Electron. Lett.* **33**, 1252 (1997).
167. F. Gaudreau, C. Carlone, A. Houdayer, and S. M. Khanna, *IEEE Trans. Nucl. Sci.* **48**, 1778 (2001).
168. S. M. Khanna, D. Estan, L. S. Erhardt, A. Houdayer, C. Carlone, A. Ionascut-Nedelcescu, S. R. Messenger, R. J. Walters, G. P. Summers, J. H. Warner, and I. Jun, *IEEE Trans. Nucl. Sci.* **51**, 2729 (2004).
169. Shun-ichi Gonda, Hiroyuki Tsutsumi, Ito Yoshiumi, Mukai Takashi, and Shin-ichi Nagahama, *Phys Stat Sol A*, **204**, 231 (2007).
170. B.-J. Kim, Y. H. Hwang, S. Ahn, F. Ren, S. J. Pearton, and J. Kim, *J. Vac. Sci. Technol. B* **33**, 051215 (2015).
171. S. M. Khanna, D. Estan, A. Houdayer, H. C. Liu, and R. Dudek, *IEEE Trans Nucl. Sci.* **51**, 3585 (2004).
172. B. H. Rose and C. E. Barnes, *J. Appl. Phys.* **53**, 1772 (1982).
173. H.-Y. Kim, J. Kim, F. Ren, and S. Jang, *J. Vac. Sci. Technol B*, **28**, 27 (2010).
174. C. S. Lee and S. Subramanian, *IEEE Trans Nucl. Sci.* **50**, 1998 (2003).
175. J. Tringe, A. Conway, T. Felter, W. Chan, J. Castelaz, V. Lordi, Y. Xia, C. Stevens, and C. Wetzel, *Nuclear Science, IEEE Transactions on*, **55**, 3633 (2008).
176. A. H. Johnson, *IEEE Trans. Nucl. Sci.* **60**, 2054 (2013).
177. C. Liu, *Optics and Spectroscopy* **113**, 153 (2012).
178. Y. L. Li, X. J. Wang, S. M. He, B. Zhang, L. X. Sun, Y. D. Li, Q. Guo, C. Q. Chen, Z. H. Chen, and W. Lu, *J. Appl. Phys.* **112**, 123515 (2012).
179. G. A. Umana-Membreno, J. M. Dell, T. P. Hessler, B. D. Nener, G. Parish, L. Faraone, and U. K. Mishra, *Appl. Phys. Lett.* **80**, 4354 (2002).
180. T. Anderson, A. Koehler, Y.-H. Hwang, Y.-L. Hsieh, S. Li, Fan Ren, J. W. Johnson, and S. J. Pearton, *J. Vac. Sci. Technol. B* **32**, 051203 (2014).
181. Y.-H. Hwang, Y.-L. Hsieh, L. Lei, S. Li, F. Ren, S. J. Pearton, A. Yadav, C. Schwarz, M. Shatkhin, L. Wang, E. Flitsiyan, L. Chernyak, A. G. Baca, A. A. Allerman, C. A. Sanchez, and I. I. Kravchenko, *J. Vac. Sci. Technol. B* **32**, 031203 (2014).
182. L. Liu, H.-H. Hwang, Y. Xi, F. Ren, V. Craciun, S. J. Pearton, G. Yang, H.- Y. Kim, and J. Kim, *J. Vac. Sci. Technol. B.* **32**, 022202 (2014).
183. E. Patrick, M. E. Law, L. Liu, C. V. Velez Cuervo, Y. Xi, and F. Ren and. S. J. Pearton, *IEEE Trans. Nucl. Sci.* **60**, 4103 (2013).
184. E. Patrick, M. Choudhury, F. Ren, S. J. Pearton, and M. E. Law, *ECS J. Solid State Sci. Technol.* **4**, Q21 (2015).
185. B. Luo, J. W. Johnson, D. Schoenfeld, S. J. Pearton, and F. Ren, *Solid-State Electron*. **45**, 1149 (2001).
186. S. Li, Y. H. Hwang, Y. L. Hsieh, F. Ren, S. J. Pearton, E. Patrick, M. E. Law, C. V. Cuervo, and D. J. Smith, *J. Vac. Sci. Tech* **32**, 021203 (2014).
187. S. Onoda, T. Ohshima, S. I. Sato, K. Yajima, H. Sasaki, Y. Nabeshima, and A. Hasuike, *IEEE Trans. Nucl. Sci.*, **60**, 4446 (2013).
188. M. Rostewitz, K. Hirche, J. Lätti, and E. Jutzi, *IEEE Trans. Nucl. Sci.*, **60**, 2525 (2013).
189. S. Bazzoli, S. Girard, V. Ferlet-Cavrois, J. Baggio, P. Paillet, and O. Duhamel, "SEE sensitivity of a COTS GaN transistor and silicon MOSFETs", *Proc. 9th Eur. Conf. Radiation Its Effects Components Syst.*, pp. 565, 2007.
190. S. Kuboyama, A. Maru, H. Shindou, N. Ikeda, T. Hirao, H. Abe, and T. Tamura, *IEEE Trans. Nucl. Sci.*, **58**, 2734 (2011).
191. A. Lidow, A. Nakata, M. Rearwin, J. Strydom, and A. M. Zafrani, *Proc. IEEE Radiation Effects Data Workshop (REDW),* 2014, pp. 1.
192. L. Scheick, *IEEE Trans. Nucl. Sci.*, **61**, 2881 (2014).
193. I. K. Samsel, E. X. Zhang, N. C. Hooten, E. D. Funkhouser, W. G. Bennett, R. A. Reed, R. D. Schrimpf, M. W. McCurdy, D. M. Fleetwood, R. A. Weller, G. Vizkelethy, X. Sun, T.-P. Ma, O. I. Saadat, and T. Palacios, *IEEE Trans. Nuclear Sci.*, **60**, 4439 (2013).
194. M. R. Pinto, "Comprehensive semiconductor device simulation for silicon USLI," Ph. D. Dissertation, Stanford University, Stanford, CA, 1990.
195. E. Patrick, D. Horton, M. Griglione, and M. E. Law, *Proc. of SISPAD, Denver,* CO, USA, 2012, pp. 217.
196. M. Farahmand, C. Garetto, E. Bellotti, K. F. Brennan, M. Goano, E. Ghillino, G. Ghione, J. D. Albrecht, and P. P. Ruden, *IEEE Trans. Elec. Dev.* **48**, 535 (2001).
197. J. Ziegler and J. Aug. 2013, "SRIM–The stopping range of ions in matter," online at: http://www.srim.org.
198. S. E. Laux, *IEEE Trans. Electron Devices*, **32**, 2028 (1985).
199. Effects of Proton-Induced Displacement Damage on GaN Power Amplifier RF Performance, Nathan Ives, MS Thesis, and MS Electrical *Engineering Department*, Vanderbilt University (August 2015).
200. R. D. Schrimpf and D. M. Fleetwood, Eds., *Radiation Effects and Soft Errors in Integrated Circuits and Electronic Devices*, (World Scientific, Singapore, (2004).
201. R. A. Reed, R. A. Weller, R. D. Schrimpf, M. H. Mendenhall, K. M. Warren, and L. W. Massengill, *IEEE Trans. Nucl. Sci.*, **53**, 3356 (2006).
202. A. M. Albadri, R. D. Schrimpf, K. F. Galloway, and D. G. Walker, *Microelectron. Rel.*, **46**, 317 (2006).

Downloaded on 2019-08-31 to IP 128.227.169.164 address. Redistribution subject to ECS terms of use (see ecsdl.org/site/terms_use) unless CC License in place (see abstract).

203. R. A. Weller, R. D. Schrimpf, R. A. Reed, A. L. Sternberg, A. S. Kobayashi, M. H. Mendenhall, L. W. Massengill, and D. M. Fleetwood, *J. Rad. Effects: Research and Engineering*, **23**(1), 129 (2007).
204. S. T. Pantelides, Y. Puzyrev, X. Shen, T. Roy, S. Dasgupta, B. R. Tuttle, D. M. Fleetwood, and R. D. Schrimpf, *Microelectron. Eng.* **90**, 3 (2012).
205. R. D. Schrimpf, D. M. Fleetwood, M. L. Alles, R. A. Reed, G. Lucovsky, and S. T. Pantelides, *Microelectron. Eng.* **88**, 1259 (2011).
206. Z. Zang, A. R. Arehart, E. C. H. Kyle, J. Chen, E. X. Zhang, D. M. Fleetwood, R. D. Schrimpf, J. S. Speck, and S. A. Ringel, *Appl. Phys. Lett.*, **106**, 022104 (2015).
207. Z. Zhang, A. R. Arehart, E. Cinkilic, J. Chen, E. X. Zhang, D. M. Fleetwood, R. D. Schrimpf, B. McSkimming, J. S. Speck, and S. A. Ringel, *Appl. Phys. Lett.*, **103**, 042102 (2013).
208. S. T. Pantelides, L. Tsetseris, M. J. Beck, S. N. Rashkeev, G. Hadjisavvas, I. G. Batyrev, B. R. Tuttle, A. G. Marinopoulos, X. J. Zhou, D. M. Fleetwood, and R. D. Schrimpf, *Solid-State Electronics* **54**, 841 (2010).

Downloaded on 2019-08-31 to IP 128.227.169.164 address. Redistribution subject to ECS terms of use (see ecsdl.org/site/terms_use) unless CC License in place (see abstract).